Topography-matching heteromultivalent nanoparticles for influenza A virus inhibition

Inaugural-Dissertation

to obtain the academic degree

Doctor rerum naturalium (Dr. rer. nat.)

submitted to the Department of Biology, Chemistry, Pharmacy

of Freie Universität Berlin

by

CHUANXIONG NIE

2020

The work presented in this thesis was conducted in the research group of Prof. Dr. Rainer Haag from **September 2017** until **October 2020** at the Department of Biology, Chemistry, Pharmacy of the Freie Universität Berlin.

1st Reviewer: Prof. Dr. Rainer Haag, Freie Universität Berlin

2nd Reviewer: PD. Dr. Thorsten Wolff, Robert Koch-Institut

Day of defense: December 03, 2020

Acknowledgement

Time flies, it has been three years since my stepping into Germany in 2017. I came here as a PhD student, seeking for opportunities to learn advanced technologies and expand my visions. Things were not easy in the very beginning. With the generous support from my family, friends, and colleagues, I have overcome all the difficulties on the path. I am glad and proud to say that I have become a different person to the one in 2017.

Rainer Haag, my supervisor, is the one who helped me to develop the professional skills. He offered me the opportunity to work in his group and introduced me the advanced technologies and things that I have never seen before. All the projects were finished under his supervision. He gave me a lot of suggestions, not only how to solve the problems I encountered, but also how to think individually, which is the most important knowledge I gained through my PhD. From him, I learnt how to design a project on my own, how to face the difficulties during the experiment, how to make a good story for the projects. I will benefit for my future from these priceless personal characters.

I would like to thank Chong Cheng, who walked with me in this scientific path. He supported the synthesis of most the compounds in my projects and helped me analyze the data and draw conclusions. He is an endless inspiration to me to keep walking to my goals. Besides the scientific support, he also helped me to get used to the German living styles and hosted a lot of parties that make me feel like home.

I would like to thank Marlena Stadtmüller, Matthias Budt, Christian Mache, Gudrun Henis and Thorsten Wolff from Robert Koch-Institut for providing me with the conditions to work with influenza A virus. I worked with them for nearly 2 years. It was a brand-new research field and they taught me everything from the beginning, like how to infection cells with influenza A virus and how to study the viral infections. I want to thank for their time and efforts for reading my results and correcting my manuscripts.

I would like to thank Matthias Wallert, Yannic Kerkhoff, and Stephan Block for supporting me with the investigation of virus binding ability. We have designed a sophisticated microscopy to quantify the weak biological interactions. Failing a lot of times, we finally managed to get the data to prove our hypothesis. I learnt a lot of biophysics, such as virus binding behaviors at the biological interfaces from them. Especially, I want to thank Stephan for reading and correcting my manuscript.

I would like to thank Daniel Lauster for support with quantifying virus binding abilities

and the endless discussions about influenza virus inhibitors. We crossed a lot sparks about how to design a novel virus inhibitor. I want to thank Sumati Bhatia and Badri Parshad for supporting the synthesis of zanamivir-based compounds, which played an important role for the design of virus inhibitors. I want to thank Elisa Quass, Katharina Achazi, Stephanie Wedephol and Jens Dernedde for the support of biological studies. I would like to thank Boris Schade, Svenja Ehrmann and Christoph Böttcher for the help with cryo-EM observations. I want to thank Wiebke Fischer and Eike Ziegler for helping me with the administration.

I want to thank all the people from Multivalency Subgroup of AG Haag for discussing the results and for helping me building up presentation skills. I want to thank all the present and former AG Haag members for creating a lovely place to work with.

Financially, I want to thank German Science Foundation (Deutsche Forschungsgemeinschaft, DFG) for the support to run the projects. Personally, I want to thank China Scholarship Council (CSC) for supporting my study in Berlin.

Finally, I would like to express my deepest acknowledgement to my family, especially my wife, Yu Pang. She supported me by coming to Germany with me and helped me sorting out all the living problems so that I can fully focus on my studies.

Thanks to the people that helped me and the ones I love.

Table of Contents

1 Introduction

1.1 Virus infection and binding at biological interface

1.1.1 Introduction to influenza A virus

Due to the globalization, pathogens nowadays can easily cross the continents with its host and cause pandemic, especially the ones with high infectivity and transmissibility.[1] The coronavirus infection disease 2019 (COVID-19) is a good example, which is caused by severe acute respiratory syndrome coronavirus 2 (SARS-CoV-2). Since the first case report in late 2019, it has caused tens of millions of infections within 10 months. All the people on earth are affected by COVID-19 due to its rapid transmission.[2-3]

Coronavirus, however, is not the only virus species that can cause mass pandemics, the infection by influenza A virus (IAV) can be equally devastating as SARS-CoV-2.[4-5] IAV has a long history of human infection, beginning with a global outbreak in 1918 in records known as Spanish Flu. That pandemic lasted for nearly 3 years and caused more than 50 million of deaths (some also say 17 million).[6] After that, IAV has hit human society with severe pandemics occasionally, each of which caused millions of infections (Figure 1a) with hundreds of thousands of deaths.[7] Nowadays, IAV has become a seasonal viral strain, which is reported to take more than half a million lives every year.[8] The possibility for a new IAV pandemic should not be underestimated, because IAV is a multi-host pathogen and it is constantly evolving with antigen mutations. People still face the possibility of highly infectious animal strains breaching the host barrier to infect human beings.[9-11]

Virology-wise, IAV is an lipid-enveloped, negative-strand RNA virus.[12] As shown in Figure 1, the virion of IAV is a 100 nm nanoparticle. The surface of IAV virion is a lipid envelop originated from its host cells. Two key proteins on the surface have been identified that control the virus binding behavior with the host cells, hemagglutinin (HA) and neuraminidase (NA).[7] HA and NA define the subtype of IAV. There are now 18 different HA antigens and 11 different NA antigens being identified. Therefore, there is a huge antigen heterogeneity for different IAV strains. The high error-rate of RNA polymerase induces the possibility of mutations, which further increases the antigen heterogeneity.

Flu vaccines have been developed in a formulation of antigens from different IAV strains and an adjuvant to boost the immune response. They have been used as powerful tools to prevent influenza infections during flu season by generating IAV neutralizing antibodies

in human body. However, the antigen heterogeneity makes it difficult to prepare a universal IAV vaccine, especially that the virus is constantly mutating.[13-15] Even though extensive efforts are devoted to monitor IAV evolution amongst animal species, it is still difficult to prepare correct vaccines for the coming IAV strains.[16-17] When infection occurred, antiviral drugs are prescribed control the transmission, e.g., zanamivir and oseltamivir.[18] However, zanamivir/oseltamivir-resisting IAV strains have emerged due to viral mutations,[19-21] there is a huge need to develop new inhibitors.

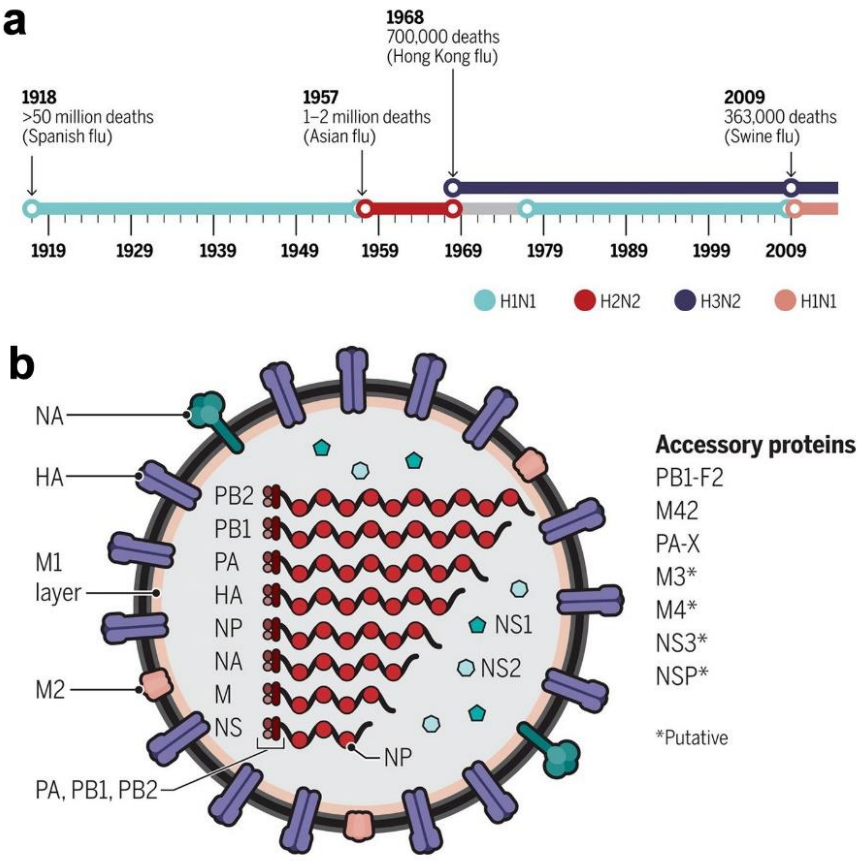

Figure 1. (a) Influenza pandemics of the past 100 years. (b) The virion of influenza A virus. From Ref [7], reprinted with permission from AAAS.

1.1.2 Virus infection in host cells

To develop a virus inhibitor, it is necessary to know how the virion evades and infects the host. As shown in Figure 2, to start the infection, the virion uses HA to bind to the sialic acid (SA) terminated receptors on host cell membrane. The interaction with HA and SA stabilizes the virion on host cell membrane and triggers the viral entry by either endocytosis or direct viral membrane fusion. After the entry, the virion is transported into the endosomes, where

the protons activate the fusion domain of HA and mediate viral-membrane fusion to release viral genome.[22] After RNA replication and protein production with the host cell machinery, the progeny virions are packaged on cell membrane and released by NA, which acts as a sialidase to cleave SA from host cell membrane.

In principle, interfering the viral infection by compounds that block one or multiple pathways in the infection cycle can result in the inhibition of viral replication.[23-24] Since the binding with the host receptors is considered to the first step of infection, most of the recent studies are focused on blocking HA-SA interaction. This has been reported in the adaptive immune response for IAV neutralization by flu vaccines. By the vaccines, HA antibodies are generated to block the receptor binding site of on HA, hence blocking the HA-SA interaction for viral entry inhibition.[25-26] However, the ability to generate HA antibodies varies in people; aged people also show deficiency to produce sufficient protective antibodies and are especially endangered during flu season.[27] The antibodies are degrading upon time and fail to provide long-term protection from seasonal outbreaks.

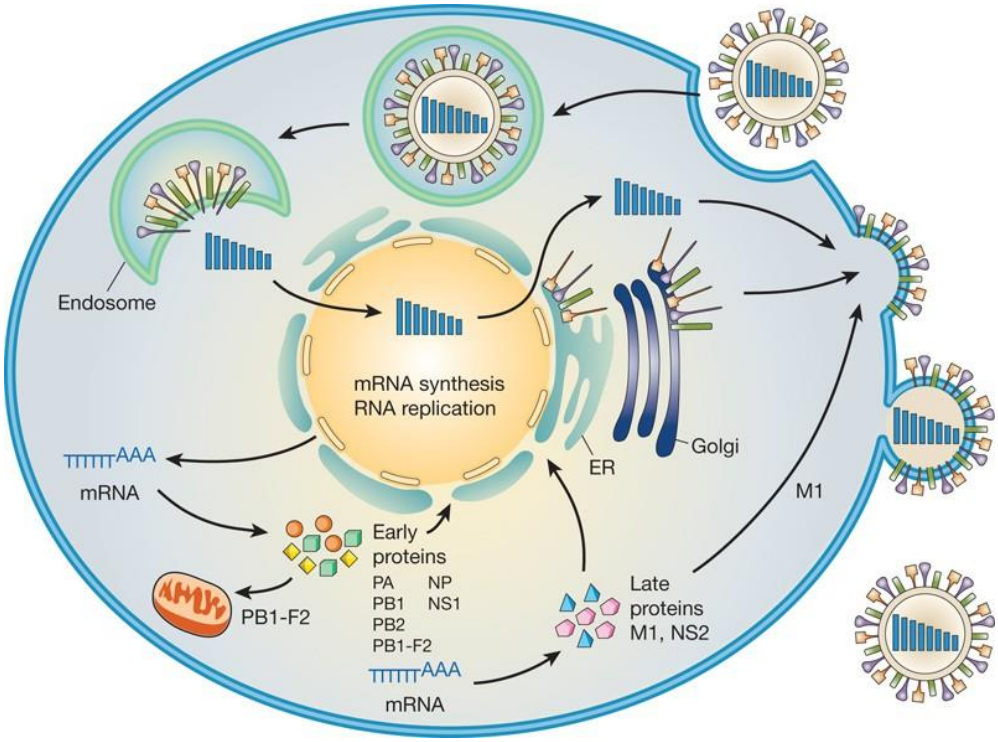

Figure 2. Infection cycle of influenza virus in the host cell. From Ref [28], reprinted with permission from Nature Publishing Group.

1.1.3 HA-NA interplay for IAV interaction with the host

Synthetic inhibitors that work similarly as the HA antibodies can compensate the deficiency of producing HA antibodies for aged people. For an effective inhibition, these inhibitors should be carefully designed with the knowledge of IAV interactions at biointerfaces. In biological systems, IAV uses HA to interaction with hosts; avian IAV binds preferably to sialic acid in 2,3-linkage and human IAV binds to sialic acid in 2,6-linkage. HA-SA interaction is the trigger for virus entry, but it is also noticed that single HA-SA binding is rather weak with a dissociation constant of 1-20 mM.[29] To facilitate virus entry, multiple SA are recruited to engage HA simultaneously to cumulate the interactions for the stabilization of virion on host cell membrane, so called multivalent interactions. Due to the weak monovalent interaction, when approaching host cell membrane, the virion is mobile on the host cell membrane when binding to SA in the beginning. Gradually, it recruits SA for multivalent and stable bindings and then viral entry occurs via endocytosis.

The dynamic virus interaction at biological interface is not only due to the weak HA-SA interaction, but also the activity of NA. NA acts as a sialidase to cleave SA group from the conjugated glycans, which is known to promote the release of progeny IAV virions from the host cells. HA and NA are presented in high numbers on viral surface in approximately 6:1 ratio. They are densely packed on the surface of IAV virion; small NA patches have also been noticed. NA-related IAV mobility has been observed in several different cases, which come to a conclusion that NA is not only necessary for the release of progeny virions from host cells, but also important for a virion to maintain its mobility when binding to its receptor. In a total internal reflection fluorescence (TIRF) microscopy set-up with a fetuin-modified support lipid bilayer, Sakai et al. noticed that an NA inhibitor could completely block the virus movement.[30] Similarly, the NA-deficient IAV virions tended to bind tightly on surface with low mobility. In another TIRF setup by Block et al., as shown in Figure 3, adding NA inhibitor was noticed to enhance virus binding to the surface with increased off-rate (related to virus residing time on the surface), indicating that virions were more stable on the surface in the presence of NA inhibitors.[31] The on-rate was modified by zanamivir, indicating that the virus binding to SA terminated ganglioside (GD1a) containing supported lipid bilayer (SLB) was enhanced by zanamivir.

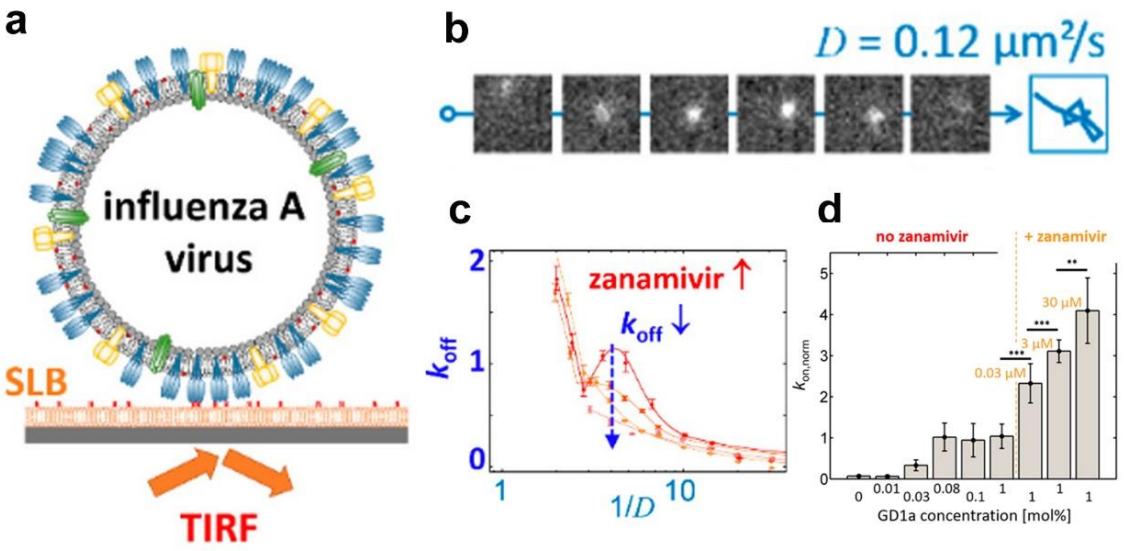

Figure 3. (a) A TIRF-based set-up to investigate IAV mobility when binding to SA receptor in a SLB. (b) Typical images for an IAV virion moving on the SLB. (c) Effects of zanamivir, a NA inhibitor, on off-rate of IAV binding to GD1a-SLB. (d) Effects of zanamivir on the on-rate of IAV binding to GD1a-SLB. From Ref [31], reprinted with permission from ACS.

The SA-cleaving ability of NA prevents the aggregation and entrapment of IAV by biological systems, e. g. mucus, ensuring the effective infection in host cells.[29] Mucus is a viscous barrier lying above the epithelial cells. Mucus consists mainly mucins with a dense charge and multiple sialic acid moieties.[32-33] When approaching to the mucus, IAV virions are trapped in the mucus layer due to the binding to sialic acid; the high viscosity of mucus limits virus penetration by diffusion. The constant propelling by the epithelial cilia promotes the renewal of mucus and the clearance pathogens trapped in there.[34] NA is therefore important for a successful mucus penetration for cleaving SA on mucins and enabling virions to travel through mucus layer. The small NA patches on IAV surface can direct the IAV movement in mucus layer and promote IAV penetration.[35] In a recent study, it is noticed that adding NA inhibitor significantly reduced the virion penetration in mucus layer and decreased the virus infectivity to the underlying epithelial cells. On the other hand, adding exogenous NA facilitated viral penetration of mucus and thus increases viral infectivity.[36] IAV mutated with NA deficiency did not transmit efficiently by aerosol droplet, despite being shed from infected animals and transmitted directly to the receipting animals, highlighting the key role of NA in the barrier penetration of IAV.[37]

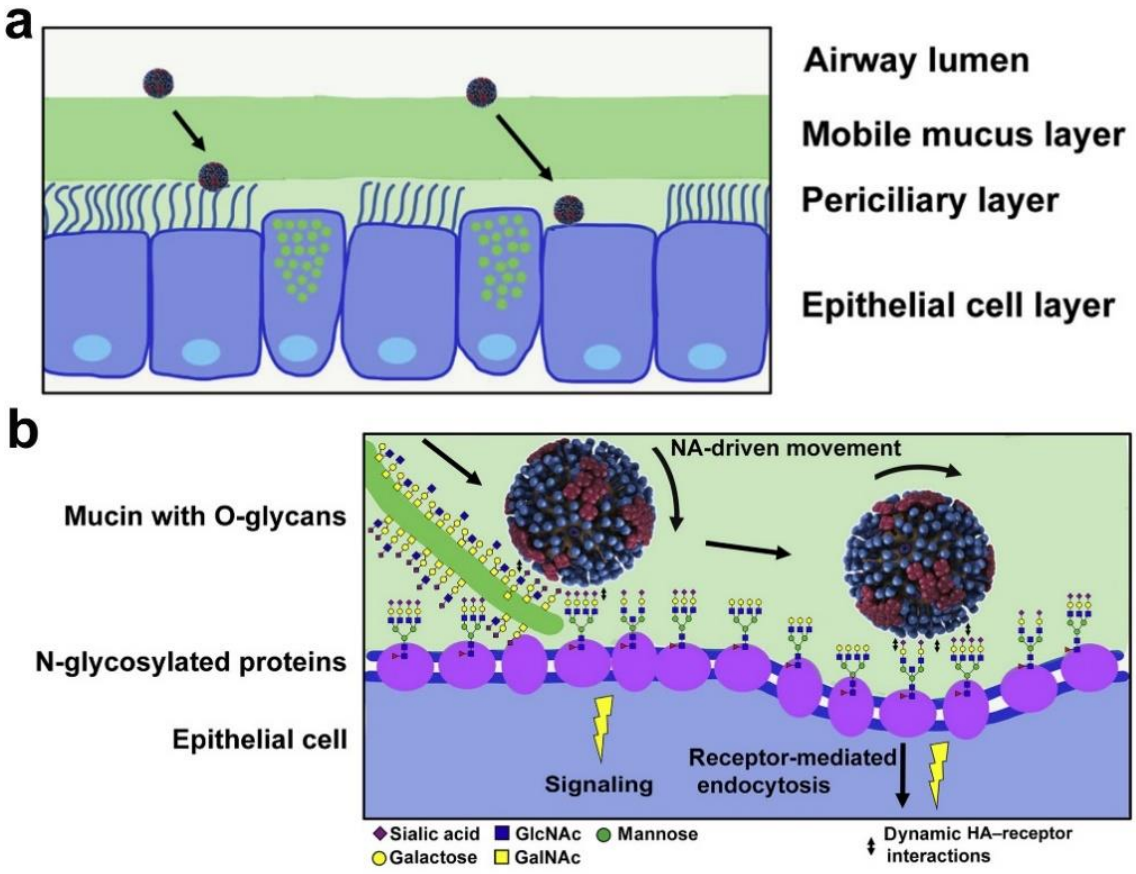

Figure 4. (a) IAV penetration of mucus barrier for the infection of epithelial cells. (b) HA-NA balance for IAV penetration of mucus and movement on the surface of epithelial cell. From Ref [33], reprinted with permission from Elsevier.

1.2 Multivalency as the principle for HA binding to block viral entry

1.2.1 SA-binding pockets on HA

For an effective virus inhibition, the virus-inhibitor binding should outperform the virus-cell binding so that the virion would preferably interact with the decoy instead of its actual receptor.[38-39] A potent binding decoy can even detach the virions that bind to its receptors via a binding competition mechanism. Therefore, for a potent inhibitor, the SA distribution should be carefully designed to maximize the interaction with HA. HA is a trimer protein with a head domain (HA1) and a stalk domain (HA2), as shown in Figure 5a. The stalk domain contains the fusion peptide that is activated by protons to mediate virus-membrane fusion for virus entry and genome release. The SA binding sites are located at the HA1 domain and multiple binding sites have been revealed for the multivalent interaction with the

SA on host cell membrane.[40] These binding pockets are spatially distributed on the head of HA trimer. Taking influenza A/X31 (H3N2) as an example, three SA binding pockets are identified in a triangle presentation on top of the HA with a distance around 4 nm as shown in Figure 5c-d. For effective influenza A/X31 (H3N2) inhibition, the distance of SA on the inhibitor should also be around 4 nm for a strong binding.[41-42]

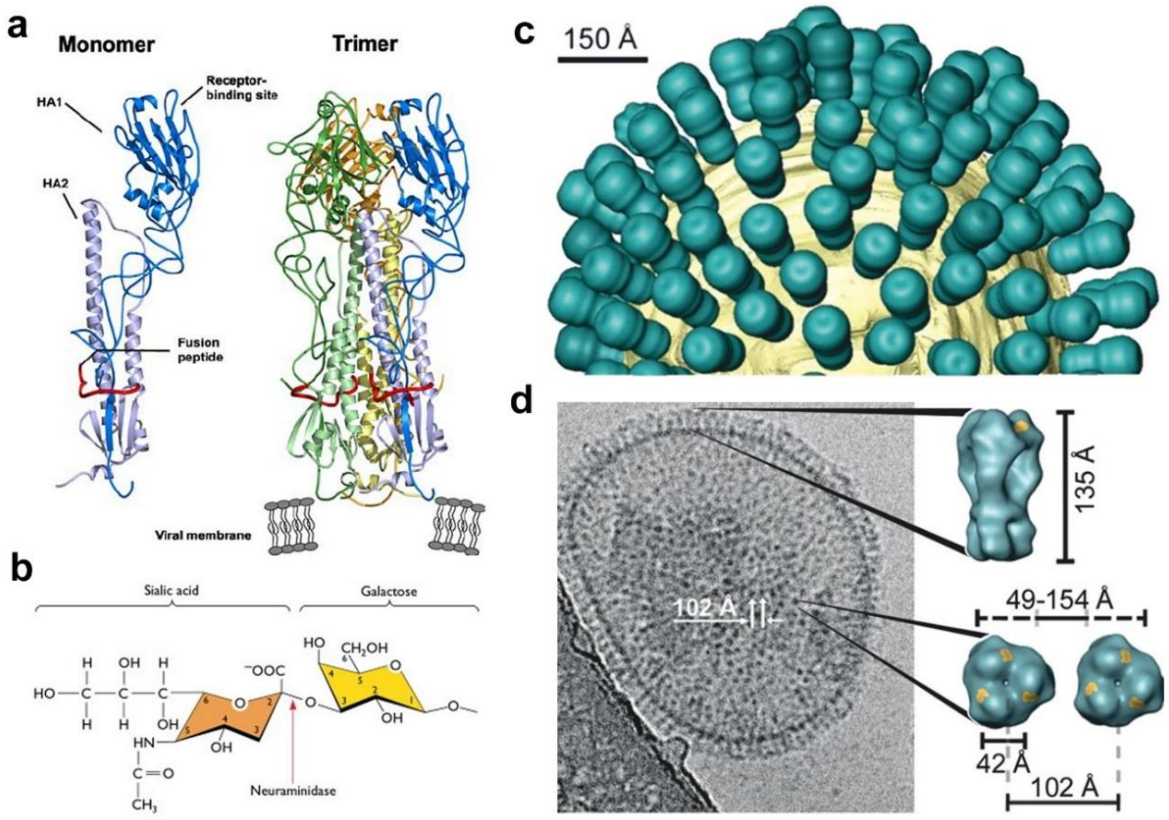

Figure 5. (a) Structure of HA. From Ref [43], reprinted with permission from SpringerLink. (b) Sialic acid receptors on host cell surface. (c) Schematic illustration of HA on an IAV virion. (d) Cryo-EM images for a virion of influenza A/X31 (H3N2) and the display of the sialic acid binding pockets (marked yellow) on HA. From Ref [40], reprinted with permission from ACS.

1.2.2 Multivalency as the principle for HA binding and blocking

Monovalent sialic acid did not show any activities due to the weak interaction (Figure 6a-b). For the simultaneous interaction with all SA binding pockets, multiple SA on a single inhibitor is needed, so called multivalent inhibitors.[38] The idea of multivalent interactions

can be noticed by multiple commercial products, e. g Velcro tapes, which utilize multiple flexible hooks to interact with targets with tight connections. For HA binding, by cumulating the weak HA-SA interaction in a single structure, the binding can be significantly improved (Figure 6c-f), especially if the inhibitors are designed with matched SA distribute to the binding pockets on HA.[38, 44] In a study by Whitesides et al., it is noticed that polymers with middle sialic acid functionalization (0.2-0.6 mole ratio) was more potent than the ones with higher or lower functionalization. Spatial matching to the SA binding pockets of HA was concluded to be the key for a potent binding, for which the intermediate sample was the one that shows matched SA distribution to the binding pockets of HA. Inspired by this study, controlling the statistical SA distribution on the inhibitor surface via different functionalization has been used as common approach to achieve robust HA binding, which has been developed with multiple polymeric scaffolds.[45-48]

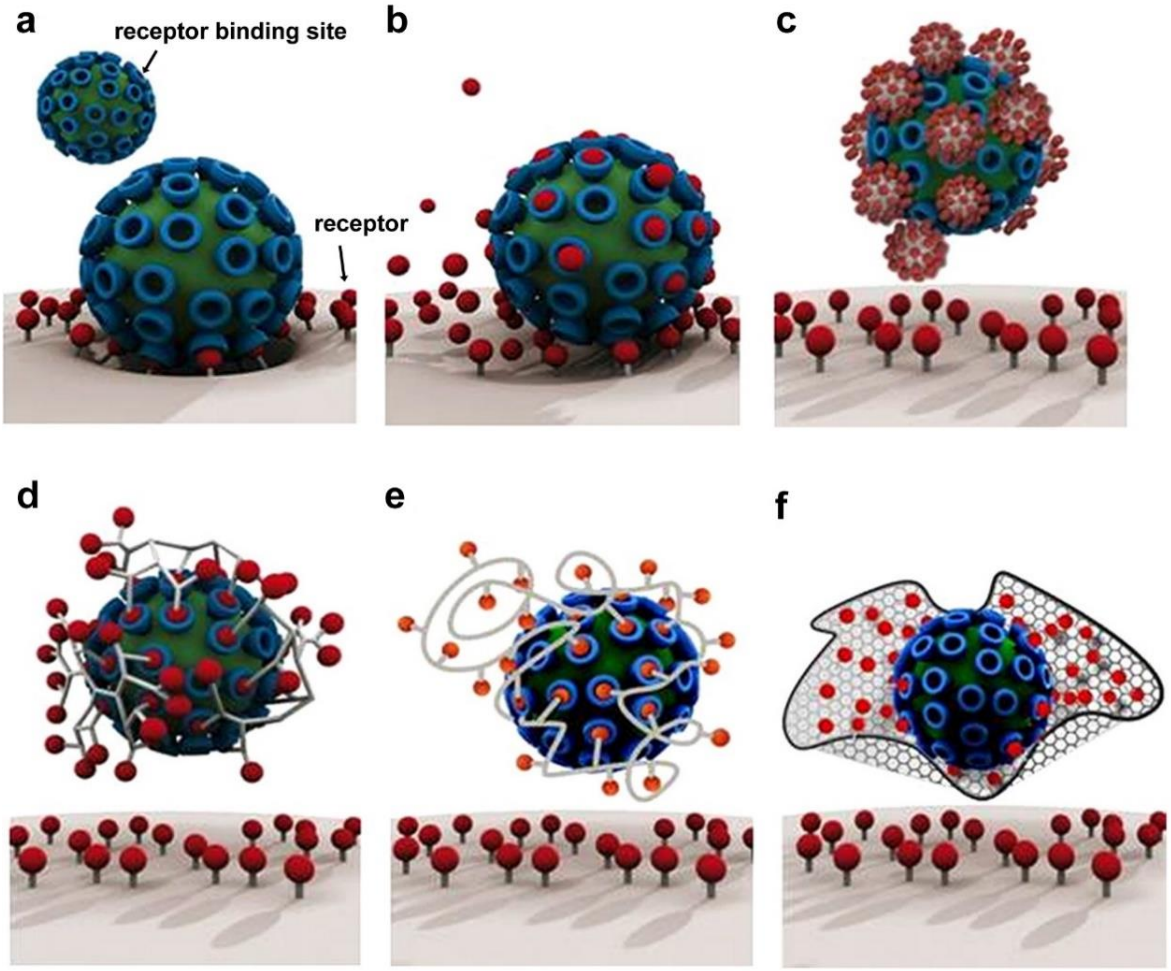

Figure 6. Multivalency as the acting principle for the design of pathogen inhibitors. (a) Without an inhibitor, a virus can bind to the receptors for cellular entry and infection. (b) The

activity of monovalent inhibitor is not ideal due to uncomplete blocking of receptor binding site. (c-f) Multivalent inhibitors can effectively block the receptor binding sites of virion and blocking its binding to receptors, including but not limited to (c) small nanoparticles, (d) dendritic structures, (e) linear structures and (f) 2D nanostructures. From Ref [38], reprinted with permission from ACS.

With the spatial distribution SA binding pockets on HA being revealed (Figure 5d), efforts have been taken for the precise topological design of inhibitors, in order to gain more insight to the virus binding behavior and study the spatial matching for HA binding. Ebara et al. used a three-armed polymer to study HA binding as shown in Figure 7a-b.[49] At the end of each 'arm', 6'-sialyllactose was introduced. By altering the length of the spacer, the end groups were distributed in a triangular shape. A detailed screening revealed the importance of spatial matching for the multivalent interactions, as even at same functionalization, the ones with topological-matched shape showed 10-fold better binding than others. The same group also designed a DNA three-way junction that matches to the sialic acid binding pockets of HA precisely (Figure 7c-d).[50] This structure showed 80,000-fold higher binding affinity towards A/Puerto Rico/08/34 (H1N1) than the sialyllactose monomer. Three-way junction showed better HA-binding ability than one-way or two-way junctions, highlighting the key role of spatial optimization for multivalent interactions.

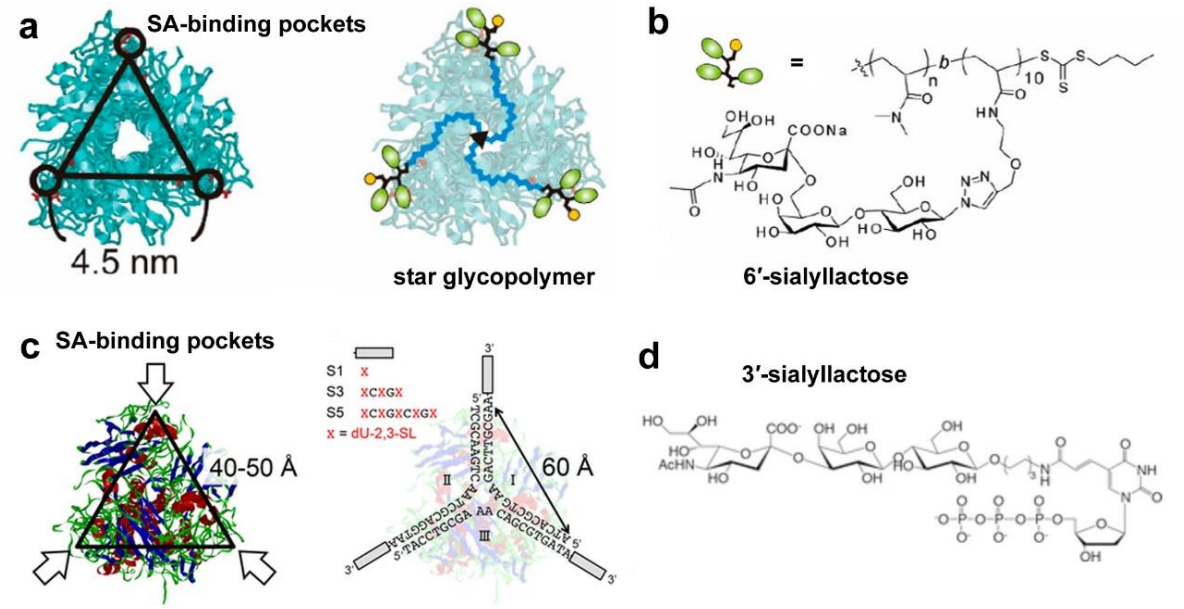

Figure 7. Spatial design of trivalent inhibitor matching to the sialic acid binding pockets of

HA, including (a) 6'-sialyllactose modified star glycopolymer [49] and (b) 3'-sialyllactose modified DNA three way junction.[50] From [49] and [50], respectively, reprinted with permission from ACS.

1.2.3 Structural factors for multivalent HA binder

Despite the ligand density/valency, the spacer flexibility and core sizes have been realized as key parameters that affect the virus-inhibitor binding as shown in Figure 8a-b. Flexible backbone/linker enables the inhibitor undergoing conformational changes to adapt the receptor binding sites, with the loss of more conformational entropy in the process.[38] In a thermodynamic investigation by Netz et al., it is pointed out that the spacer flexibility is closely related to the dissociation of monovalent interactions (K_{mono}).[51] They defined critical monovalent dissociation constant (K_{mono}*) as the constant for a spacer length when bivalent structures show equal binding to the monovalent structures, indicating that there is no cumulative effects for multivalency in this case. In the case that $K_{mono} < K_{mono}$*, a broader range of spacer length will exist where divalent structure outperforms the monovalent structure for the binding. In the case that $K_{mono} > K_{mono}$*, monovalent binder is better because the entropy lose overcomes the gain in binding energy.

Since that monovalent HA-SA interaction exhibit a dissociation constant of 1-20 mM, the divalent inhibitor with stiff spacer is expected to be better than the flexible one, which has been proven by a comparison between DNA- and PEG-based sialic acid models.[40] Perfectly designed DNA structures exhibited better binding that the optimal PEG structures. The adoption of different conformations enables the flexible inhibitors to overcome the steric obstruction in binding to the receptors without steric strain, where the rigid ones that are not perfectly designed cannot do so. Therefore, when designing the IAV inhibitors, the monovalent affinity should be carefully considered for the usage of flexible or rigid spacers. The idea is proved by a study from Pallavi et al., whereas trivalent sialoside structures were synthesized in rigid or flexible backbone and compared for IAV binding as shown in Figure 8c-e.[52] Although these flexible structures showed millimolar binding constant, the rigid one dominated flexible compound with binding constant in micromolar range. They also emphasized the necessity of the optimizing the spacer length for inhibitor design as increased conformational penalties for long PEG spacers was noticed from the molecular dynamic simulations.

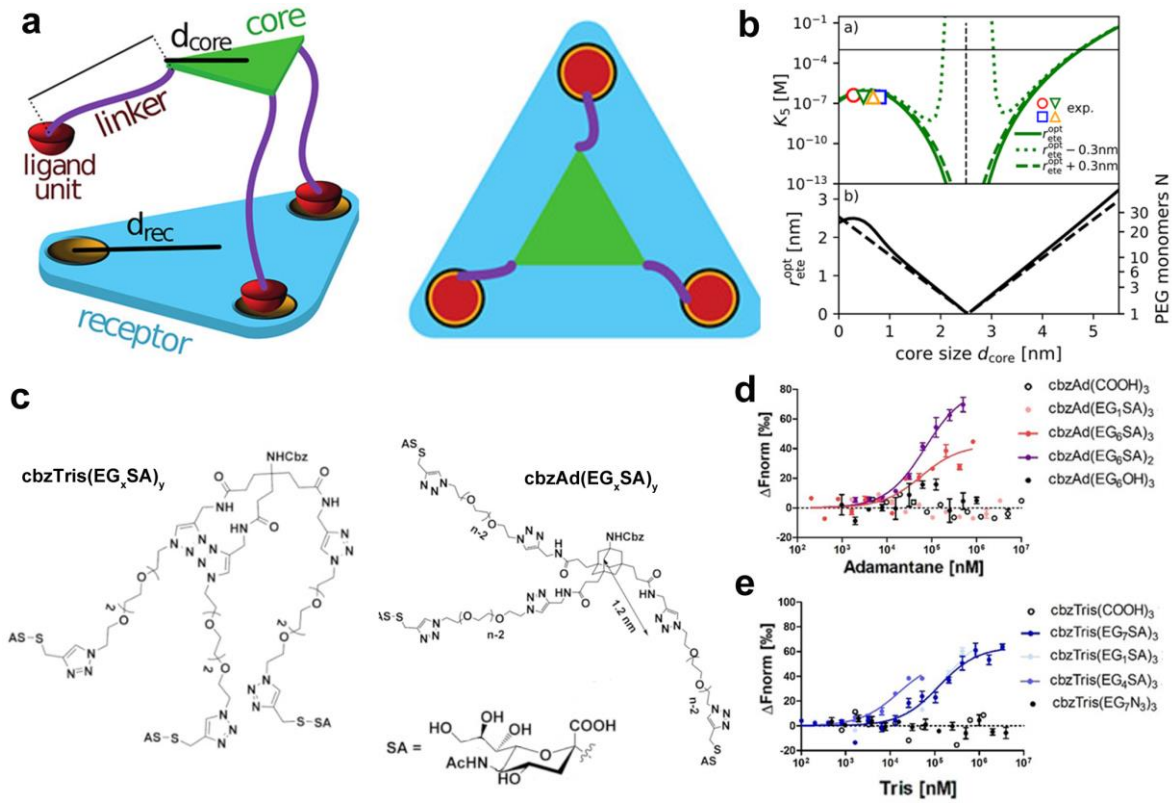

Figure 8. (a) Schematic illustration for the matching of ligands to the receptor binding sites for the design of virus inhibitors. (b) Influence of ligand core size d_{core} for the binding. From [53], reprinted with permission from ACS. (c) Typical structures for the rigid (adamantane) and flexible (4-(((Benzyloxy)carbonyl)amino)-4-(2-carboxyethly)heptanedioic acid, TRIS) cores for HA binding. (d-e) Microscale thermophoresis measurements with intact R18 labeled influenza A/X31 (H3N2) virions against (d) different adamantane-based or (e) TRIS-based constructs. From [52], reprinted with permission from Wiley.

1. 3 Rationally designed IAV inhibitors

1.3.1 Synthetic polysialyated structures for IAV inhibition

With the principles mentioned above, numerous polysialyated structures have been developed in recent years.[38] Kwon et al. revealed the importance of nanostructured polysialyllactose to achieve effective IAV inhibition as shown in Figure 9a.[54] A dendritic polymer, polyamidoamine (PAMAM), was used as the core for the sialyllactose functionalization. Dendritic structure is rigid due to the internal steric hinderance, so the

distance of the sialyllactose on PAMAM can be statistically controlled via the degree of functionalization. The PAMAM-sialyllactose conjugate with a spacing around 3 nm showed the best binding and inhibition of influenza A/California/04/2009 (H1N1). The SA binding pockets was roughly 4 nm distanced for this virion, highlighting the importance of spatial matching for the design of IAV inhibitors.

How the valency and scaffold flexibility affect the virus binding and inhibition was thoroughly studied in a recent report by Bhatia et al.[41] Polyglycerol was used as the polymeric platform for multivalent display of sialic acid as shown in Figure 9b. It was noticed that, at a suitable valency that allowed the matching of sialic acid to the binding pockets, the binding was maximized. It is also revealed that flexible scaffold (linear polyglycerol, LPG) was much better than rigid scaffold (dendritic polyglycerol, dPG), due to the ability to adapt to the SA-binding pockets of HA by changing polymer backbone conformation. The robust virus-inhibitor binding enabled potent virus inhibition, with which four orders of magnitude of reduction of virus titer was achieved. For a precise spatial design of polysialyated structure, Lauster et al. developed a phage-capsid-based IAV inhibitor that exhibited a well-defined sialic acid display matching the SA-binding pockets as shown in Figure 9c.[42] Such a rationally designed inhibitor showed robust binding with HA and blocked the virus binding to the host cells. As a result, potent virus inhibition and efficient prevention of virus infection were achieved, revealed by *in vitro* cell culture, *ex vivo* lung tissue culture, and *in vivo* mouse tests.

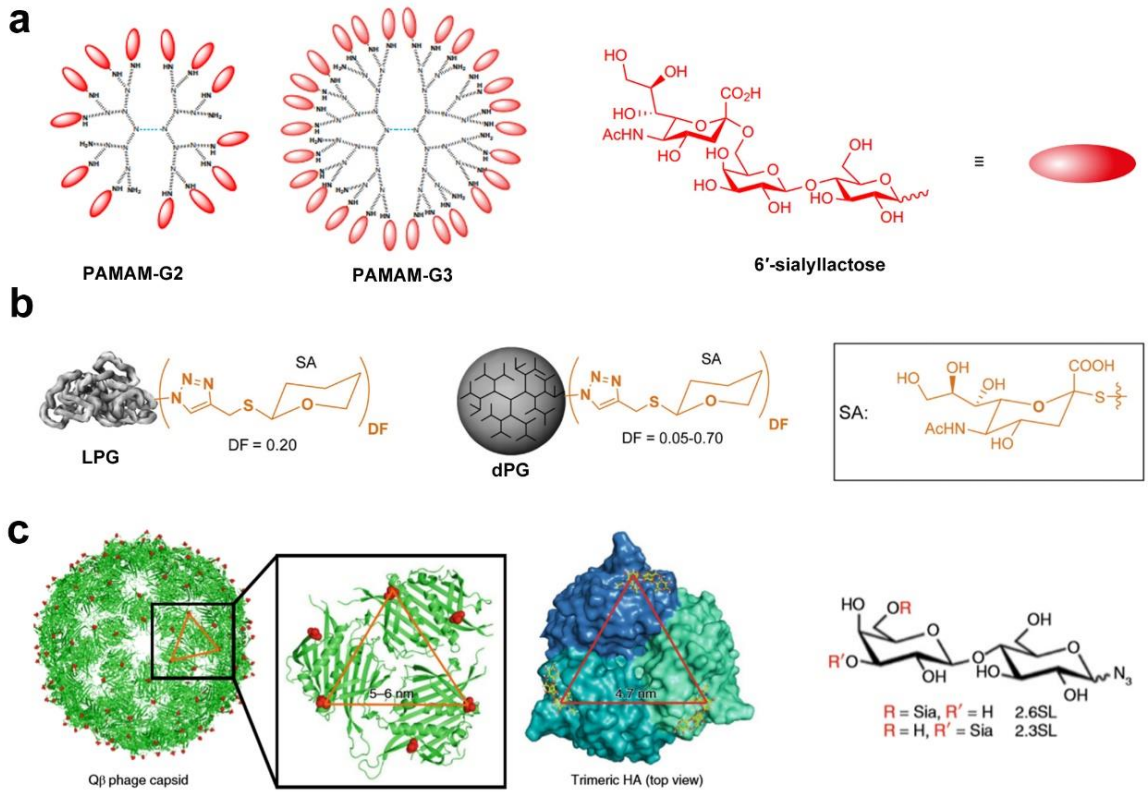

Figure 9. (a-c) Examples for the polysialyated structures for the inhibition of influenza A virus. The scaffold materials are (a) PAMAM dendrimers, (b) linear and dendritic polyglycerol, and (c) Qβ-phage capsid. From Ref [54], Ref [41], and Ref [42], reprinted with permission from Elsevier and Nature Publishing Group, respectively.

1.3.2 Virucidal structures for irreversible deactivation of virions

In addition to receptor blocking, Stellacci group has further promoted the design of virus inhibitors via a 'virucidal' mechanism as shown in Figure 10a-b.[55-56] Even being multivalent, the virus interaction with its binder is still reversible. Upon dilution, the binder can detach from the virion, especially at the concentration below its IC50 value, and the virus would be infectious again. To preserve inhibitory activity upon dilution, they came up with an idea of virucidal compounds. These compounds not only interact with the virion but also deactivate the virions irreversibly via destroying the lipid structures or deform the surface proteins by hydrophobic interactions. In a recent report, they have synthesized a cyclo-dextrin-based virucidal compounds for IAV inhibition as shown in Figure 10c.[57] They noticed that only the sialic acid linked with a hydrophobic alkane spacer showed virucidality towards IAV, the one with hydrophilic PEG spacer was virustatic. The specificity of the inhibitor was also noticed as the one with 6' sialyl-N-acetyllactosamine (6'SLN) showed

superior activity on human IAV strains and 3’ sialyl-N-acetyllactosamine (3’SLN) worked on avian IAV strains, depending on the HA binding preference of the IAV. However, for the designing of virucidal compounds, the cytotoxicity should be carefully investigated as these amphiphilic compounds may also disrupt the cell membranes.

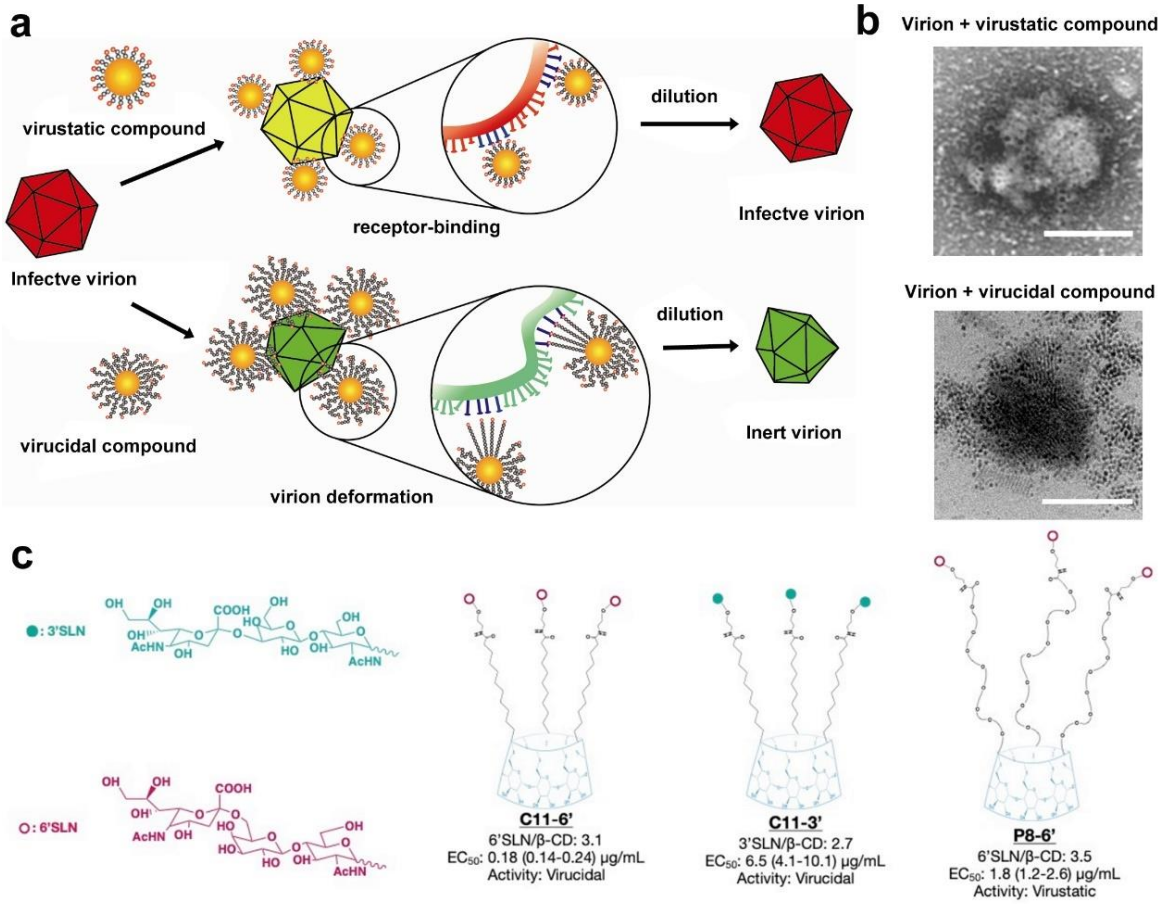

Figure 10. (a) The acting mechanism for virustatic and virucidal compounds. (b) Typical cryo-EM images of a virion incubated with virustatic and virucidal compounds respectively. From Ref [55], reprinted with permission from Nature Publishing Group. (c) Sialyllactose modified compounds for the irreversible deactivation of IAV virions. From Ref [57].

1.3.3 Nanoparticles-based virus inhibitors

Combination of multivalent polymeric structures and nanomaterials leads to the development of novel nano-inhibitors. Compared with polymeric structures, these nano-inhibitors offer the possibility to control ligand display in a nanoscale dimension, which can improve spatial hinderance of viral particles as shown in Figure 11a-b.[58] In a theoretical study by Netz et

al.,[58] it was noticed that at low virus concentration, the IC50 of an inhibitor predominantly depended on the multivalent interactions, which exponentially increased with the inhibitor/virus contact area. One major conclusion from the study is that larger inhibitors often show better binding than the small ones at low virus concentration so that only steric shielding effects can be observed for the binding, instead of forming virus/inhibitor clusters. Considering that the concentration of viruses in the body fluids of infected individuals is quite low, larger inhibitors would be of major advantage than the smaller ones. It is also pointed out that the optimal size for a globular binder is 1/3 of the target.

The hypothesis is supported by a recent study by Block et al., where they proved that 2.6MDa dPG with size around 30 nm showed better influenza A/X31 (H3N2) binding ability than the 10kDa dPG with the same sialic acid functionalization.[59] The size of IAV virions is around 100 nm. Papp et al. also noticed that the size of the inhibitor could alter the binding.[60] Sialic acid-modified gold nanoparticles (AuNP) were synthesized for IAV binding and they noticed that only 14 nm AuNP showed inhibitory effects towards A/X31 (H1N1), while the 2 nm AuNP did not show any significant impact. This is probably due to the smaller AuNP could not hinder the HA effectively from the binding with the receptors on host cell membrane.

The inhibitor flexibility significantly influents the virus/inhibitor binding, which is even more pronounced than the polymer-based inhibitors. Compared with globular stiff structure, the flexible ones can change it morphology upon binding, hence maximize the interacting area and steric shielding for virus inhibition. In a report by Ziem et al., it was found out the dendritic polyglycerol sulfate (dPGS) was not active for the inhibition of Orthopoxvirus, but once dPGS was conjugated to graphene surface, a potent inhibitor was obtained because of the steric hinderance by the 2D flexible graphene materials.[61] Even the study was performed on IAV, their study pointed out that soft/flexible substrates are promising platform to develop virus inhibitors, due to its ability to adapt to the virion and maximize the interface area for increased steric shielding.[62-64] For the proof of concept, Bhatia et al. synthesized polyglycerol nanogels with different flexibilities with sialic acid on the surface and compared their efficiency for IAV inhibition (Figure 11c).[63] They noticed that IAV virion binding could induce deformation of the nanogel at the binding site to increase the interface area and enhance the binding, as shown in Figure 11d. The enhanced binding led to the enhanced inhibition of IAV infection by blocking the virions from the cells.

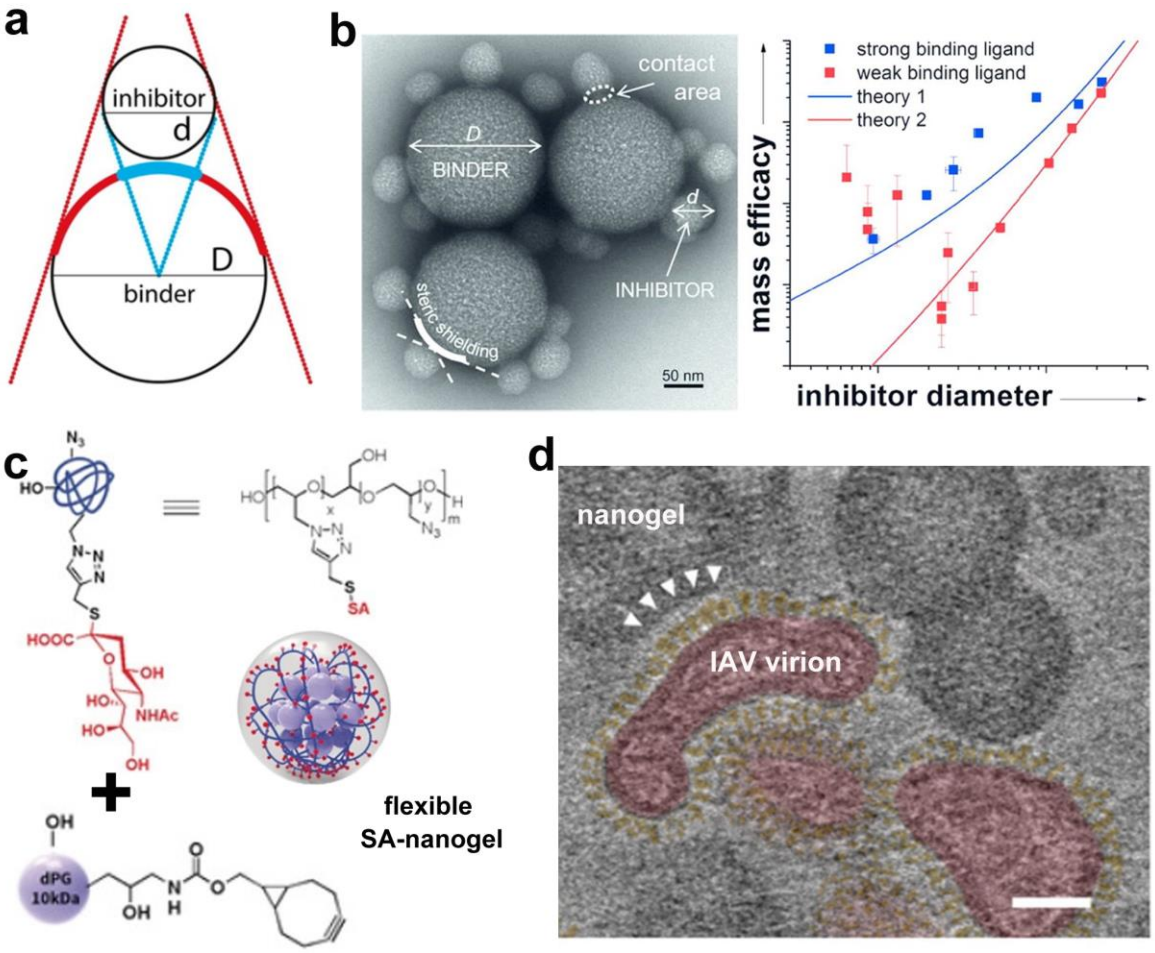

Figure 11. (a) Schematic illustration for the spatial hindering by the inhibitor. (d) Negative-stained TEM images for the binding between binders and inhibitors. (b) Combination of the experimental and theoretical volume normalized number of inhibitors, P(d/D)3, required to inhibit a binder from attaching to a planar surface. From Ref [58], reprinted with permission from ACS. (c) Synthesis of flexible SA-nanogel via the click conjugation of LPG-SA with dPG. (d) Cryo-EM image for interaction between flexible SA-nanogel and IAV virion. The binding sites are marked with white triangles. The IAV virion are marked red, while the HA and NA are marked orange. Scale bar: 50 nm. From Ref [63], reprinted with permission from Wiley.

1.3.4 The need for new structures for virus inhibition

Even though significant progress has been made for the developing of multivalent binding decoys for IAV inhibition, the status is not satisfactory for the lack of a broad-spectrum virus inhibitor. As mentioned above, the HAs from different IAV subgroups are highly heterogenic, which means that the SA-binding pockets vary for different IAV strains. The structures

mentioned above are mostly designed with a fixed SA display. Therefore, they may only be active on a very limited range of IAV strains. The intra-trimer targeting of HA from different subgroups can hardly be achieved by the synthetic polymers. For example, the phage-capsid inhibitor that Lauster reported showed HA inhibition against H3N2 IAV strains (specifically, A/X31 (H3N2) and A/Panama/2007/1999 (H3N2)), but not against H1N1 strains (A/Puerto Rico/8/1934 (H1N1), A/WSN/1933 (H1N1), etc.).[42] The activity of PAMAM-based inhibitors from Kwon et al. was rather limited to H1N1 strains.[54] Additionally, IAV is a highly mutative viral strain, the constant mutation of HA makes it even more difficult to prepare a broad-spectrum inhibitor.[65-66] The treatment by HA inhibitors could also promote IAV mutations with resistance.[67-69]

Also, because that IAV is mutating and evolving, a broad-spectrum virus inhibitor is quite needed as a countermeasure for the next IAV pandemic. To do that, the concept of multivalency should be further improved with more binding dynamics being considered for the inhibitor design. More efforts should be devoted to this field, seeking for new opportunities for broad-spectrum IAV inhibitors.

1. 4 Cellular membrane vesicle as a novel virus binder

1.4.1 Cellular membrane coating nanotechnology

Cellular membrane is the outermost layer of a cell for the biological interactions, and it is the interface for the cells to sense the surrounding microenvironment and communicate with other cells. Numerous receptors carrying different functions anchors on cell membrane through hydrophobic transmembrane domains. These receptors, made of carbohydrates or proteins, are the structural basis for the cell recognition at biological systems. For example, Cluster of Differentiation 47 (CD47) is expressed on most of the human cells and it delivers a ‘do-not-eat-me’ signal to macrophages to avoid immune clearance.[70] The lipid-based structure of cellular membrane enables the receptors to be highly mobile and to maintain its function at different conditions.

Inspired by its versatile functions, scientists have begun research to make synthetic nanoparticles exhibiting similar functions as cells by transferring the membrane receptors to the surface of nanoparticles.[71] Recent developments of nano- and bio- technology have allowed the extraction of whole membrane of cells and transfer it onto a nanoparticle surface, making a highly biocompatible bio-interfaces for biomedical applications, as shown in Figure

12.[72-73] Typically, the cells are disrupted mechanically and the cellular membrane is isolated from other structures via centrifugation. As the membrane is highly mobile, it can follow the curvature of the nanoparticle and stabilize by hydrophobic interactions. During the membrane transfer, all the membrane components, including the lipid bilayer, membrane proteins and glycans, are also transferred on the nanoparticle surface in an outside-out orientation.[73]

As most of the biological interactions occur via the interaction with cell membrane, the cell membrane-coated nanoparticles behave like cells when being injected into animals. For instance, nanoparticles coated with red blood cell membrane (RBCm) exhibited reduced clearance and prolonged circulation time.[74-75] This was because of the transferring of CD47 onto the nanoparticle surface, the lipid structure ensured that CD47 was at its native form. Nanoparticles cloaked with platelet membrane were able to target pathogens, thrombus and tumors, like platelets.[73, 76] The cell membrane-coated nanostructures have been used for tumor therapy,[77-79] bio-absorbents,[80] and vaccine development.[81-83] The *in vivo* studies demonstrated the safety of cell membrane coated nanoparticles for biomedical applications, as no adverse effects are noticed.[72]

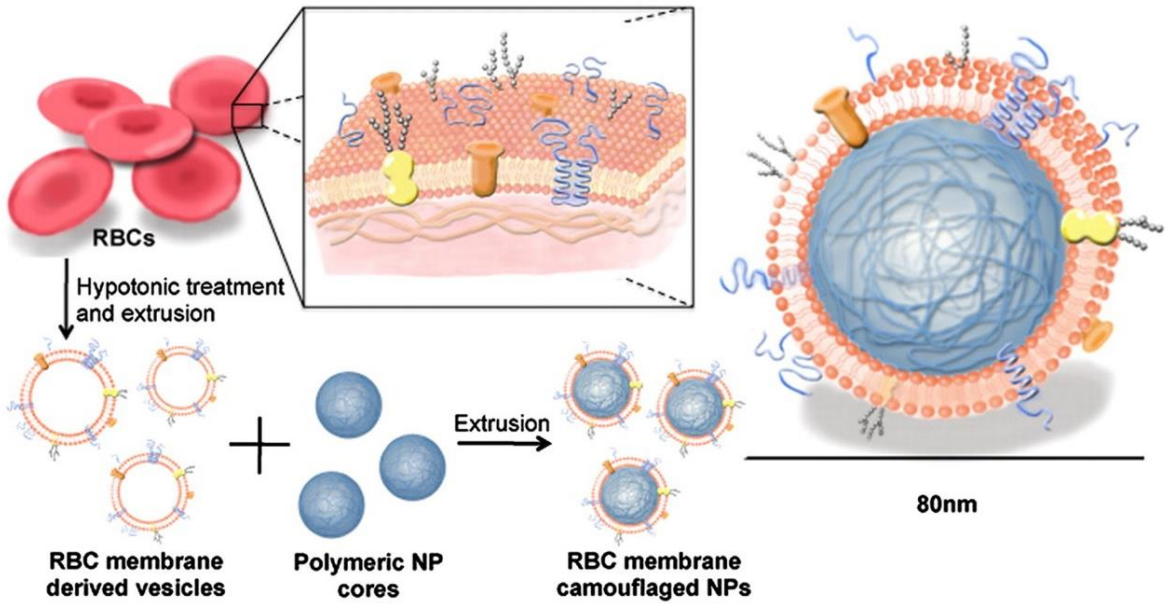

Figure 12. Red blood cell membrane coated nanoparticles for biomedical applications. From Ref [74], reprinted with permission from National Academy of Sciences.

1.4.2 Cellular membrane vesicles for virus binding

As mentioned above, the viral receptors anchored the membrane of host cells. Therefore, the cellular-based structures may also be used for virus binding. de Carvalho et al. revealed that the exosomes of CD4+ T-cells could be used to inhibit the infection human immunodeficiency virus 1 (HIV-1) *in vitro*. These exosomes exhibited the same protein profile as the CD4+ T-cells, ensuring the binding with HIV-1 virion and competing with actual CD4+ T-cells for gp120 interaction.[84] The emerging cell-engineering technologies can be future used to modify the surface of cells for virus binding. In a report by Liu et al., the HepG2 cells were engineered to express human sodium taurocholate co-transporting polypeptide (hNTCP) as the receptor for hepatitis B virus (HBV), as shown in Figure 13.[85] The budded hNTCP membrane vesicles are revealed to be able to bind to HBV virions with high sensitivity and specificity. The infection of HBV is effectively blocked hNTCP membrane vesicle, which is proven both *in vitro* cell culture and *in vivo* chimeric mouse models.

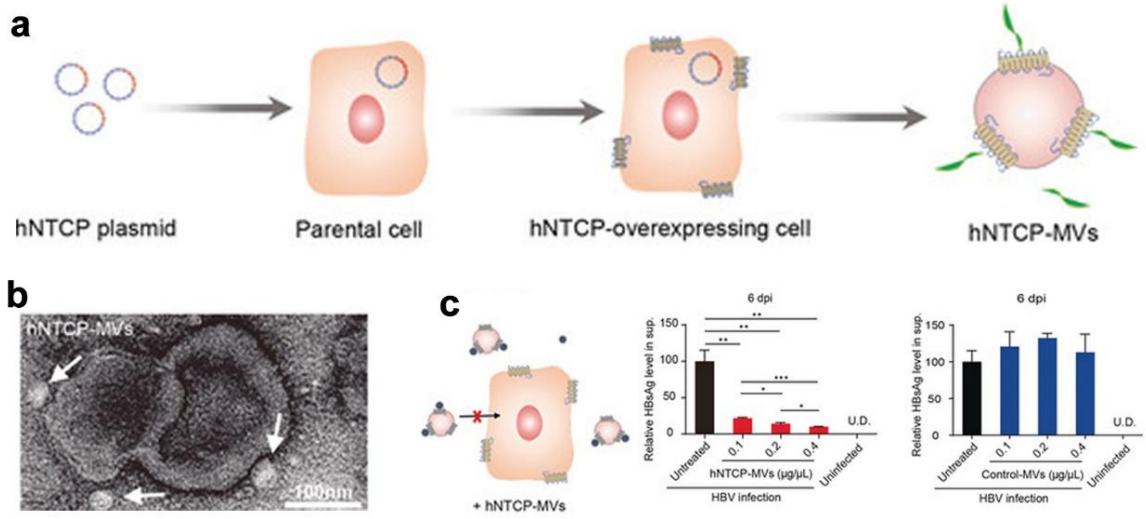

Figure 13. hNTCP-engineered cell membrane vesicles for HBV infection inhibition. (a) Generation of hNTCP cell membrane vesicles. (b) Binding of hNTCP membrane vesicles to HBV virions. (c) *In vitro* HBV infection inhibition by hNTCP membrane vesicles. From Ref [85], reprinted with permission from Wiley.

Membrane vesicles can be solution to the broad-spectrum virus inhibitors. Membrane fluidity and the possibility of lateral diffusion of membrane proteins enable attachment factors to adjust and possibly even be recruited by virions as needed, which indicates that the

cellular membrane vesicle might overcome the HA heterogeneity of different IAV strains and work as a broad-spectrum IAV inhibitor. Additionally, the receptor on the cell membrane, e.g., the receptor density, can be tuned via gene engineering. On the other hand, preparing polymeric inhibitor requires extensive synthetic efforts to prepare a big library of candidate compounds and multiple screening steps to identify active ones. The preparation of cellular membrane-based inhibitors is considered to simple and easy. The membrane isolation can be completed within a few hours, making it suitable to prepare inhibitors for sudden and unexpected pandemics. It is envisioned that the combination of cellular membranes vesicles with engineered nanoparticles can lead to the development of novel IAV inhibitors. However, this has not been studied in detail.

2 Scientific goals

RBCs exhibit a natural multivalent display of SA for IAV binding. Despite the heterogenicity of HA, most of the IAV virions from different subtypes bind strongly to red blood cells, casing aggregation of the cells, namely, hemagglutination. Recent development of biotechnology has allowed the extraction of RBCm and the coating of RBCm onto synthetic nanoparticles surface without interfering the proteins and glycans of RBCm.[74] Cellular membrane is a fluid system, on which the anchored receptors remain mobile. Therefore, it has the potential to adapt to the sialic acid binding pocket of HA and overcome the heterogenicity of HA. It is envisioned that the combination of RBCm with nanoparticles can lead to broad-spectrum IAV inhibitors.

To be a potent inhibitor, the virus binding ability of the cell membrane structures should be further improved. As the membrane is originated from the host cells, when applying to the cells, the virus binding preference to the membrane vesicle is considered to be the same as it to the host cells. In this case, some virions may still interact with the host cells for virus entry and infection. To improve virus-binding ability, heteromultivalency and topography matching principle may be considered.

For IAV, NA acts as a sialidase to cleave HA-SA interactions for virus release. As introduced above, the NA-HA interplay plays an important role for maintaining viral mobility at the biointerface. It can also interfere the IAV/inhibitor binding, especially for the cellular membrane-based structures. Inhibiting the activity of NA can reduce the negative impact of NA on IAV/inhibitor binding. In earlier studies, it has been proven that when NA is inhibited, the binding between IAV virion and host cells is significantly enhanced. The addition of NA inhibitor may also provide additional binding sites for IAV virion, which further improves the IAV/inhibitor binding.

If the membrane is coated onto a nanoparticle for a nanoparticle-based inhibitor, the core material can be designed to improve the IAV/inhibitor binding, e.g., maximizing the interface area via match topography can also increase virus binding ability. As monovalent HA-SA is weak, the virions are mobile when firstly interacting with the membrane-based inhibitors. In this case, increasing the interface area can facilitate the multivalent virus binding and reduce the possibility of virus escape via crawling and gliding. With the development of nanomaterials science, many kinds of nanoparticles with special shapes have been synthesized, including nanorods,[86] nanocubes,[87] nanofibers,[88] nanobowls,[89]

spiky nanoparticles,[90] etc. It is envisioned that these nanostructures will exhibit different binding patterns compared with spherical nanoparticles or 2D nanosheets.

Given to the above introduction about research background, we believe there is still a huge need for developing influenza inhibitors integrating the knowledge from materials science, cellular biology, and virology. The scientific goal of this PhD study is to overcome the challenges for broad-spectrum and potent influenza inhibitors. The following research projects are proposed to achieve the goal:

1. The membrane of RBC will be extracted and its ability to binding IAV virions will be studied thoroughly, including transmission electron microscope (TEM), total internal reflection fluorescence (TIRF) microscope and hemagglutination inhibition (HAI) assay. The binding ability will be compared with different human IAV strains and investigate the potential of RBCm to be a broad-spectrum inhibitor. The inhibitory effects of RBCm will be studied be cellular infection assays, including the investigation of cellular infections (staining of infected cells) and virus replications (plaque assays).

2. Nanoparticles with different morphologies will be synthesized for RBCm coating, including spiky nanostructures that target the nanostructures on IAV surface, and concave nanostructures that match the curvature and size of IAV virion. The IAV binding ability of RBCm-coated nanoparticles will be quantified by western blot, while the inhibitory activity will be investigated by HAI assay, cellular infection assays and so on.

3. For heteromultivalent inhibition of both HA and NA, zanamivir, a commercial and approved NA inhibitor, will be used. To facilitate zanamivir incorporation, a lipidic zanamivir will be synthesized. The IAV binding of RBCm-zanamivir surface will be investigated in detail by HAI assay and TIRF microscopy.

4. Finally, the heteromultivalent and topography matching RBCm-coated nanoparticles will be developed integrating the information from 1-3 as a novel broad-spectrum IAV inhibitor (Figure 14). The inhibitory activity will be studied thoroughly by cellular infection assays with different human IAV strains. The cellular toxicity will also be carefully evaluated to translate to potential *in vivo* experiment.

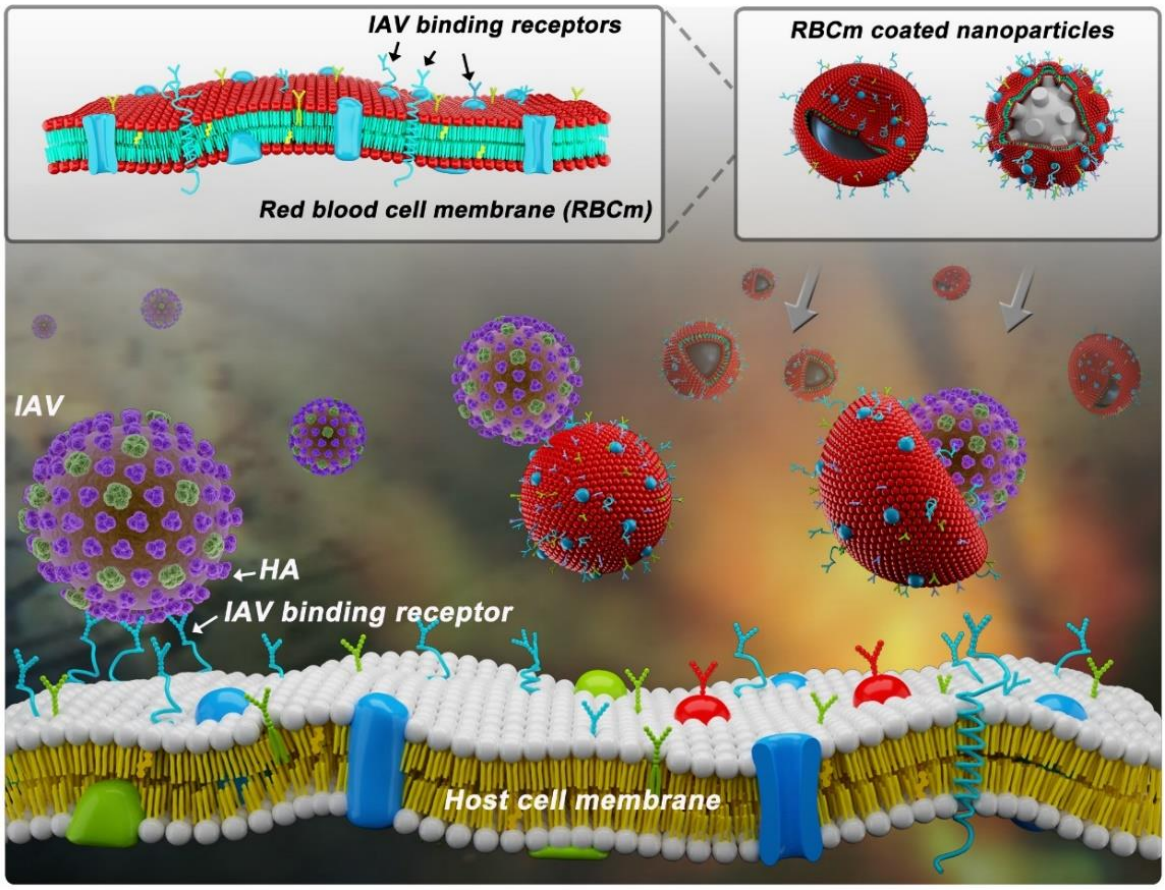

Figure 14. Preparation of RBCm-coated heteromultivalent structures as the binding decoys to prevent IAV infection.

3 Publications

3.1 Spiky nanostructures as topography matching principle for influenza A virus inhibition

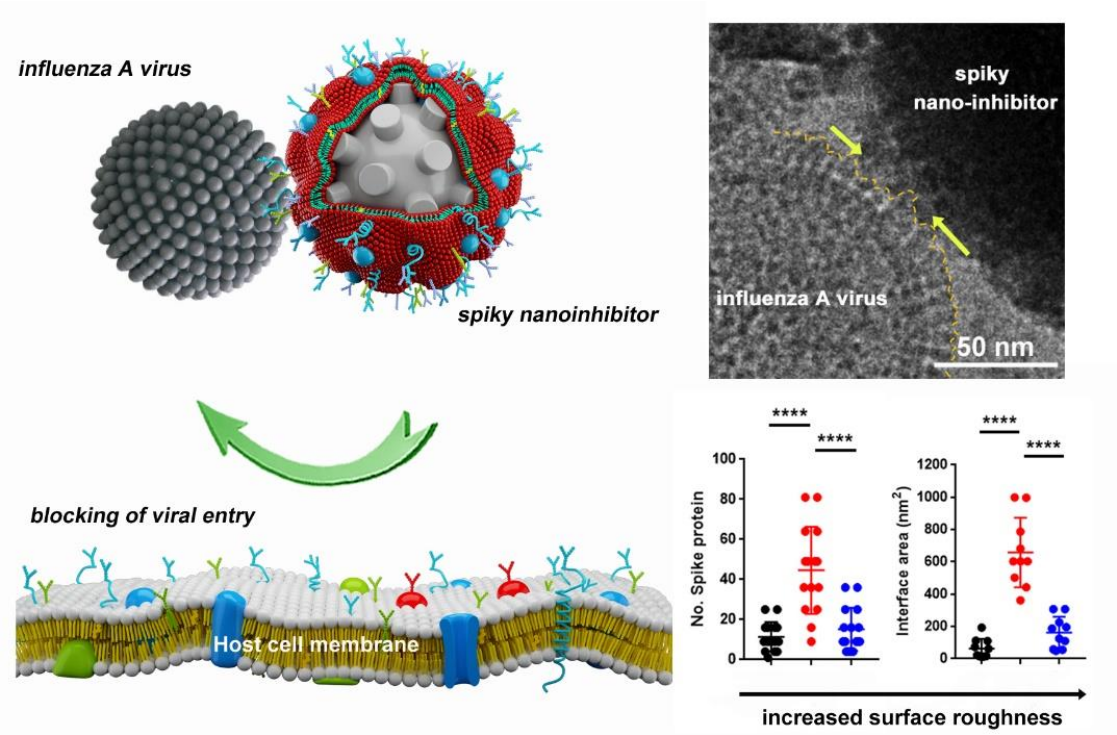

Chuanxiong Nie, Marlena Stadtmüller, Hua Yang, Yi Xia, Thorsten Wolff, Chong Cheng, Rainer Haag

Nano Lett., **2020**, *20*, 7, 5367–5375

https://doi.org/10.1021/acs.nanolett.0c01723

Author contribution:

Chuanxiong Nie synthesized the materials, performed the experiment, and wrote the manuscript.

Marlena Stadtmüller supported the virology experiment.

Hua Yang and Yi Xia performed the geometry analysis.

Thorsten Wolff, Chong Cheng, and Rainer Haag supervised the project and edited the manuscript.

3.2 Topology-matching design of an influenza A virus inhibitor with dual mode of action

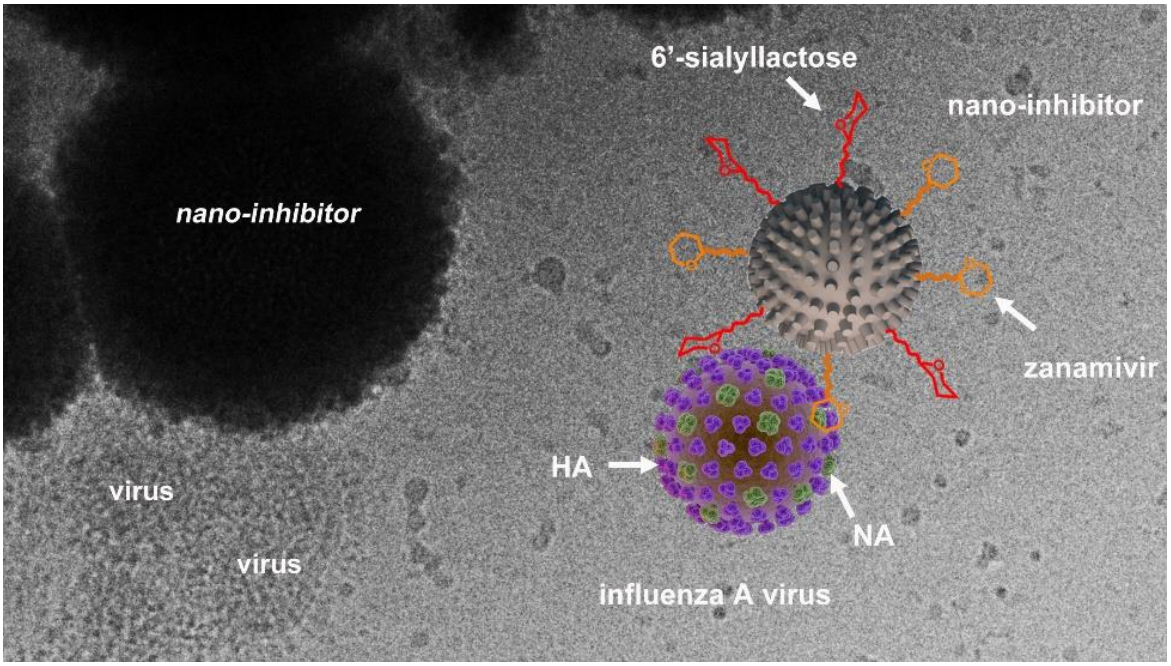

Chuanxiong Nie, Badri Parshad, Sumati Bhatia, Chong Cheng, Marlena Stadtmüller, Alexander Oehrl, Yannic Kerkhoff, Thorsten Wolff, Rainer Haag

Angew. Chem. Int. Ed., **2020**, 59, 15662-15666.

https://doi.org/10.1002/anie.202004832

Author contribution:

Chuanxiong Nie synthesized the materials, performed the experiment, and wrote the manuscript.

Badri Parshad, Sumati Bhatia, Chong Cheng, and Alexander Oehrl supported the synthesis of the materials.

Marlena Stadtmüller supported the virology experiment.

Yannic Kerkhoff supported the analysis of the results.

Thorsten Wolff and Rainer Haag supervised the project and edited the manuscript.

3.3 Heteromultivalent topology-matched nanostructures as potent and broad-spectrum influenza A virus inhibitors

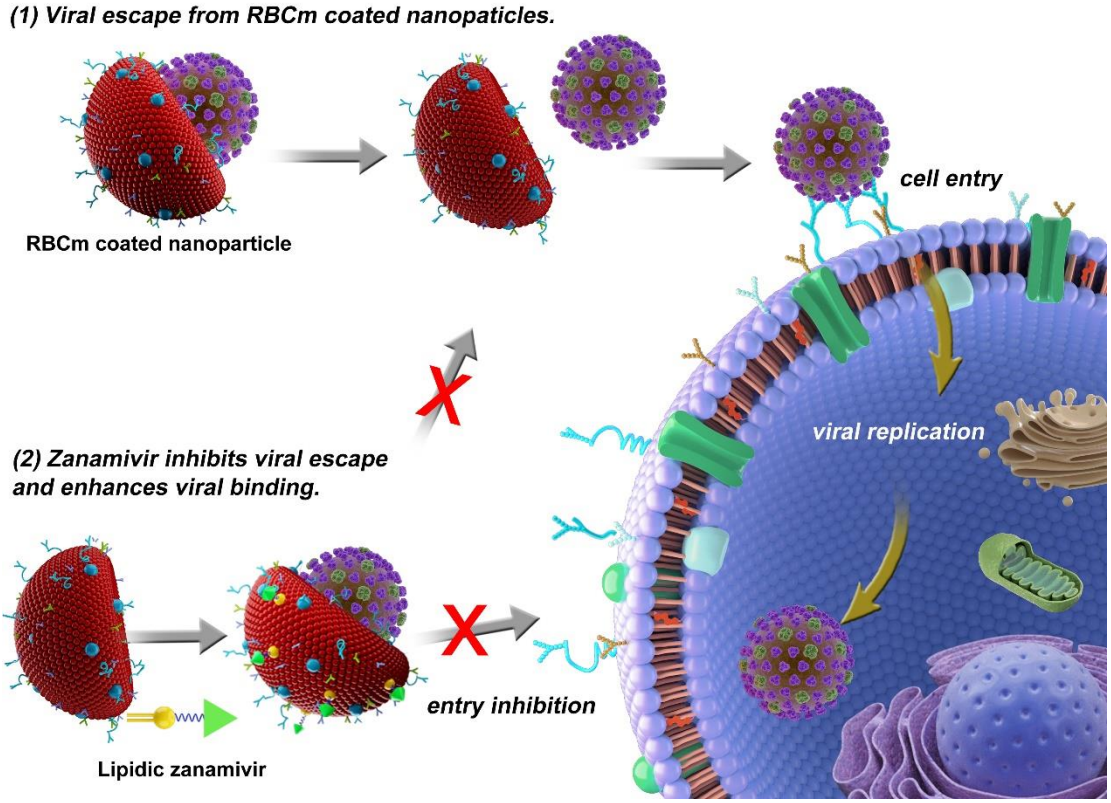

Chuanxiong Nie, Marlena Stadtmüller, Badri Parshad, Matthias Wallert, Yannic Kerkhoff, Sumati Bhatia, Stephan Block, Chong Cheng, Thorsten Wolff, Rainer Haag

Sci. Adv., **2020**, Accepted.

Author contribution:

Chuanxiong Nie synthesized the materials, performed the experiment, and wrote the manuscript.

Marlena Stadtmüller supported the virology experiment.

Badri Parshad and Sumati Bhatia supported the synthesis of the materials.

Matthias Wallert and Yannic Kerkhoff supported the analysis of the results.

Stephan Block, Chong Cheng, Thorsten Wolff, and Rainer Haag supervised the project and edited the manuscript.

Heteromultivalent topology-matched nanostructures as potent and broad-spectrum influenza A virus inhibitors

Chuanxiong Nie[1,2], Marlena Stadtmüller[2], Badri Parshad[1,3], Matthias Wallert[1], Vahid Ahmadi,[1] Yannic Kerkhoff[1], Sumati Bhatia[1], Stephan Block[1,*] Chong Cheng[1,4]*, Thorsten Wolff[2,*], Rainer Haag[1,*]

[1] Institut für Chemie und Biochemie Organische Chemie, Freie Universität Berlin, Takustr. 3, 14195 Berlin, Germany
[2] Unit 17, Influenza and Other Respiratory Viruses, Robert Koch-Institut, Seestr. 10, 13353 Berlin, Germany
[3] Department of Chemical Engineering and Biotechnology, University of Cambridge, Cambridge CB3 0AS, UK
[4] College of Polymer Science and Engineering, State Key Laboratory of Polymer Materials Engineering, West China Hospital, Sichuan University, Chengdu, 610065, China

* Corresponding authors.
E-mail addresses: stephan.block@fu-berlin.de (S. Block), chong.cheng@scu.edu.cn (C. Cheng), WolffT@rki.de (T. Wolff), haag@zedat.fu-berlin.de (R. Haag).

Abstract. Herein, we report the topology-matched design of heteromultivalent nanostructures as potent and broad-spectrum virus entry inhibitors based on the host cell membrane, which can be easily achieved. Initially, we investigate the virus binding dynamics to validate the better binding performance of the heteromultivalent moieties as compared to homomultivalent ones. Next, the heteromultivalent binding moieties are transferred to nanostructures with a bowl-like shape matching the viral spherical-surface. Unlike the conventional homomultivalent-inhibitors, the heteromultivalent ones exhibit an IC50 of 32.4 ± 13.7 μg/mL due to the synergistic multivalent effects and the topology-matched shape. At a dose without causing cellular toxicity, >99.99% reduction of virus propagation has been achieved. By this strategy, the efforts of developing virus inhibitors can be significantly improved. Since that multiple binding sites (receptor binding domain, furin cleaverage site, fusion domain etc.) have also been identified on the S-protein of SARS-CoV-2, we envision that the use of heteromultivalent nanostructures may also be applied to develop a potent inhibitor to prevent coronavirus infection.

INTRODUCTION.

The fast development of broad-spectrum solutions to prevent and inhibit viral infections is of great societal need. COVID19, which is caused by severe acute respiratory syndrome coronavirus 2 (SARS-CoV-2), has become a global health problem with tens of millions of infections and hundreds of thousands of fatalities by now.(*1, 2*) Besides coronaviruses, influenza A virus (IAV) is also a highly infectious pathogen circulating in human beings and many other kinds of animal species.(*3, 4*) Due to a high error rate of the viral RNA polymerase, human IAV evolution is accompanied by unpredictable antigenic drift and may involve the acquisition of mutations conferring resistance to many current

antivirals.(*5, 6*) Therefore, methods to develop potent and broad-spectrum viral inhibitors to fast respond to the unexpected outbreak are urgently required.(*7, 8*)

The viral infection cycle starts with the binding to the receptors on the host cell. Blocking the viral entry via a binding decoy has been proved to be effective for many types of viruses, e. g. the use of multivalent mannose structures is reported to be effective for inhibiting Ebola virus infection, which is one of few options to fight with Ebola infection.(*9-12*) For IAV, two glycoproteins have been identified to be associated with the binding behavior on the cellular membrane, hemagglutinin (HA) and neuraminidase (NA). The multivalent binding between the HA and sialic acid on the host cell triggers the viral entry. Therefore, polysialylated structures with synthetic scaffolds have been designed for IAV inhibition.(*13-15*) However, as the HA binding pockets vary in different IAV strains, developing broad-spectrum IAV inhibitors become a challenge. Inter-trimer targeting of IAV can hardly be achieved with synthetic polysialyated structures. To this point, the cellular membrane-based materials may accomplish. The cellular membrane is a highly stable self-assembled structure with a native display of virus binding receptors. In principle, the native cell membrane can be a robust IAV binder as it has the native, dynamic, and multivalent sialic acid display for the binding of various IAVs. Moreover, the extraction of the cellular membrane is easier than synthesizing multivalent nanostructures matching the sialic acid binding pockets on HA.

For the viral binding at the cell membrane, NA can cleave sialic acid from attached host cell surface factors for the release of progeny virions. As a result of the HA-NA interplay, the interactions between IAV virus and host cells are transient and need to be dynamically balanced during early and late time-points of infection, respectively.(*16, 17*) Therefore, for the potent inhibition of both HA and NA, the heteromultivalent nanostructures are required to block both proteins. This is, however, rarely achieved, as most of the current antiviral strategies rely on homomultivalent engagement of HA.(*13, 14, 18*) Herein, we aim for generating a highly potent IAV inhibitor by combining three different bioinspired design incentives: (*i*) coating the inhibitor surface with a cell-derived membrane that serves as a native source of sialic acids (Fig. 1a), (*ii*) complementing the cell-derived membrane with zanamivir (Zan), an approved NA inhibitor, that enhance the IAV-membrane interaction by heteromultivalent binding (Fig. 1b), and (*iii*) employing a concave inhibitor topology-matched shape that further enhances the IAV-membrane interaction by maximizing the total interaction area (Fig. 1c).

RESULTS.

RBCm as a potent binder but not inhibitor towards IAV.

As most of the human IAV strains bind to red blood cells actively, we firstly investigated if membranes extracted from red blood cellss are efficient IAV binder. Vesicles made of red blood cell membranes (RBCm) are obtained by disrupting human red blood cells and centrifugation, and the obtained RBCm vesicles have the same protein presentation to the red blood cells (Fig. S1, Supplementary Materials). The binding between RBCm and IAVs is investigated by an assay based on total internal reflection fluorescence (TIRF) microscopy (Fig. 1d).(*19*) The ganglioside GD1a-containing supported lipid bilayer (SLB) is created at a glass interface, and TIRF microscopy is used

to monitor the transient binding of IAVs to this SLB. Subsequent application of single-virus tracking allows for extracting various information about the multivalent IAV-sialic acid interaction, such as the rate of IAV attachment to the sialic acid-containing SLB, and IAV mobility and off-rate distributions.(*19*)

A decrease in the IAV attachment rate for increasing RBCm vesicle concentration is observed, indicating that RBCm vesicle can bind with IAV and block its interaction with GD1a SLB. The IC50 value from this measurement is 2.9 ± 1.2 μg/mL. From the hemagglutination inhibition assays of A/X31 (H3N2), A/PR/8/34 (H1H1), A/Panama/2007/1999 (H3N2), and A/Bayern/63/2009 (H1N1pdm), the broad-spectrum IAV binding ability of the RBCm vesicles is confirmed with a binding constant (Ki_{HAI}) in the nanomolar range (Table 1). The cellular infection assay, where the MDCK-II cells, a host cell for IAV infection, are infected by influenza A/X31 (H3N2) in the presence of 100 μg/mL RBCm vesicles, revealed the broad-spectrum inhibition potential of the RBCm vesicles. However, the inhibitory activity of RBCm vesicle is not ideal; only a small decrease in infected cells is noticed, as shown in Fig. 1e. The reduction of virus titre for RBCm vesicle is two orders of magnitudes (Fig. 1f).

It should also be noted that even RBCm is quite similar as the membrane of MDCK-II cells, the sialic acids, especially the underlying glycan structures, differ from each other. The membrane of MDCK-II cells is obtained and its binding with influenza A/X31 (H3N2) is studied via hemagglutination inhibition assays.(*20, 21*) MDCK-II cell membrane exhibits a Ki_{HAI} of 1.6 ± 0.5 nM, which is lower than RBCm in the same assay (8.4 ± 4.2 nM). As a binding decoy, the binding to the inhibitor should outperform the binding to the actual receptor to achieve potent inhibition.(*22*) When applying RBCm to MDCK-II cells, the virions may still bind to the actual sialic acid receptor on MDCK-II cells due to the higher binding affinity and then start the infection cycle. Therefore, to develop a potent IAV inhibitor with RBCm, the virus binding ability must be further improved.

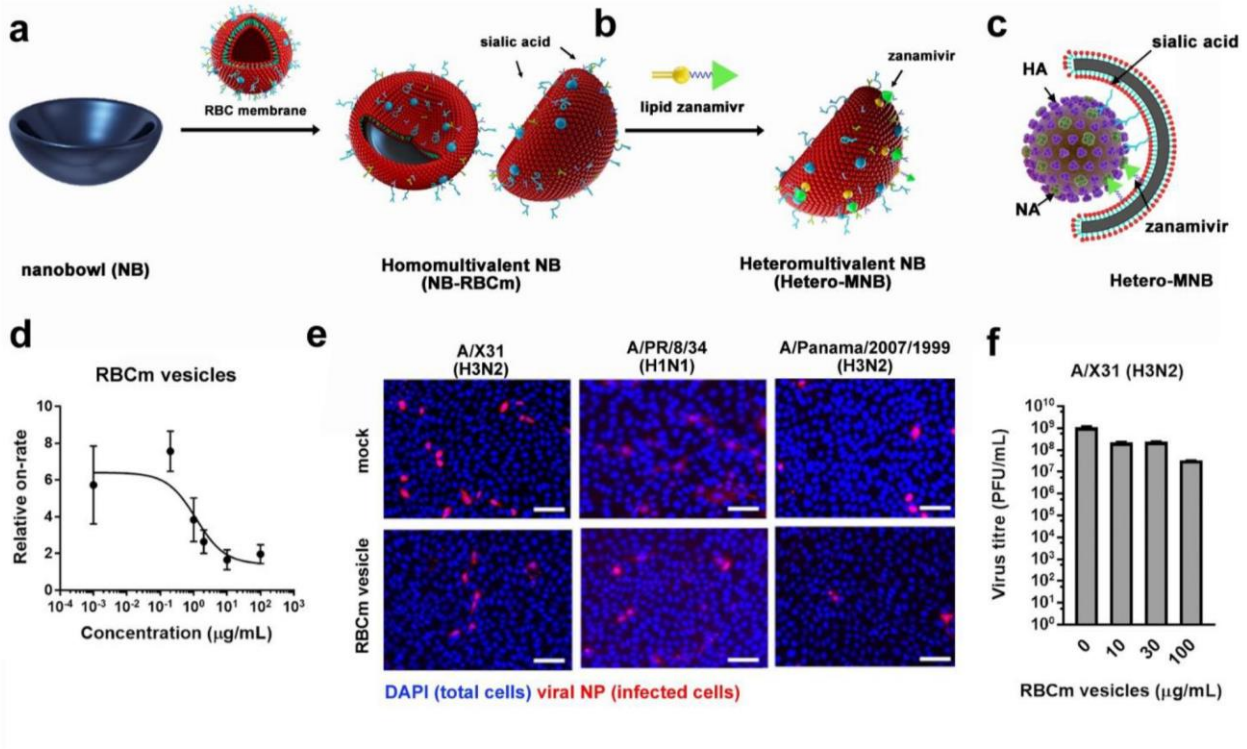

Fig. 1. (a, b) Design and synthesis of a heteromultivalent nanobowl (Hetero-MNB) for influenza A virus (IAV) inhibition, including the coating of RBCm onto the nanbowl surface and the further modification with lipidic zanamivir. (c) Proposed binding patterns between IAV and the Hetero-MNB, whereas sialic acid and zanamivir bind to HA and NA, respectively, and the bowl-shape with facilitating the capping to the surface of the virus particle. (d) Inhibition curves for RBCm vesicles at different concentrations from a TIRF setup. Values are expressed as mean ±SD, n=4. (e) Typical immuno-fluorescent staining images of viral nucleoprotein (NP) to show the infected cells with the treatment of RBCm vesicles. Scale bar: 50 μm. Multiplicity of infection: 0.1. (f) Propagation of IAV in the presence of RBCm vesicles. Values are expressed as mean ±SD, n=4.

Table 1. The binding constant of RBCm vesicles of different IAV strains from hemagglutination inhibition assay. Values are expressed as mean ±SD, n=4.

	KiHAI (μg/mL)	**KiHAI (nM sialic acid)**
A/X31 (H3N2)	41.6 ± 20.6	8.4 ± 4.2
A/PR/8/34 (H1N1)	23.4 ± 9.0	4.8 ± 1.8
A/Panama/2007/1999 (H3N2)	27.3 ± 7.8	5.5 ± 1.7

Heteromultivalent surface for enhanced virus binding.

Two concepts are introduced for improving the virus binding ability of RBCm: ***(1)*** additional NA inhibitors to further promote the viral binding to the RBCm, and ***(2)*** transferring the RBCm to a nanoparticle surface with matched topology to the IAV virion to maximize the interaction area (Fig. 1b and 1c). In order to prove the first concept that heteromultivalent targeting of both HA and NA on IAV can further promote virus binding, hybrid vesicles of RBCm with an approved NA inhibitor, zanamivir (Zan), are obtained. Zanamivir is firstly functionalized with lipid structure and then formed

into a lipid vesicle (Fig. S2-S3, Supplementary Materials). The hybrid RBCm-Zan vesicle is obtained via co-sonication. The binding of IAV virions for the vesicles is checked by hemagglutination inhibition assays (Table 2). The addition of free zanamivir decreases Ki_{HAI} value for RBCm vesicles, indicating that inhibiting NA can improve the virion binding, due to the inhibition of HA-sialic acid cleavage. The NA activity for RBCm-Zan treated virions is similar to those treated by 'RBCm + Free Zan' (Fig. S4, Supplementary Materials), but a lower Ki_{HAI} value is noticed. This means besides the NA inhibitory activity, and zanamivir may also provide an additional binding for the virion and RBCm vesicle, which is analyzed in detail via TIRF microscopy.

The TIRF-based assay is now operated using SLBs which have been fused with RBCm vesicles, Zan-conjugated lipids, or a mixture of both, allowing to determine changes in the IAV binding dynamics that are caused by the presence of different glycostructures (RBCm-originating sialic acid, Zan-conjugated lipids, or a combination of both; Fig. 2). In this analysis, RBCm vesicles are fused with POPC-based vesicles, allowing to form "hybrid" SLBs containing RBCm material and serving as a homomultivalent inhibitor.(*23*) A heteromultivalent SLB membrane is generated by incorporating lipidic Zan in the RBCm hybrid SLB (RBCm-Zan).

Application of the TIRF assay indicates that the rate of IAV attachment to the heteromultivalent surface of RBCm-Zan shows 3-fold higher values with respect to the Zan- or RCBm-SLB (Fig. 2b). Furthermore, single-virus tracking also provides information about the motion of IAV while being SLB-bound. On RBCm-SLBs, most of the mobile tracks are very short, indicating that the viruses stay at the surface for less than 1 s before being released (Fig. 2c, Fig. S5a, and Video S1, Supplementary Materials). This behavior is qualitatively similar to IAVs interacting with GD1a-containing SLBs.(*19*) The addition of Zan-conjugated lipids, however, strongly increases the duration of the mobile population, which now exhibits very long tracks, and thus the IAV residence time being much larger than 1 s (Fig. 2c, Fig. S5b and Video S2, Supplementary Materials). This behaviour is observed for both membranes, the homomultivalent Zan-SLBs and the heteromultivalent RBCm-Zan-SLB. Hence, while IAVs show only short residence times to sialic acid-containing SLBs, the NA-Zan interaction generates very large IAV residence times to Zan-containing SLBs. These findings are in line with the observation that the binding between Zan with NA is predominant to the binding between sialic acid and IAV,(*24*) and with the concept that the inhibitory effect of Zan on NA plays a beneficial role for the permanent binding, as NA is able to cleave the binding between HA and sialic acid as sialidase. Hence, while a notable fraction of IAVs exhibit only short residence times to sialic acid-containing SLBs and can, therefore, bind to a small number of sialic acids, the addition of lipid-Zan strongly extends the IAV residence time by the formation of NA-Zan interactions. In the heteromultivalent SLB, this behavior keeps the IAVs sufficiently long at the membrane to allow for binding a large number of sialic acids, thereby promoting the IAV attachment rate and IAV entrapment by the membrane. Thus, the heteromultivalent membrane provide a much better binding compared to homomultivalent ones.

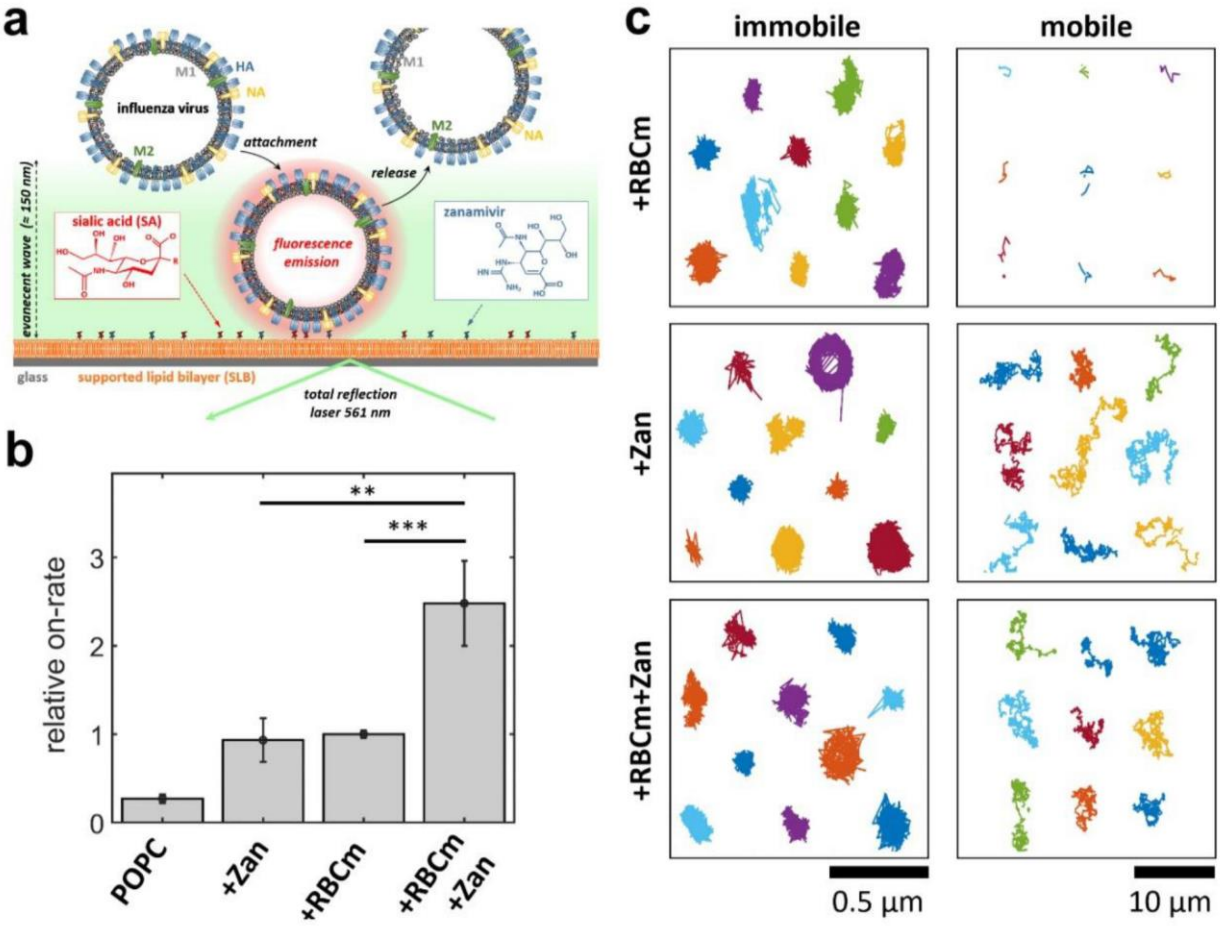

Fig. 2. (a) TIRF-based assay for assessing the interaction of IAVs with homo- or heteromultivalent membranes. The corresponding glycostructures (either sialic acids or lipid-conjugated zanamivir) are incorporated in a supported lipid bilayer (SLB) and the IAV-SLB interaction is recorded using TIRF microscopy. Application of single-virus tracking allows for extracting changes of (b) the rate of IAV attachment to the membranes and (c) the motion of SLB-bound IAVs, when employing the different homo- and heteromultivalent structures. Each color represents the track of a single virion. Values in (e) are expressed as mean ± SEM, n=10. **p<0.01, ***p < 0.001 by Student t-test. Note the different scale bars used for the immobile and mobile IAVs in (c).

Table 2. The binding constant of samples against A/X31 (H3N2) from hemagglutination inhibition assay. Values are expressed as mean ±SD, n=4.

	Ki_{HAI} (µg/mL)	**Ki_{HAI} (nM sialic acid)**
RBCm	41.6 ± 20.6	8.4 ± 4.2
MDCK-II membrane	6.8 ± 1.9	1.6 ± 0.5
RBCm vesicles + free Zan	11.7 ± 4.5	2.4 ± 0.9
RBCm-Zan hybrid vesicles	5.9 ± 2.3	1.2 ± 0.5
NB-RBCm	51.9 ± 23.8	3.1 ± 1.4
NB-RBCm + Zan	19.5 ± 7.8	1.2 ± 0.5
Hetero-MNB	13.7 ± 3.9	0.8 ± 0.2

Nanobowl with a matched surface towards IAV virion for virus binding.

In order to prove the second concept that matching topology can benefit the virus binding, bioinert and biostable nanoparticles with sphere (nanosphere, NS) and bowl-like (nanobowl, NB) morphologies are synthesized, as shown in Fig. 3a and Fig. S6-S7, Supplementary Materials.(*25*) The nanoparticle is homomultivalently coated with RBCm (Fig. S8-S9, Supplementary Materials), named as NS-RBCm and NB-RBCm, respectively. The coating is carried out via co-sonicating RBCm vesicle with NS and NB.(*26, 27*) Cellular membrane is a highly dynamic lipid system with the ability to deform and adapt to the surrounding environment. In the coating process, the high-power sonication drives the membrane vesicle to follow the curvature of nanobowl. After the sonication, the membrane is stabilized on the surface of nanoparticle via hydrophobic interactions. Finally, free membrane vesicles are removed by centrifugation.

The IAV virion is a nano-sized sphere around 100 nm in diameter, and in our synthesis, a nanobowl with a concave structure around 120 nm is selected as it matches the size of the IAV virus to benefit multivalent interactions (Fig. 3a). The binding for the NS-RBCm and NB-RBCm is studied by a prophylactic infective assay (Fig. S10, Supplementary Materials). Less infected cells and higher cell viability are noticed for NB-RBCm than those for NS-RBCm. The IC50 for NB-RBCm is about 4 times lower than that of NS-RBCm, as shown in Fig. 3b. The better inhibition by the NB-RBCm should be attributed to its matched shape to the IAV virion, which can promote the binding of the virus, as proved by our binding test in Fig. S11, Supplementary Materials.

Geometry analysis of the virus binding to NS-RBCm and NB-RBCm is performed with the model of a convex virion binding to convex or concave inhibitor, respectively, as shown in Fig. 3c. The IAV virion is illustrated as a particle around 100 nm. The steric shielding by the inhibitor is estimated by placing new inhibitors with the same curvature, which are marked with dashed lines.(*28*) The actual contact between the virion and inhibitor is marked white with an angle of Θ_1, while the steric shielding by the inhibitor is marked purple with an angel of Θ_2. In these two cases, the actual contact area is quite similar, but the steric shielding is different. Concave inhibitor creates a much larger steric shielding than a convex inhibitor; therefore, it shows better virus inhibition than the convex one. Another difference between them is the edge distance. The concave inhibitor is much closer to the virion than the convex one. Monovalent sialic acid-HA interaction is weak with a dissociation constant of 1-20 mM.(*17, 29*) When binding to a surface, e. g. cellular membrane, the virion remains mobile in the begining. This is what we have observed from TIRF that IAV virions remain mobile when binding to RBCm. The virion is transiently interacting with RBCm and then stabilize on the surface via multivalent interactions. Many other studies also reported that influenza virions are mobile when binding at the biological interfaces.(*17, 30-32*) Therefore, we presume that in the case of convex inhibitor (NS), a virion could be released by crawling and gliding, especially that NA is constantly cleaving the sialic acid-HA interaction. For a concave inhibitor (NB), the small edge distance enables a virion to recruit binding ligands more easily for multivalent interaction and then stabilize.

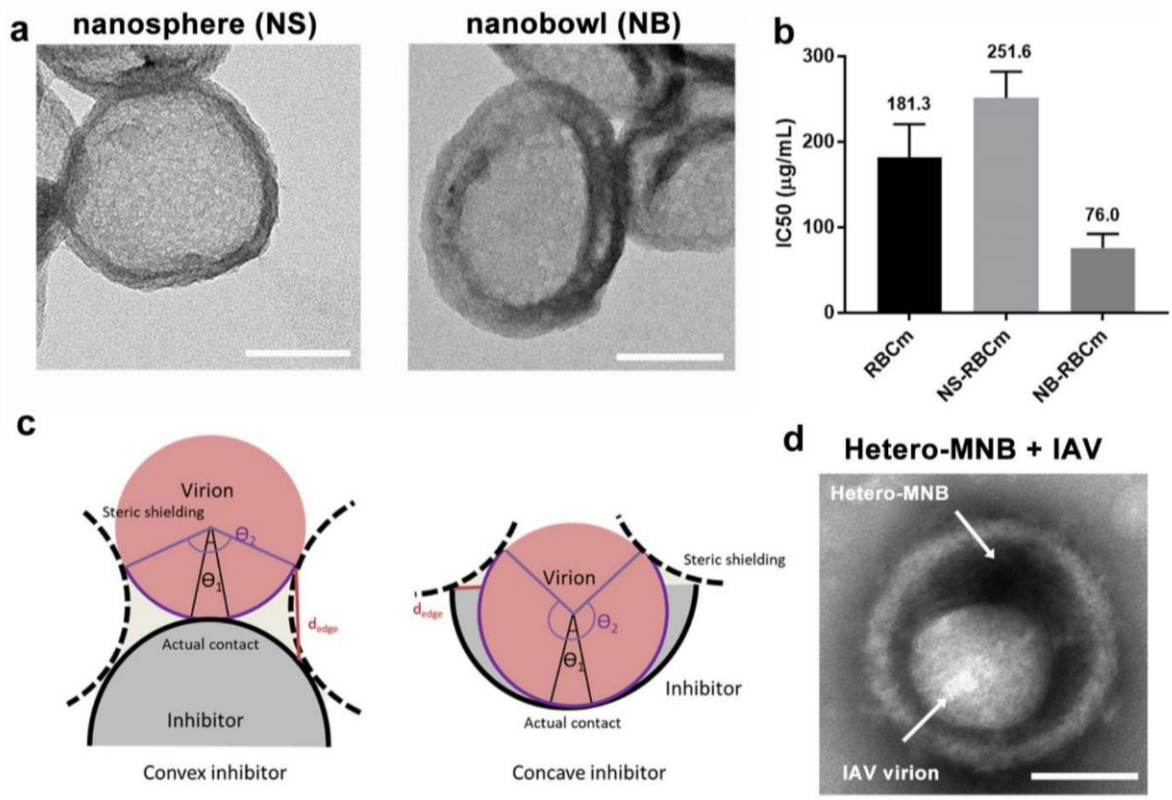

Fig. 3. (a) HR-TEM images for the nanosphere (NS) and nanobowl (NB) with RBCm coating, respectively. Scale bar: 50 nm. (b) IC50 values for the homomultivalent NS-RBCm and NB-RBCm. Values are expressed as mean ± SD, n=4. (c) Geometry analysis for a virion binding to a convex inhibitor and concave inhibitor. The actual contact between them is marked with Θ_1; the steric shielding by the inhibitor is marked with purple lines with Θ_2. Steric shielding is estimated by placing new inhibitors with the same curvature. (d) Negatively stained HR-TEM image for the IAV particle binding with the Hetero-MNB. Scale bar: 50 nm. Images for other samples are shown in Fig. S11, Supplementary Materials.

Heteromultivalent nanobowl as a potent and broad-spectrum IAV inhibitor.

Finally, concepts *(1)* and *(2)* are combined into a heteromultivalent nanobowl (Hetero-MNB) for the *in vitro* viral inhibition studies, which is obtained by inserting the lipid-Zan to NB-RBCm. The negatively stained HR-TEM images in Fig. 3c reveal the binding between IAV virion and Hetero-MNB. The hemagglutination inhibition assay (Table 2) reveals that the Hetero-MNB is more predominant than NB-RBCm for viral binding. As a result of heteromultivalent inhibition of HA and NA, the IAV virion binding to MDCK-II cells is significantly inhibited as shown in Fig. 4a-c. Little-to-none virus particles are detected on the surface of MDCK-II cells by flow cytometry and fluorescence microscopy, indicating the entry of virus is effectively blocked by the inhibitors.

Next, we investigate whether the Hetero-MNB is able to inhibit the virus infection at the entry step by counting cells expressing IAV nucleoprotein (NP) (Fig. 4d-e, and Fig. S12-S13, Supplementary Materials). The treatment of NB-RBCm and Hetero-MNB reduces the infectivity of A/X31 (H3N2) significantly, and Hetero-MNB shows better inhibitory effects than NB-RBCm. We have tested the

inhibition towards 4 typical human IAV strains (A/X31 (H3N2), A/PR/8/34 (H1N1), A/Panama/2007/1999 (H3N2), and A/Bayern/63/2009 (H1N1pdm)). The Hetero-MNB shows broad-spectrum inhibition as little to none infected cells are observed in these four tests. The cell viability test further verifies the inhibitory effects of Hetero-MNB (Fig. 4e), whereas the cells are more viable after the treatment by Hetero-MNB. Herein, Hetero-MNB reveals an IC50 value of 32.4 ± 13.7 μg/mL. It should be noted that Hetero-MNB shows no clear toxicity in MDCK-II cells (Fig. S14, Supplementary Materials). The CC50 value is 2.4 ± 0.5 mg/mL, corresponding to a selective index of 74.07.

In addition to the cellular infections, the ability to reducing viral propagation is also studied by plaque assay for the samples, as shown in Fig. 4g. In this test, to investigate if they can be used as a therapeutic agent, the inhibitors are used after the cells have been infected by the viruses. Both the NB-RBCm and Hetero-MNB reduced viral titres. Hetero-MNB outperforms the homomultivalent ones with 4 orders of magnitude of reduction, which corresponds to inhibitory effects higher than 99.99%. Fig. 4h further illustrates that the Hetero-MNB is active against the typical IAV strains circulating in humans, revealing its potential to be a broad-spectrum IAV inhibitor.

IAV mutation with zanamivir resistance has been noticed recently.(*33, 34*) We also tested hetero-MNB for the inhibition of a zanamivir resisting strain (influenza A/BLN/28/2012) via cellular infection assays (Fig. S15, Supplementary Materials).(*35*) Hetero-MNB can inhibit viral replication with two orders of magnitudes reduction of virus titre. However, in this case, because NA has mutated, NB-Zan does not show any inhibitory effects; Hetero-MNB and NB-RBCm shows similar activities. Considering the inhibitory effects of RBCm, it is also believed that NB-RBCm and Hetero-MNB can be one possible solution to inhibit zanamivir resisting IAV strains.

The inhibitory activity of RBCm-based structures might be lower than the rationally designed polysialylated structures,(*14, 15, 36*) but compared with their complicated synthetic process and high costs, the approach in this study is much simpler, sparing the efforts of preparing and screening a big library of candidate compounds. If a significant alternation of sialic acid binding sites occurs, the synthetic polysialylated structures may lose the activity. The easy preparation of RBCm-based inhibitors makes it a good candidate to prepare for such a case. Even if IAV mutates to not bind RBC anymore, we still have the option of taking the membrane from its host cells, e. g. A549 cells and MDCK-II cells, for inhibitor development. It should be noted that the extraction of A549 and MDCK-II cells membrane takes more efforts and needs further optimization for large-scale production. The idea of cell membrane-based inhibitors can also be used in other viral strains, especially for the outbreak of a novel virus.

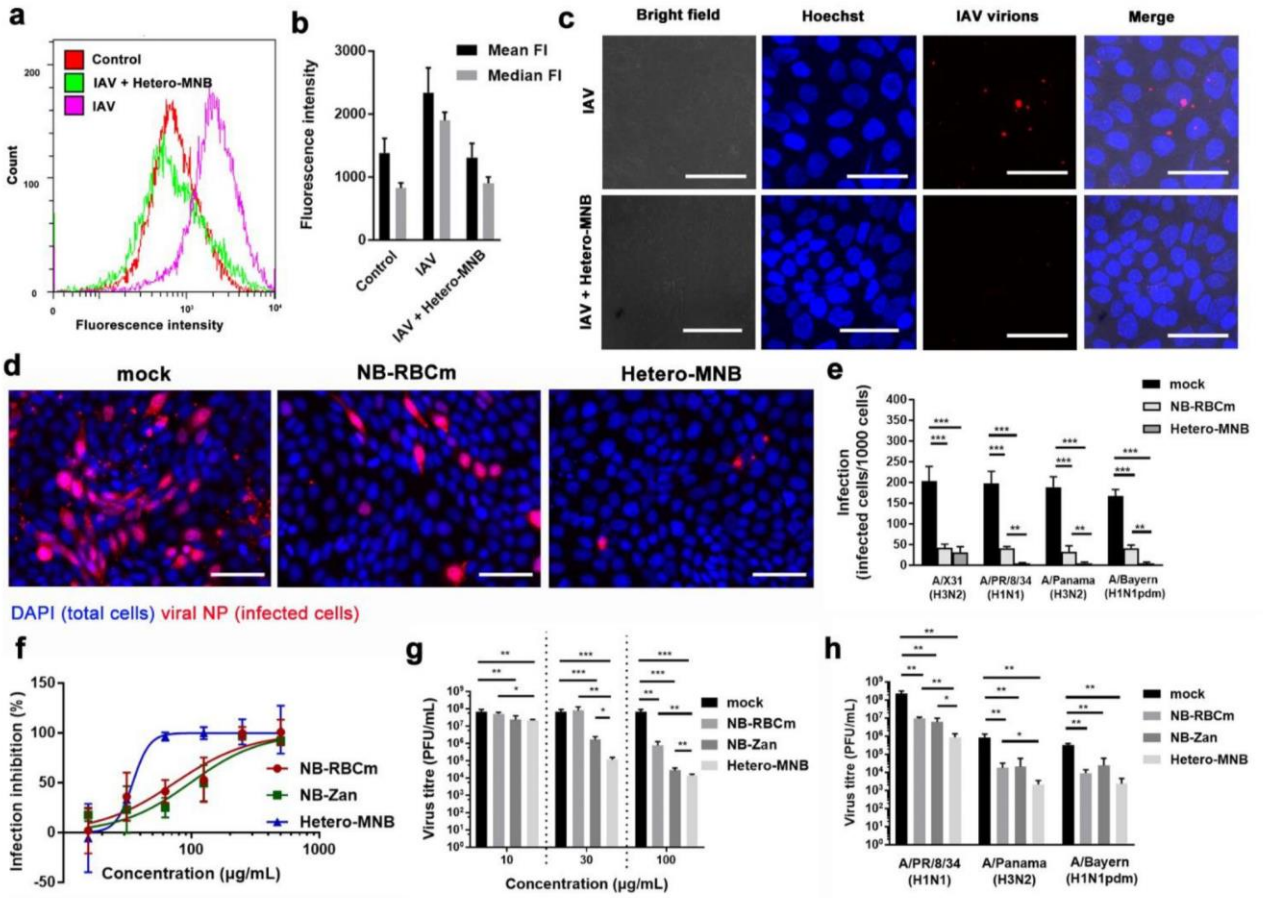

Fig. 4. (a) Flow cytometry for the virus attachment to MDCK-II cells and (b) corresponding mean and median fluorescence intensities (FI) for the samples. The error bars are generated by the CytExpert Acquisition and Analysis Software Version 2.3. (c) Projection CLSM images for the viral attachment to MDCK-II cells in the presence of Hetero-MNB. Scale bar: 20 μm. (d) Typical immune-fluorescence images to show the IAV (A/X31 (H3N2)) infection in the presence of the inhibitors. Other images are shown in Fig. S12-S13, Supplementary Materials. Scale bar: 100 μm. (e) Detection of viral nucleoprotein in cells infected with four typical human IAV strains, including A/X31 (H3N2), A/PR/8/34 (H1N1), A/Panama/2007/1999 (H3N2), A/Bayern/63/2009 (H1N1pdm) in the presence or absence of inhibitors. (f) The inhibition of A/X31 (H3N2) of the inhibitors at different dosages revealed by cell viability. (g) Inhibition towards IAV propagation (A/X31 (H3N2)) for the inhibitors. (h) Inhibition towards IAV propagation for the inhibitors against three other IAV strains, including A/PR/8/34 (H1N1), A/Panama/2007/1999 (H3N2), A/Bayern/63/2009 (H1N1pdm). The inhibitors are used after the first cycle of infection. Inhibitor dosage: 100 μg/mL. Values are expressed as mean ± SD, n=4. *p< 0.05, **p<0.01, ***p<0.001 by Student t-test, respectively.

CONCLUSIONS.

The development of heteromultivalent RBCm inhibitors with a topology-matched design is believed to expand the toolbox for fighting the pathogens as alternatives for the rapidly emerging resistance to the current drugs and therapies. In our study, the combination of the specific binding

capabilities of sialic acid and Zan provide a unique heteromultivalent dynamic viral binding decoy to achieve potent interactions with IAV, which is much better than the conventional homomultivalent ones. When coated onto a fitting bowl-shaped nanostructure, the heteromultivalent membrane exhibits 99.99% viral inhibition due to the synergistic multivalent effects and topology-matched shape at a dose causing no cellular toxicity. The IC50 value is 32.4 ± 13.7 μg/mL (1.8 ± 0.8 nM sialic acid) with a selective index of 74.07. We also proved that Hetero-MNB could serve as a broad-spectrum binding decoy and entry inhibitors for human IAV strains. Furthermore, this unique strategy using bioinspired heteromultivalent topology-matching nanostructures is a general approach to fabricate broad virus inhibitors and might compete with new or mutated viruses better than specifically designed drugs. Recent studies have pointed out the *in vivo* safety of RBCm coated nanoparticles, of which the intravenous injection does not induce any adverse effects in mice.(*26, 37*) They have been used for the development of *in vivo* drug delivery vehicle, toxin absorber, and vaccine platform.(*37-39*) The potential antigenicity of a foreign cell membrane can be addressed by taking the RBCs from the host. The protocol for membrane extraction is simple and can be finished within one day. Therefore, it is believed that cell membranes can serve as a promising platform to develop virus inhibitors.

There are many similarities between SARS-CoV-2 and IAV, not only in disease symptoms but also in the infection cycles. SARS-CoV-2 uses its spike protein (S-protein) to interact with the angiotensin-converting enzyme 2 (ACE2) on host cells' surface to mediate cellular entry. Structural analysis of S-protein has revealed several binding sites for potential inhibitor design.(*40, 41*) On the head of S protein (S1 domain) locates the receptor-binding domain (RBD) that interacts with ACE2. The stalk domain (S2 domain) contains a fusion peptide that triggers the virus fusion with host cells to release the viral genome for replication. A furin cleavage site is identified at the S1/S2 region, the cleavage by furin or TMPRSS2 is necessary to activate RBD interaction with ACE2. It has also been revealed by a recent study that these domains can be targeted separately by non-competing antibodies. Antibodies cocktails showed significantly improved virus neutralization ability compared to monovalent antibodies.(*42, 43*) Taking together the information from this study, it is believed that the heteromultivalent display of ligands that target different domains on S-proteins can result in a potent SARS-CoV-2 inhibitor.(*44, 45*) The membrane of the host cells, e. g. Vero E6 cell, may be used as one target to the RBD.(*46*) For the design of such an inhibitor, the platform supporting the ligands should be rationally designed to facilitate multiple interactions with heteromultivalency.

Materials and methods.

Materials and Characterizations.

All chemicals and solvents are reagent or HPLC grade, used as received, and purchased from Sigma (Steinheim, Germany) unless stated otherwise. The deionized water used is purified using a Millipore water purification system with a minimum resistivity of 18.0 MΩ·cm. The human RBCs are obtained from Haema Blutspendezentrum, Berlin, Germany.

^{1}H NMR spectra are recorded on a Bruker Avance 3 operating at 400 MHz or 500 MHz, at concentrations of 100 mg·mL^{-1}. The chemical shifts are reported in δ (ppm) values and referenced for different solvents. The spectra of Matrix-Assisted Laser Desorption/Ionization Time-of-Flight Mass

Spectroscopy (MALDI-ToF MS) are recorded using a Bruker Ultra-flex III in the positive ion mode using a linear pathway (LP). Saturated Alpha-cyano-4-hydroxycinnamic acid in methanol is used as the matrix. The sample is prepared via the "dried-droplet method" by dropping 0.5 μL of a mixture of the matrix and the polymer solution (1:1). The mixture is placed on the target plate and allowed to air dry. Fourier transform infrared (FTIR) Spectra are obtained with Nicolet iS50, Thermofisher. Dynamic light scattering (DLS) measurements are performed using Malvern Zetasizer Nano ZS (Malvern Instruments GmbH, Herrenberg, Germany). All samples are measured at a constant scattering angle of 173° at 25 °C and freshly prepared just before measurement in DI water or PBS buffer (1 mM, pH 7.4). Ultrasonic bath (Model: SONOREX, RK255 HZ, made in Germany) is used to disperse materials in solvents. Scanning electron microscope (SEM): The morphology of the nanoparticle is observed by ultra-high-resolution FE-SEM (Hitachi S-4800). The samples are dried in the oven and then attached to the sample supports using carbon tape. All the samples are observed directly without gold coating. For the non-conductive substrates, the gold coating is deposited with about 1-2 nm. Fluorescence images are taken on ZEISS Axio Observer (Carl Zeiss Microscopy GmbH, Jena, Germany). Transmission electron microscopy (TEM): Droplets (~5 μL, ~ 0.02 mg/mL) of the sample solution are placed on ultrathin carbon film on copper grids (Ted Pella, Inc. USA), and the supernatant liquid is removed by blotting with a piece of filter paper. The grids are air-dried at least 40 min and are subsequently transferred into a TEM machine, Talos L120c transmission electron microscope (ThermoFisher Scientific, USA), and operated at 200 kV.

Viruses and cells.

MDCK-II (Madin-Darby canine kidney epithelial) cells are maintained in monolayer cultures in DMEM (supplemented with 10% fetal calf serum, 2 mM L-glutamine, 100 mg/ml streptomycin and 100 units/ ml penicillin) at 37°C and 5% CO_2. IAV strains, A/Panama/2007/1999 (H3N2), A/X31 (H3N2), A/PR/8/34 (H1N1), A/Bayern/63/2009 (H1N1) and A/BLN/28/2012 are taken from the strain collection of Unit 17 at the Robert Koch Institut (Berlin, Germany) and propagated in ten-day-old embryonated chicken eggs. The stock virus is quantitated by plaque titration on MDCK-II cells.

Extraction of RBC membrane (RBCm) and coating of RBCm onto the nanoparticle surface.

The RBCm is obtained by a hypotonic treatment and ultracentrifugation process. The human RBCs are firstly washed with PBS buffer (pH 7.4) at 4 °C for at least 4 times to remove the residual platelets and blood proteins and then treated overnight with DI water-diluted PBS buffer (0.25×) at 4 °C. The RBCm is collected by centrifugation at 10, 000 rpm for 5 min and then washed with PBS buffer extensively and then frozen at -20 °C for storage.

Extraction of MDCK-II cells membrane.

MDCK-II cells are cultured DMEM medium (supplemented with 10% fetal calf serum, 2 mM L-glutamine, 100 mg/ml streptomycin, and 100 units/ ml penicillin) at 37°C and 5% CO2). The cells are harvested by trypsin and collected by centrifugation at 1000 rpm for 5 min. The cells are washed 3 times with PBS and then placed in cold Tris buffer (pH = 7.4) containing 10 mM Tris, 10 mM $MgCl_2$, and 1×EDTA-free protease inhibitor. The cells are then disrupted by homogenizing with dounce homogenizer on ice. The solution is centrifuged at 5000 rpm for 5 min, the supernatant containing membrane vesicles is then centrifuged at 100,000 × g for 2 h (Optimal L-100XP, Beckman Coulter). The pellet is washed with PBS and centrifuged again at 100,000 × g for 2 h. The resuspended cell

membrane vesicles are extruded through 400 nm polycarbonate membranes (Millipore) and stored at -80°C.

Hemagglutination inhibition assay.

The samples are diluted in 25 uL PBS two-foldly in a U-shaped 96 well plate. 25μL IAV solution (in PBS, containing 4 HA unit) is mixed with the samples by pipetting and incubated for 30 min at room temperature. Afterward, 50 μL of 1% chicken red blood cells are added to each well and incubated for another 30 min at room temperature. The hemagglutination is observed by tilting the plates. The sample concentration of the last well-showing inhibition of hemagglutination is recorded the binding constant Ki_{HAI}.

Total internal reflection fluorescence (TIRF) microscopy.

TIRF microscopy is used to quantify the interaction of single, R18-labelled IAV with different glycostructures embedded in SLBs with different compositions as described.(*19*) The glycostructures originated from native RBCm vesicles, zanamivir-conjugated lipids, or both. This method provides information about various properties of the IAV-membrane interaction, such as the attachment rate to the membrane, IAV mobility, and off-rate distributions regarding the different membrane compositions. The conduction of measurements is shown in Supplementary Materials.

Synthesis of spherical and bowl-like nanoparticles.

First, the resorcinol-formaldehyde coated SiO_2 nanoparticle is synthesized via a one-step reaction according to an earlier report with slight modifications. Briefly, 2.5 mL ammonia aqueous solutions (30 wt.%) is added into 100 mL ethanol/water (v/v 2/1) and stirred for 1 h at room temperature. With vigorous stirring, 3 mL TEOS (19.2 mmol), 0.2 g resorcinol (4.5 mmol), and 0.7 mL formaldehyde solution (37 wt. % in H_2O, 9 mmol) are added sequentially. The reaction is ceased by 10-minute centrifugation at 10,000 rpm after 3 h, 6 h and 24 h, respectively. The final products are washed 5 times with water and collected by centrifugation at 10,000 rpm for 10 min and then lyophilized. The nanocomposites are carbonized at 600 °C, 700 °C, and 800 °C (5 °C/min) for 1 hour with argon, respectively. The SiO_2 core is then removed by etching in 2 M NaOH for 2 days at 60 °C, and different types of hollow nanocarbons, including the spherical and bowl-like nanoparticles, can be obtained by centrifugation at 10,000 rpm for 10 min and washed extensively by water. Afterward, the nanoparticles are carbonized again at 1100 °C (5 °C/min) for 1 hour with argon to fix the morphology.

Coating of RBCm onto the nanoparticle surface.

The RBCm is coated onto the nanoparticle surface with horn sonication (Sonopuls Ultrasonic Homogenizers HD 2200, BANDELIN electronic GmbH & Co. KG, Berlin, Germany) at 4 °C for 30min, and then the RBCm coated nanocarbons are isolated by centrifugation at 5,000 rpm for 5 min and washed for at least 4 times with PBS buffer. The morphology of the RBCm coated nanoparticles is studied by SEM and TEM. For a better view of RBCm, the sample is stained with 1% sodium phosphotungstate before the measurement. The protein content is studied by the Pierce BCA assay kit (23225, ThermoFisher, USA) according to manual instructions. The RBCm coating weight ratio is then estimated by the protein contents following the equation:

$$\text{Coating ratio (wt.\%)} = \frac{Protein\ content\ (RBCm\ coated\ nanoparticle)}{Protein\ content\ (RBCm)} \times 100\%$$

For SDS page, 10 μg of samples are loaded to 10% polyacrylamide (PAM) gel, and the gel is run

at 200 V for 1 h and then stained with 10% (v/v) Coomassie Blue solution and the imaged by ChemiDoc MP imaging system (Bio-Rad Laboratories GmbH, München, Germany). The sialic acid content for the RBCm coated nanocarbons is studied by Sialic Acid (NANA) Assay Kit (ab83375, Abcam, UK) according to the instructions by the provider.

Virus binding tests.

For the western blot test, 5 μL concentrated A/X31 (H3N2) virus solution (protein content: 0.72 mg/mL) is incubated with 15 μL 1 mg/mL solution with different nano-inhibitors for 45 min at 37 °C. Then, the mixture is centrifuged at 10, 000 rpm for 10 min to collect the virus bound nano-inhibitors. The precipitant is washed 3 times with PBS and loaded onto a 10% PAM gel. After running at 200 V for 1 h, the proteins are transferred onto the PVDF membrane, which is then blocked by 3 wt.% milk powder. The nucleoprotein is marked by influenza A NP monoclonal antibody (HYB 156-01-02, Invitrogen, USA) and HRP conjugated secondary antibody (G-21040, Invitrogen, USA). Then chemiluminescent detection is performed using Pierce™ ECL Western Blotting Substrate (32106, ThermoFisher Scientific, USA). The intensities of the bands are analyzed by ImageJ pro.

Virus attachment and inhibition.

To study virus attachment, 100 μL A/X31 (H3N2) solution (protein content: 0.73 mg/mL) is incubated with 10 μL 20 μM octadecyl rhodamine B chloride (R18, O246, ThermoFisher Scientific, USA) in PBS for 45 min firstly. The free R18 is removed by spinning column (3300 rpm, 2 min; Protein A HP SpinTrap™, GE Healthcare, Germany). Then, 10 μL labeled virus is incubated with a 90 μL nano-inhibitor solution (100 μg/mL) for 45 min at 37 °C. The mixture is then taken to incubate with MDCK-II cells for 1 h on ice. The unbound virus is removed by washing with PBS. The cell nucleus is stained with DAPI, and then the cells are visualized by fluorescence microscopy. For a quantitative analysis of virus attachment, the mixture of labeled virus and nano-inhibitor is incubated with 100,000 MDCK-II cells for 1 h, and then the unbounded virus is removed by centrifugation at 1500 rpm for 2 min. The cells are washed 3 times with PBS and then analyzed by flow cytometry (CytoFLEX S, Beckman Coulter GmbH, Krefeld, Germany).

For the infection inhibition test, 0.2×10^6 PFU of A/X31 (H3N2) virus is treated with the nano-inhibitors for 45min at 37 °C and then used to infect MDCK-II cells. After 45 min of infection, the cells are washed twice by PBS and cultured in DMEM medium (0.1% BSA, 1100 mg/ml streptomycin, and 100 units/ ml penicillin). After 24 h, the cells are washed with PBS, fixed with 4% formaldehyde, and permeabilized with 0.5% Triton X-100. The infected cells are marked by influenza A NP monoclonal antibody (HYB 156-01-02, Invitrogen, USA) and Alexa Fluor 594 coupled secondary antibody (A-11032, Invitrogen, USA). The cell nucleus is stained using DAPI. The infection is estimated by counting infected cells from at least 10,000 cells in total and expressed as the number of infected cells per 1,000 cells.

Multicyclic viral replication inhibition test.

MDCK-II cells are firstly infected with IAV at the MOI of 0.01 and cultured in infection medium (DMEM, 0.1% BSA, 1% L-glutamine, 1% Penicillin-Streptomycin, 1 μg/mL TPCK-Trypsin) containing the nano-inhibitors for 24 h. The virus in the supernatants are then titred by plaque assay on MDCK-II cells and are expressed as plaque-forming units per mL (PFU/mL).

References and notes.

References

1. C. Wang, P. W. Horby, F. G. Hayden, G. F. Gao, A novel coronavirus outbreak of global health concern. *The Lancet* **395**, 470-473 (2020).
2. N. Zhu, D. Zhang, W. Wang, X. Li, B. Yang, J. Song, X. Zhao, B. Huang, W. Shi, R. Lu, P. Niu, F. Zhan, X. Ma, D. Wang, W. Xu, G. Wu, G. F. Gao, W. Tan, A Novel Coronavirus from Patients with Pneumonia in China, 2019. *N. Engl. J. Med.* **382**, 727-733 (2020).
3. J. K. Taubenberger, D. M. Morens, The Pathology of Influenza Virus Infections. *Annu. Rev. Pathol.* **3**, 499-522 (2008).
4. W. W. Thompson, D. K. Shay, E. Weintraub, L. Brammer, C. B. Bridges, N. J. Cox, K. Fukuda, Influenza-Associated Hospitalizations in the United States. *JAMA* **292**, 1333-1340 (2004).
5. J. D. Bloom, L. I. Gong, D. Baltimore, Permissive Secondary Mutations Enable the Evolution of Influenza Oseltamivir Resistance. *Science* **328**, 1272-1275 (2010).
6. F. Carrat, A. Flahault, Influenza vaccine: The challenge of antigenic drift. *Vaccine* **25**, 6852-6862 (2007).
7. N. S. Laursen, R. H. E. Friesen, X. Zhu, M. Jongeneelen, S. Blokland, J. Vermond, A. van Eijgen, C. Tang, H. van Diepen, G. Obmolova, M. van der Neut Kolfschoten, D. Zuijdgeest, R. Straetemans, R. M. B. Hoffman, T. Nieusma, J. Pallesen, H. L. Turner, S. M. Bernard, A. B. Ward, J. Luo, L. L. M. Poon, A. P. Tretiakova, J. M. Wilson, M. P. Limberis, R. Vogels, B. Brandenburg, J. A. Kolkman, I. A. Wilson, Universal protection against influenza infection by a multidomain antibody to influenza hemagglutinin. *Science* **362**, 598-602 (2018).
8. M. J. P. van Dongen, R. U. Kadam, J. Juraszek, E. Lawson, B. Brandenburg, F. Schmitz, W. B. G. Schepens, B. Stoops, H. A. van Diepen, M. Jongeneelen, C. Tang, J. Vermond, A. van Eijgen-Obregoso Real, S. Blokland, D. Garg, W. Yu, W. Goutier, E. Lanckacker, J. M. Klap, D. C. G. Peeters, J. Wu, C. Buyck, T. H. M. Jonckers, D. Roymans, P. Roevens, R. Vogels, W. Koudstaal, R. H. E. Friesen, P. Raboisson, D. Dhanak, J. Goudsmit, I. A. Wilson, A small-molecule fusion inhibitor of influenza virus is orally active in mice. *Science* **363**, eaar6221 (2019).
9. A. Muñoz, D. Sigwalt, B. M. Illescas, J. Luczkowiak, L. Rodríguez-Pérez, I. Nierengarten, M. Holler, J.-S. Remy, K. Buffet, S. P. Vincent, J. Rojo, R. Delgado, J.-F. Nierengarten, N. Martín, Synthesis of giant globular multivalent glycofullerenes as potent inhibitors in a model of Ebola virus infection. *Nat. Chem.* **8**, 50-57 (2016).
10. J. Ramos-Soriano, J. J. Reina, B. M. Illescas, N. de la Cruz, L. Rodríguez-Pérez, F. Lasala, J. Rojo, R. Delgado, N. Martín, Synthesis of Highly Efficient Multivalent Disaccharide/[60]Fullerene Nanoballs for Emergent Viruses. *J. Am. Chem. Soc.* **141**, 15403-15412 (2019).
11. L. Rodríguez-Pérez, J. Ramos-Soriano, A. Pérez-Sánchez, B. M. Illescas, A. Muñoz, J. Luczkowiak, F. Lasala, J. Rojo, R. Delgado, N. Martín, Nanocarbon-Based Glycoconjugates as Multivalent Inhibitors of Ebola Virus Infection. *J. Am. Chem. Soc.* **140**, 9891-9898 (2018).
12. B. M. Illescas, J. Rojo, R. Delgado, N. Martín, Multivalent Glycosylated Nanostructures To Inhibit Ebola Virus Infection. *J. Am. Chem. Soc.* **139**, 6018-6025 (2017).
13. S.-J. Kwon, D. H. Na, J. H. Kwak, M. Douaisi, F. Zhang, E. J. Park, J.-H. Park, H. Youn, C.-S. Song, R. S. Kane, J. S. Dordick, K. B. Lee, R. J. Linhardt, Nanostructured glycan architecture is important in the inhibition of influenza A virus infection. *Nat. Nanotech.* **12**, 48 (2016).
14. S. Bhatia, D. Lauster, M. Bardua, K. Ludwig, S. Angioletti-Uberti, N. Popp, U. Hoffmann, F. Paulus, M. Budt, M. Stadtmüller, T. Wolff, A. Hamann, C. Böttcher, A. Herrmann, R. Haag, Linear polysialoside outperforms dendritic analogs for inhibition of influenza virus infection in vitro and in vivo. *Biomaterials* **138**, 22-34 (2017).
15. D. Lauster, S. Klenk, K. Ludwig, S. Nojoumi, S. Behren, L. Adam, M. Stadtmüller, S. Saenger, S. Zimmler, K. Hönzke, L. Yao, U. Hoffmann, M. Bardua, A. Hamann, M. Witzenrath, L. E. Sander, T. Wolff, A. C. Hocke, S. Hippenstiel, S. De Carlo, J. Neudecker, K. Osterrieder, N. Budisa, R. R. Netz, C. Böttcher, S. Liese, A. Herrmann, C. P. R. Hackenberger, Phage capsid nanoparticles with defined ligand arrangement block influenza virus entry. *Nat. Nanotech.* **15**, 373-379 (2020).

16. R. Wagner, M. Matrosovich, H.-D. Klenk, Functional balance between haemagglutinin and neuraminidase in influenza virus infections. *Rev. Med. Virol.* **12**, 159-166 (2002).
17. E. de Vries, W. Du, H. Guo, C. A. M. de Haan, Influenza A Virus Hemagglutinin–Neuraminidase–Receptor Balance: Preserving Virus Motility. *Trends Microbiol.* **28**, 57-67 (2020).
18. D. Lauster, M. Glanz, M. Bardua, K. Ludwig, M. Hellmund, U. Hoffmann, A. Hamann, C. Böttcher, R. Haag, C. P. R. Hackenberger, A. Herrmann, Multivalent Peptide–Nanoparticle Conjugates for Influenza-Virus Inhibition. *Angew. Chem. Int. Ed.* **56**, 5931-5936 (2017).
19. M. Müller, D. Lauster, H. H. K. Wildenauer, A. Herrmann, S. Block, Mobility-Based Quantification of Multivalent Virus-Receptor Interactions: New Insights Into Influenza A Virus Binding Mode. *Nano Lett.* **19**, 1875-1882 (2019).
20. H. Sun, J. Su, Q. Meng, Q. Yin, L. Chen, W. Gu, P. Zhang, Z. Zhang, H. Yu, S. Wang, Y. Li, Cancer-Cell-Biomimetic Nanoparticles for Targeted Therapy of Homotypic Tumors. *Adv. Mater.* **28**, 9581-9588 (2016).
21. R. H. Fang, C.-M. J. Hu, B. T. Luk, W. Gao, J. A. Copp, Y. Tai, D. E. O'Connor, L. Zhang, Cancer Cell Membrane-Coated Nanoparticles for Anticancer Vaccination and Drug Delivery. *Nano Lett.* **14**, 2181-2188 (2014).
22. N. Parveen, G. E. Rydell, G. Larson, V. P. Hytönen, V. P. Zhdanov, F. Höök, S. Block, Competition for Membrane Receptors: Norovirus Detachment via Lectin Attachment. *J. Am. Chem. Soc.* **141**, 16303-16311 (2019).
23. H. Pace, L. Simonsson Nyström, A. Gunnarsson, E. Eck, C. Monson, S. Geschwindner, A. Snijder, F. Höök, Preserved Transmembrane Protein Mobility in Polymer-Supported Lipid Bilayers Derived from Cell Membranes. *Anal. Chem.* **87**, 9194-9203 (2015).
24. F. Wen, X.-F. Wan, Influenza Neuraminidase: Underrated Role in Receptor Binding. *Trends Microbiol.* **27**, 477-479 (2019).
25. H. Zhang, M. Yu, H. Song, O. Noonan, J. Zhang, Y. Yang, L. Zhou, C. Yu, Self-Organized Mesostructured Hollow Carbon Nanoparticles via a Surfactant-Free Sequential Heterogeneous Nucleation Pathway. *Chem. Mater.* **27**, 6297-6304 (2015).
26. E. Ben-Akiva, R. A. Meyer, H. Yu, J. T. Smith, D. M. Pardoll, J. J. Green, Biomimetic anisotropic polymeric nanoparticles coated with red blood cell membranes for enhanced circulation and toxin removal. *Sci. Adv.* **6**, eaay9035 (2020).
27. R. H. Fang, A. V. Kroll, W. Gao, L. Zhang, Cell Membrane Coating Nanotechnology. *Adv. Mater.* **30**, 1706759 (2018).
28. J. Vonnemann, S. Liese, C. Kuehne, K. Ludwig, J. Dernedde, C. Böttcher, R. R. Netz, R. Haag, Size Dependence of Steric Shielding and Multivalency Effects for Globular Binding Inhibitors. *J. Am. Chem. Soc.* **137**, 2572-2579 (2015).
29. J. L. Cuellar-Camacho, S. Bhatia, V. Reiter-Scherer, D. Lauster, S. Liese, J. P. Rabe, A. Herrmann, R. Haag, Quantification of Multivalent Interactions between Sialic Acid and Influenza A Virus Spike Proteins by Single-Molecule Force Spectroscopy. *J. Am. Chem. Soc.* **142**, 12181-12192 (2020).
30. P. H. Hamming, N. J. Overeem, J. Huskens, Influenza as a molecular walker. *Chem. Sci.* **11**, 27-36 (2020).
31. M. D. Vahey, D. A. Fletcher, Influenza A virus surface proteins are organized to help penetrate host mucus. *eLife* **8**, e43764 (2019).
32. M. Lakadamyali, M. J. Rust, H. P. Babcock, X. Zhuang, Visualizing infection of individual influenza viruses. *Proc. Natl. Acad. Sci.* **100**, 9280-9285 (2003).
33. A. C. Hurt, J. K. Holien, M. Parker, A. Kelso, I. G. Barr, Zanamivir-Resistant Influenza Viruses with a Novel Neuraminidase Mutation. *J. Virol.* **83**, 10366-10373 (2009).
34. R. Trebbien, S. S. Pedersen, K. Vorborg, K. T. Franck, T. K. Fischer, Development of oseltamivir and zanamivir resistance in influenza A(H1N1)pdm09 virus, Denmark, 2014. *Eurosurveillance* **22**, 30445 (2017).
35. B. Rath, X. Chen, V. Spies, S. Muehlhans, P. Obermeier, F. Tief, L. Seeber, K. Karsch, J. Milde, H. Skopnik, Prospective surveillance of antiviral resistance in hospitalized infants less than 12 months of age with A (H3N2)

influenza infection and treated with oseltamivir. *Antivir Ther* **22**, 515Ğ522 (2017).

36. M. Waldmann, R. Jirmann, K. Hoelscher, M. Wienke, F. C. Niemeyer, D. Rehders, B. Meyer, A Nanomolar Multivalent Ligand as Entry Inhibitor of the Hemagglutinin of Avian Influenza. *J. Am. Chem. Soc.* **136**, 783-788 (2014).
37. B. T. Luk, R. H. Fang, C.-M. J. Hu, J. A. Copp, S. Thamphiwatana, D. Dehaini, W. Gao, K. Zhang, S. Li, L. Zhang, Safe and Immunocompatible Nanocarriers Cloaked in RBC Membranes for Drug Delivery to Treat Solid Tumors. *Theranostics* **6**, 1004-1011 (2016).
38. C.-M. J. Hu, R. H. Fang, J. Copp, B. T. Luk, L. Zhang, A biomimetic nanosponge that absorbs pore-forming toxins. *Nat. Nanotech.* **8**, 336-340 (2013).
39. C.-M. J. Hu, R. H. Fang, B. T. Luk, L. Zhang, Nanoparticle-detained toxins for safe and effective vaccination. *Nat. Nanotech.* **8**, 933-938 (2013).
40. M. Hoffmann, H. Kleine-Weber, S. Schroeder, N. Krüger, T. Herrler, S. Erichsen, T. S. Schiergens, G. Herrler, N.-H. Wu, A. Nitsche, M. A. Müller, C. Drosten, S. Pöhlmann, SARS-CoV-2 Cell Entry Depends on ACE2 and TMPRSS2 and Is Blocked by a Clinically Proven Protease Inhibitor. *Cell* **181**, 271-280.e278 (2020).
41. A. C. Walls, Y.-J. Park, M. A. Tortorici, A. Wall, A. T. McGuire, D. Veesler, Structure, Function, and Antigenicity of the SARS-CoV-2 Spike Glycoprotein. *Cell* **181**, 281-292.e286 (2020).
42. A. Baum, B. O. Fulton, E. Wloga, R. Copin, K. E. Pascal, V. Russo, S. Giordano, K. Lanza, N. Negron, M. Ni, Y. Wei, G. S. Atwal, A. J. Murphy, N. Stahl, G. D. Yancopoulos, C. A. Kyratsous, Antibody cocktail to SARS-CoV-2 spike protein prevents rapid mutational escape seen with individual antibodies. *Science*, eabd0831 (2020).
43. Y. Wu, F. Wang, C. Shen, W. Peng, D. Li, C. Zhao, Z. Li, S. Li, Y. Bi, Y. Yang, Y. Gong, H. Xiao, Z. Fan, S. Tan, G. Wu, W. Tan, X. Lu, C. Fan, Q. Wang, Y. Liu, C. Zhang, J. Qi, G. F. Gao, F. Gao, L. Liu, A noncompeting pair of human neutralizing antibodies block COVID-19 virus binding to its receptor ACE2. *Science* **368**, 1274-1278 (2020).
44. S. Xia, M. Liu, C. Wang, W. Xu, Q. Lan, S. Feng, F. Qi, L. Bao, L. Du, S. Liu, C. Qin, F. Sun, Z. Shi, Y. Zhu, S. Jiang, L. Lu, Inhibition of SARS-CoV-2 (previously 2019-nCoV) infection by a highly potent pan-coronavirus fusion inhibitor targeting its spike protein that harbors a high capacity to mediate membrane fusion. *Cell Res.* **30**, 343-355 (2020).
45. S. Xia, L. Yan, W. Xu, A. S. Agrawal, A. Algaissi, C.-T. K. Tseng, Q. Wang, L. Du, W. Tan, I. A. Wilson, S. Jiang, B. Yang, L. Lu, A pan-coronavirus fusion inhibitor targeting the HR1 domain of human coronavirus spike. *Sci. Adv.* **5**, eaav4580 (2019).
46. Q. Zhang, A. Honko, J. Zhou, H. Gong, S. N. Downs, J. H. Vasquez, R. H. Fang, W. Gao, A. Griffiths, L. Zhang, Cellular Nanosponges Inhibit SARS-CoV-2 Infectivity. *Nano Lett.* **20**, 5570-5574 (2020).

Acknowledgments:

General: Dr. Pamela Winchester is sincerely acknowledged for language polishing the manuscript. We would like to acknowledge the assistance of the Core Facility BioSupraMol in Freie Universität Berlin supported by the DFG and Zhongkebaice Technology Service Co. Ltd. Beijing, China for materials characterizations.

Funding: The authors gratefully acknowledge financial support from Deutsche Forschungsgemeinschaft (DFG) through grants from the Collaborative Research Center (SFB) 765. C. N. acknowledges the support from the China Scholarship Council (CSC). C. C. acknowledges the support of the National Key R&D Program of China (2019YFA0110600, 2019YFA0110601), the Science and Technology Project of Sichuan Province (2020YFH0087, 2020YJ0055), Special Funds

for Prevention and Control of COVID-19 of Sichuan University (2020scunCoV-YJ-20005) and SKLFPM, Donghua University (YJ202005), State Key Laboratory of Polymer Materials Engineering (Grant No. sklpme2019-2-03), Fundamental Research Funds for the Central Universities, Ten Thousand Youth Talents Plan, and Alexander von Humboldt Fellowship.

Author contributions: C. N. and C. C. synthesized the materials. T. W. provided the IAV strains and supervised the virus infection tests. C. N. and M. S. performed the virus infection inhibition tests. M. W., Y. K. and St. B. designed and performed TIRFM analysis. B. P. and Su. B. synthesized functionalized Zanamivir molecules. V. A. perfomed MALDI-ToF analysis. C. C, T. W., and R. H. designed and supervised the project. C. N, C. C., T. W., and R. H. wrote and edited the manuscript.

Competing interests: All other authors declare that they have no competing interests.

Data and materials availability: All data needed to evaluate the conclusions in the paper are present in the paper and/or the Supplementary Materials. Additional data related to this paper may be requested from the authors.

Figures and Tables.

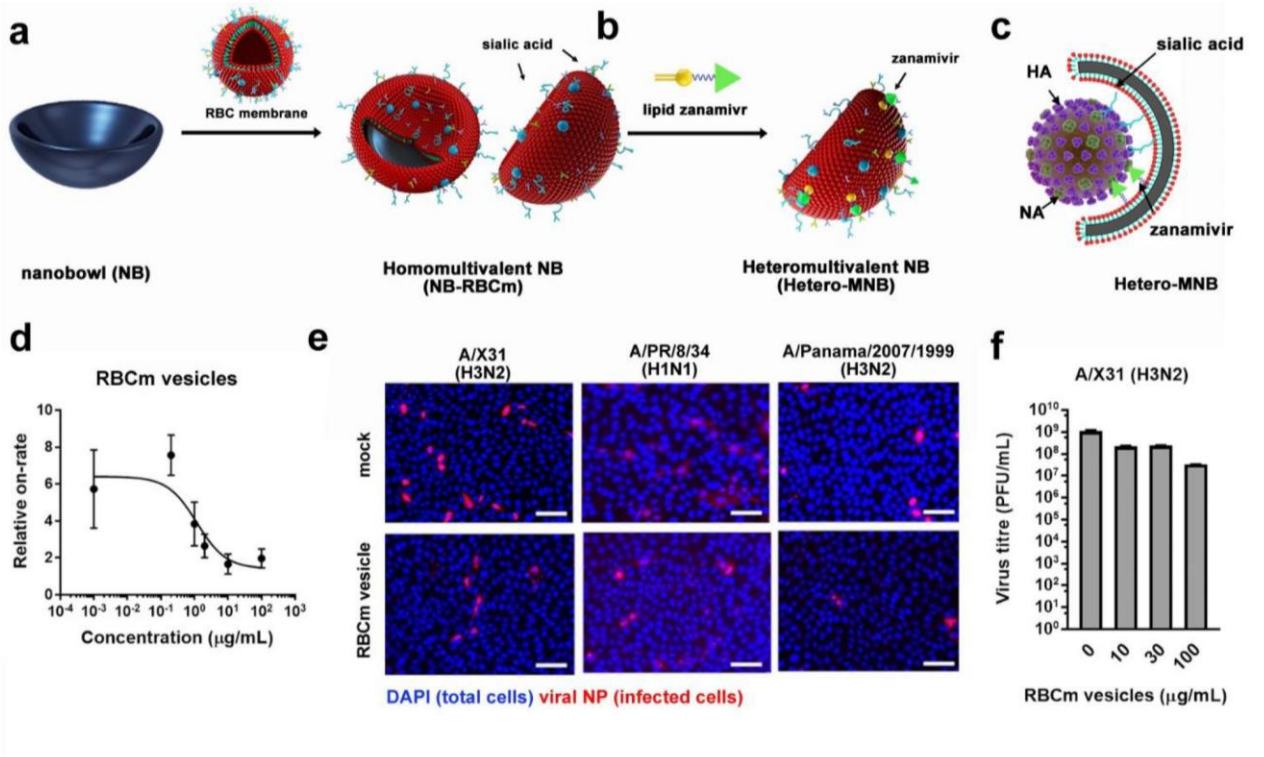

Fig. 1. (a, b) Design and synthesis of a heteromultivalent nanobowl (Hetero-MNB) for influenza A virus (IAV) inhibition, including the coating of RBCm onto the nanbowl surface and the further modification with lipidic zanamivir. (c) Proposed binding patterns between IAV and the Hetero-MNB, whereas sialic acid and zanamivir bind to HA and NA, respectively, and the bowl-shape with facilitating the capping to the surface of the virus particle. (d) Inhibition curves for RBCm vesicles at different concentrations from a TIRF setup. Values are expressed as mean ±SD, n=4. (e) Typical immuno-fluorescent staining images of viral nucleoprotein (NP) to show the infected cells with the treatment of RBCm vesicles. Scale bar: 50 μm. Multiplicity of infection: 0.1. (f) Propagation of IAV in the presence of RBCm vesicles. Values are expressed as mean ±SD, n=4.

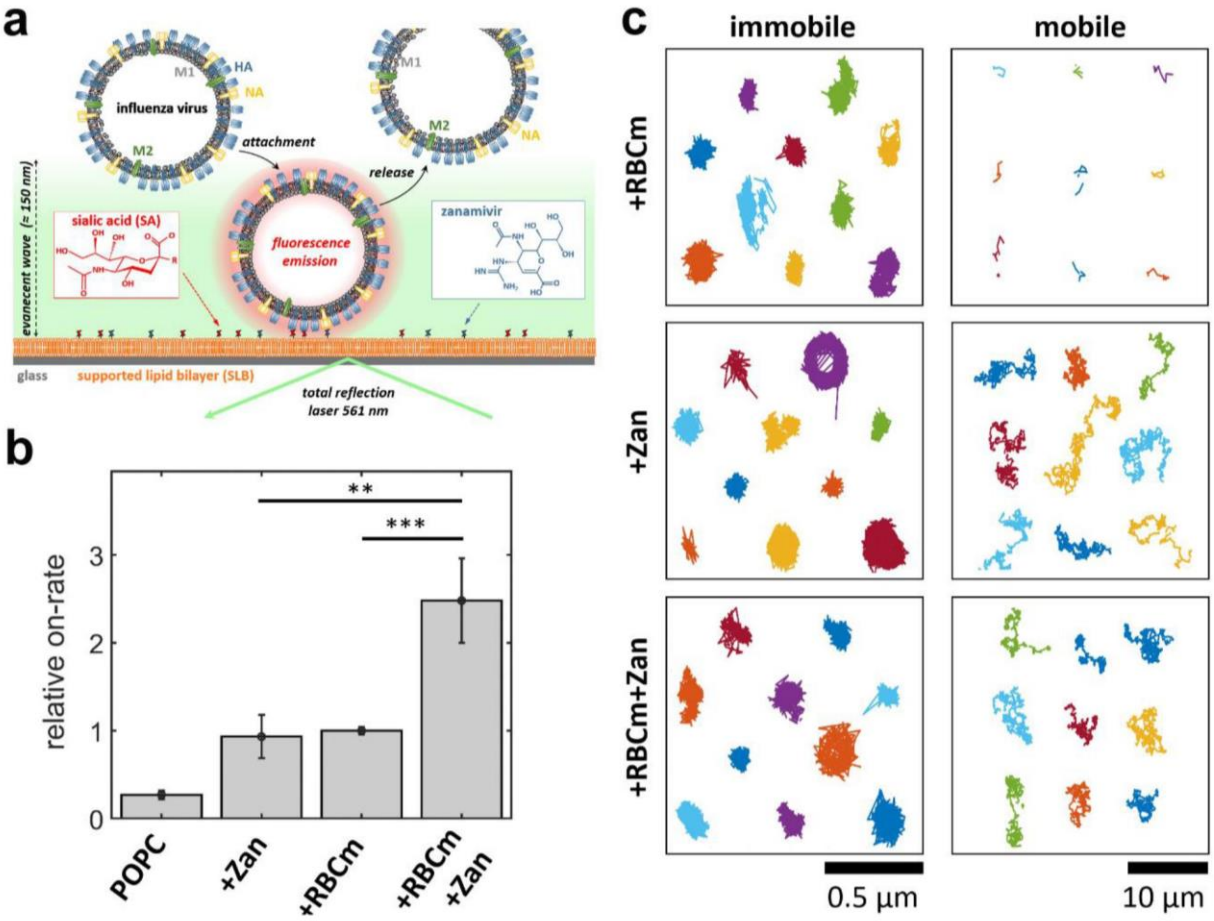

Fig. 2. (a) TIRF-based assay for assessing the interaction of IAVs with homo- or heteromultivalent membranes. The corresponding glycostructures (either sialic acids or lipid-conjugated zanamivir) are incorporated in a supported lipid bilayer (SLB) and the IAV-SLB interaction is recorded using TIRF microscopy. Application of single-virus tracking allows for extracting changes of (b) the rate of IAV attachment to the membranes and (c) the motion of SLB-bound IAVs, when employing the different homo- and heteromultivalent structures. Each color represents the track of a single virion. Values in (e) are expressed as mean ± SEM, n=10. **p<0.01, ***p < 0.001 by Student t-test. Note the different scale bars used for the immobile and mobile IAVs in (c).

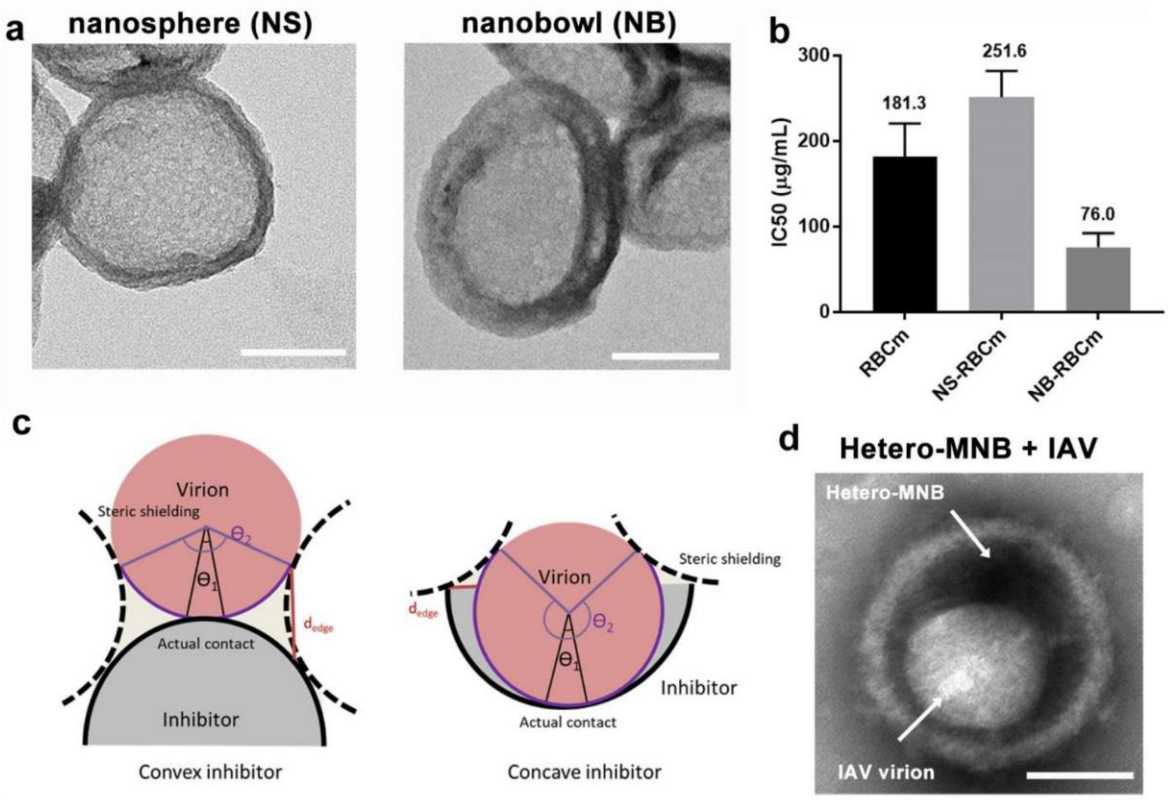

Fig. 3. (a) HR-TEM images for the nanosphere (NS) and nanobowl (NB) with RBCm coating, respectively. Scale bar: 50 nm. (b) IC50 values for the homomultivalent RBCm coated NS (NS-RBCm) and NB (NB-RBCm). Values are expressed as mean ± SD, n=4. (c) Geometry analysis for a virion binding to a convex inhibitor and concave inhibitor. The actual contact between them is marked with Θ_1; the steric shielding by the inhibitor is marked with purple lines with Θ_2. Steric shielding is estimated by placing new inhibitors with the same curvature. (d) Negatively stained HR-TEM image for the IAV particle binding with the Hetero-MNB. Scale bar: 50 nm.

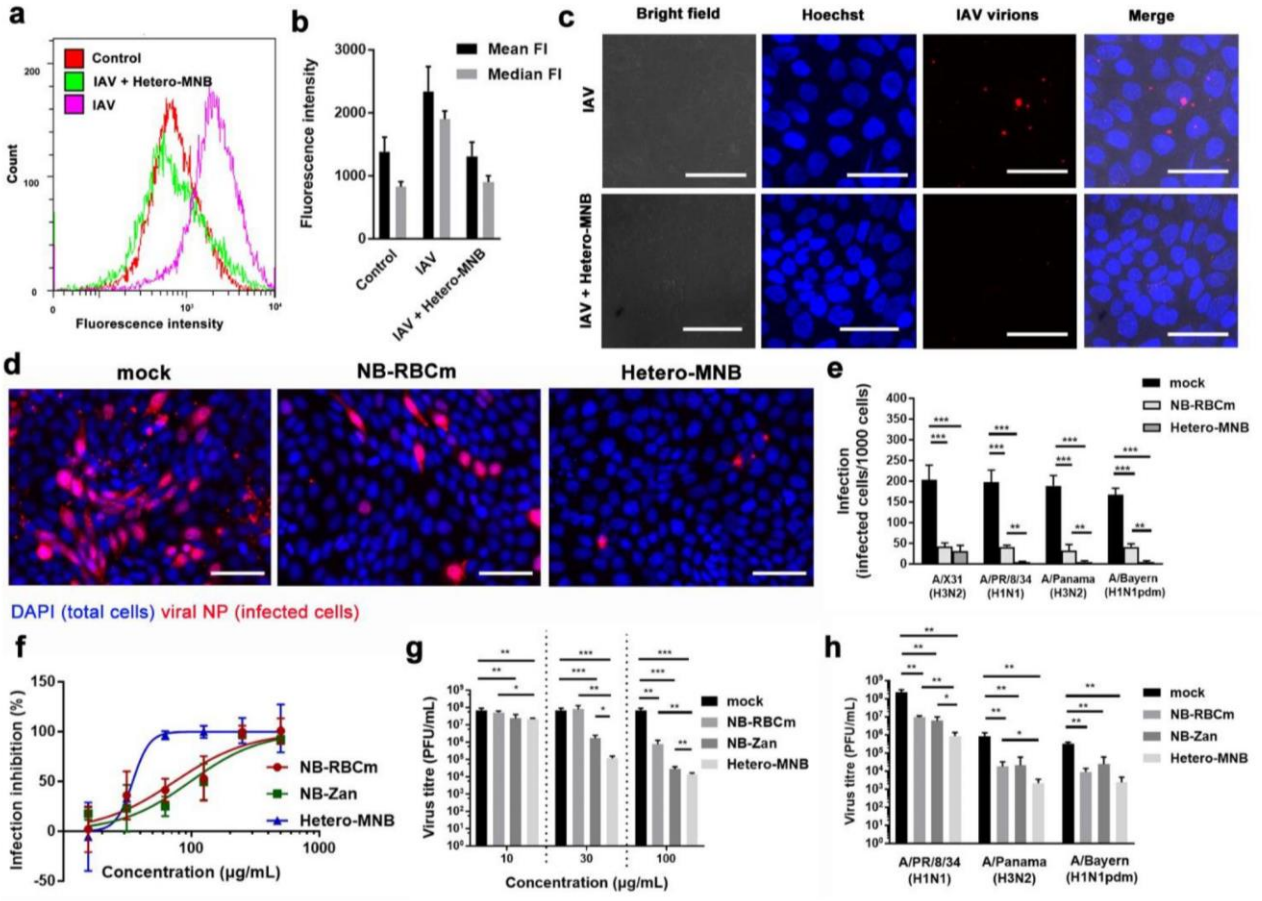

Fig. 4. (a) Flow cytometry for the virus attachment to MDCK-II cells and (b) corresponding mean and median fluorescence intensities (FI) for the samples. The error bars are generated by the CytExpert Acquisition and Analysis Software Version 2.3. (c) Projection CLSM images for the viral attachment to MDCK-II cells in the presence of Hetero-MNB. Scale bar: 20 μm. (d) Typical immune-fluorescence images to show the IAV (A/X31 (H3N2)) infection in the presence of the inhibitors. Other images are shown in Fig. S11-S12, Supplementary Materials. Scale bar: 100 μm. (e) Detection of viral nucleoprotein in cells infected with four typical human IAV strains, including A/X31 (H3N2), A/PR/8/34 (H1N1), A/Panama/2007/1999 (H3N2), A/Bayern/63/2009 (H1N1pdm) in the presence or absence of inhibitors. (f) The inhibition of A/X31 (H3N2) of the inhibitors at different dosages revealed by cell viability. (g) Inhibition towards IAV propagation (A/X31 (H3N2)) for the inhibitors. (h) Inhibition towards IAV propagation for the inhibitors against three other IAV strains, including A/PR/8/34 (H1N1), A/Panama/2007/1999 (H3N2), A/Bayern/63/2009 (H1N1pdm). Inhibitor dosage: 100 μg/mL. Values are expressed as mean ± SD, n=4. *p< 0.05, **p<0.01, ***p<0.001 by Student t-test, respectively.

Table 1. The binding constant of RBCm vesicles of different IAV strains from hemagglutination inhibition assay. Values are expressed as mean ±SD, n=4.

	KiHAI (μg/mL)	KiHAI (nM sialic acid)
A/X31 (H3N2)	41.6 ± 20.6	8.4 ± 4.2
A/PR/8/34 (H1N1)	23.4 ± 9.0	4.8 ± 1.8
A/Panama/2007/1999 (H3N2)	27.3 ± 7.8	5.5 ± 1.7

Table 2. The binding constant of samples against A/X31 (H3N2) from hemagglutination inhibition assay. Values are expressed as mean ±SD, n=4.

	KiHAI (μg/mL)	KiHAI (nM sialic acid)
RBCm	41.6 ± 20.6	8.4 ± 4.2
MDCK-II membrane	6.8 ± 1.9	1.6 ± 0.5
RBCm vesicles + free Zan	11.7 ± 4.5	2.4 ± 0.9
RBCm-Zan hybrid vesicles	5.9 ± 2.3	1.2 ± 0.5
NB-RBCm	51.9 ± 23.8	3.1 ± 1.4
NB-RBCm + Zan	19.5 ± 7.8	1.2 ± 0.5
Hetero-MNB	13.7 ± 3.9	0.8 ± 0.2

Supplementary Materials:

Materials and Methods

Figs. S1-S15

Movies S1-S2

Science
AAAS

Supplementary Materials for

Heteromultivalent topology-matched nanostructures as potent and broad-spectrum influenza A virus inhibitors

Chuanxiong Nie, Marlena Stadtmüller, Badri Parshad, Matthias Wallert, Vahid Ahmadi, Yannic Kerkhoff, Sumati Bhatia, Stephan Block, Chong Cheng, Thorsten Wolff, Rainer Haag

Correspondence to: stephan.block@fu-berlin.de (S. Block), chong.cheng@scu.edu.cn (C. Cheng), WolffT@rki.de (T. Wolff), haag@zedat.fu-berlin.de (R. Haag).

This PDF file includes:

Other Supplementary Materials for this manuscript include the following:

Materials and Methods

Characterazations

^{1}H NMR spectra are recorded on a Bruker Avance 3 operating at 400 MHz or 500 MHz, at concentrations of 100 mg·mL^{-1}. The chemical shifts are reported in δ (ppm) values and referenced for different solvents. The spectra of Matrix-Assisted Laser Desorption/Ionization Time-of-Flight Mass Spectroscopy (MALDI-ToF MS) are recorded using a Bruker Ultra-flex III in the positive ion mode using a linear pathway (LP). Saturated Alpha-cyano-4-hydroxycinnamic acid in methanol is used as the matrix. The sample is prepared via the "dried-droplet method" by dropping 0.5 µL of a mixture of the matrix and the polymer solution (1:1). The mixture is placed on the target plate and allowed to air dry. Fourier transform infrared (FTIR) Spectra are obtained with Nicolet iS50, Thermofisher. Dynamic light scattering (DLS) measurements are performed using Malvern Zetasizer Nano ZS (Malvern Instruments GmbH, Herrenberg, Germany). All samples are measured at a constant scattering angle of 173° at 25 °C and freshly prepared just before measurement in DI water or PBS buffer (1 mM, pH 7.4). Ultrasonic bath (Model: SONOREX, RK255 HZ, made in Germany) is used to disperse materials in solvents. Scanning electron microscope (SEM): The morphology of the nanoparticle is observed by ultra-high-resolution FE-SEM (Hitachi S-4800). The samples are dried in the oven and then attached to the sample supports using carbon tape. All the samples are observed directly without gold coating. For the non-conductive substrates, the gold coating is deposited with about 1-2 nm. Fluorescence images are taken on ZEISS Axio Observer (Carl Zeiss Microscopy GmbH, Jena, Germany). Transmission electron microscopy (TEM): Droplets (~5 µL, ~ 0.02 mg/mL) of the sample solution are placed on ultrathin carbon film on copper grids (Ted Pella, Inc. USA), and the supernatant liquid is removed by blotting with a piece of filter paper. The grids are air-dried at least 40 min and are subsequently transferred into a TEM machine, Talos L120c transmission electron microscope (ThermoFisher Scientific, USA), and operated at 200 kV.

Total internal reflection fluorescence (TIRF) microscopy

TIRF microscopy was used to quantify the interaction of single, R18-labelled Influenza A viruses (IAV) with different glycostructures embedded in supported lipid bilayers (SLBs) with different compositions as described.*(19)* The glycostructures originated from native red blood cell membrane (RBCm) vesicles, zanamivir-conjugated lipids, or both. This method provides information about various properties of the IAV-membrane interaction, such as the attachment rate to the membrane, IAV mobility, and off-rate distributions regarding the different membrane compositions. The measurements have been conducted as follows:

Materials:

POPC (1-palmitoyl-2-oleoyl-glycero-3-phosphocholine), and C16-PEG5k (N-palmitoyl-sphingosine-1-{succinyl[methoxy(polyethylene glycol)5000]}) were purchased from Avanti Polar Lipids Inc. (Alabaster, AL). DSPE-PEG-Zan was synthesized, as shown in Fig. S3. RBCm vesicles were produced by disrupting human red blood cells and centrifugation as mentioned above. R18 (octadecyl rhodamine B chloride), calcium chloride (≥97 %), and Liquinox cleaning solution were obtained from Sigma Aldrich (Steinheim, Germany). Phosphate buffered saline was acquired from Carl Roth GmbH + Co. KG (Karlsruhe, Germany).

Supported Lipid Bilayer (SLB) Formation:

For the TIRF measurements, two batches of liposomes were generated, the lipid composition of which are: (*batch 1*) 96.2 wt% POPC + 3.8 wt% C16-PEG5k and (*batch 2*) 95.2 wt% POPC + 3.8 wt% C16-PEG5k + 1 wt% DSPE-PEG-Zan. The liposomes were generated by mixing the

lipids (dissolved in chloroform) in a round flask, followed by drying the mixture in a steam of dry nitrogen and in vacuum. After drying, the lipids were hydrated using PBS buffer (pH 7.4) to the lipid content of 1 mg/mL, followed by small volume extrusion with a 100 nm polycarbonate membrane. *Batch 1* lacks any IAV attachment factors and allows to assess the unspecific IAV-POPC interaction, while *batch 2* exposes the sialic acid-analog zanamivir, allowing to assess the homomultivalent IAV-zanamivir interaction.
In order to assess the IAV-RBCm interaction, two additional batches were generated by mixing 90 µL of either *batch 1* or *2* (lipid content 1 mg/mL) with 10 µL of RBCm vesicles (1 mg/mL). The combination of *batch 1* + RBCm vesicles allows for assessing the homomultivalent IAV-SA interaction, while *batch 2* + RBCm vesicles yield information about the binding enhancement by heteromultivalent presentation of SA and zanamivir. The principle of generating hybrid liposome solutions combining synthetic and native liposomes is performed in this study by mixing the liposome solutions, followed by ultrasonication of the solutions at 37 °C for 30 minutes, inducing transfer of material between the different liposome populations.
Prior to SLB formation, glass slides (No. 1 coverslips, 25 mm; Menzel Glas, Braunschweig, Germany) were cleaned in a 0.5 vol% aqueous Liquinox solution of at 80 °C for 75 min. Afterwards the glass slides were rinsed intensively with deionized water (Milli-Q; Merck Millipore, Burlington, MA) and dried at room temperature. Home-made polydimethylsiloxane (PDMS) piece with 6 wells was placed on the glass, and the (hybrid-)vesicle solution (lipid content 0.33 mg/mL) was incubated in each well for approximately 10 minutes. The SLB is then self-forming by adsorption and rupturing at high densities of the vesicles on the glass surface.*(26)* Non-adsorbed vesicles were washed away by replacing the supernatant 10 times with PBS (pH 7.4).
TIRF microscopy measurements:
An Nikon Eclipse Ti-E microscope (Nikon, Tokyo, Japan), equipped with a 100x Plan-Apo oil immersion objective (NA 1.45, Nikon, Tokyo, Japan), a Zyla 4.2 sCMOS camera (Andor, Oxford, UK), and a white light source (Lumen 200; Prior Scientific, Cambridge, UK), was used to record videos of IAVs interacting with (hybrid) SLBs with different membrane compositions. TIRF microscopy videos with 1000 frames (acquisition rate 9 frames per second, exposure time 100 ms, 2 x 2 binning, the field of view 130 µm x 130 µm, pixel size 130 nm x 130 nm) were recorded for each measurement condition to quantify the transient interaction of the IAVs with the (h)SLB using single virus tracking and the equilibrium fluctuation analysis, *(23, 24)* implemented by self-created MATLAB scripts.*(19)*

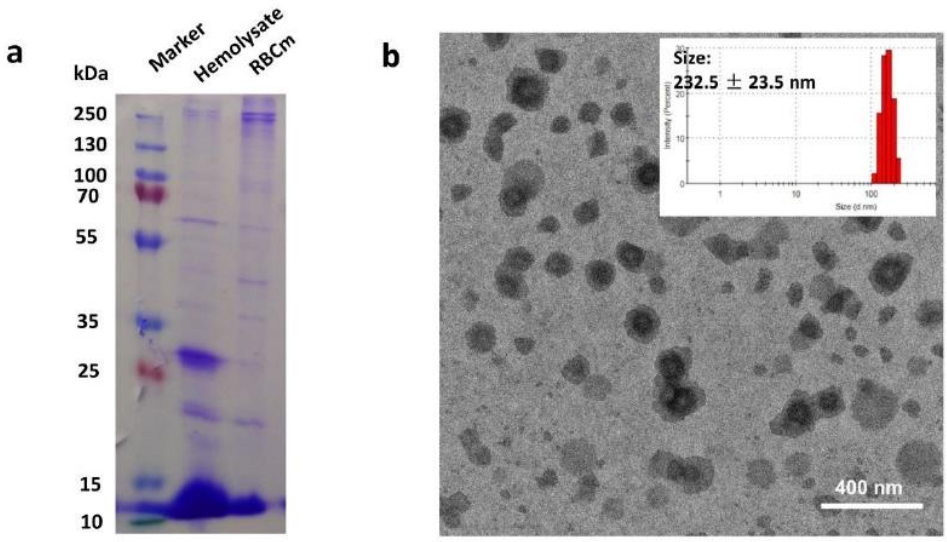

Fig. S1. Extraction of RBCm from red blood cells.

(a) SDS page image that shows the protein components of lysed RBC and RBCm. (b) TEM images for RBCm and corresponding size distribution by DLS. Scale bar: 400 nm.

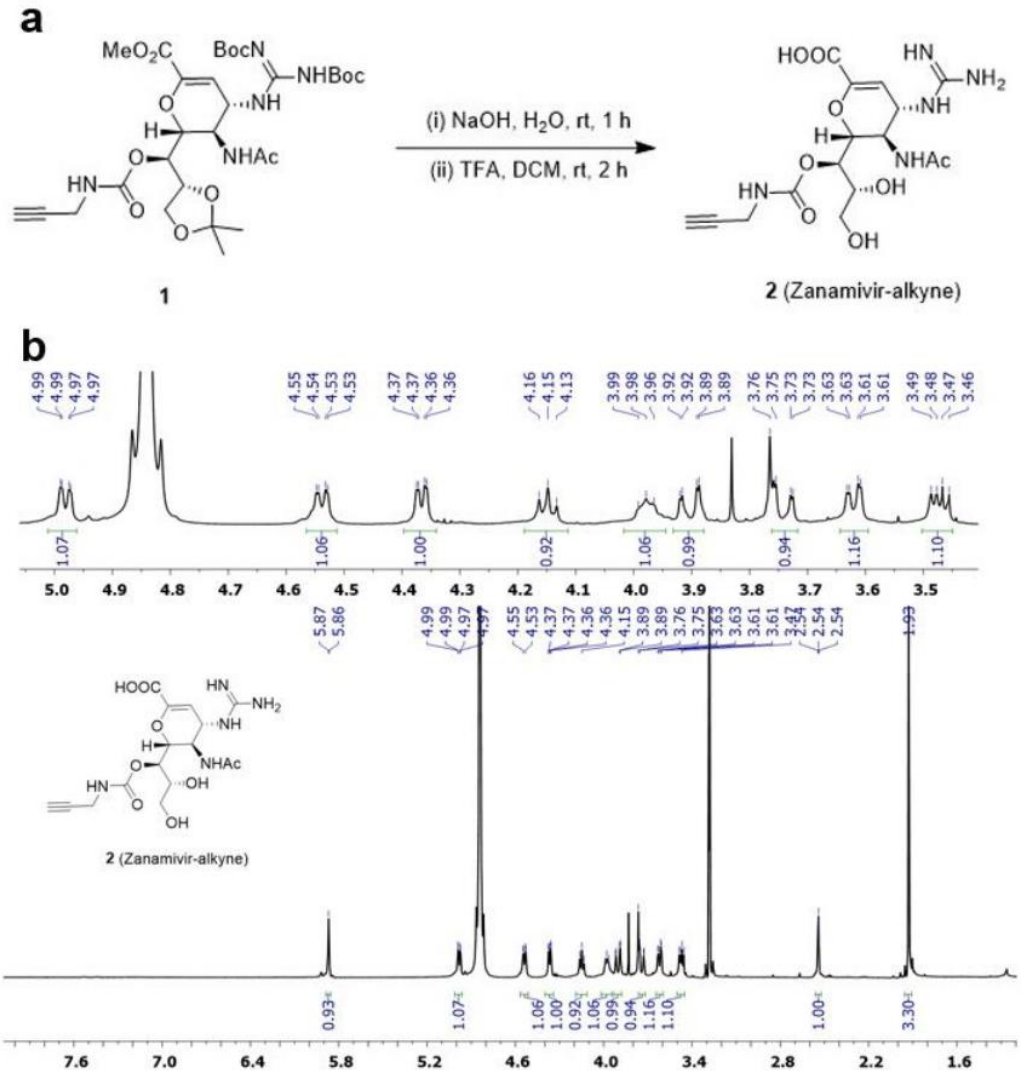

Fig. S2. Synthesis of zanamivir-alkyne.
(a) Synthesis of zanamivir-alkyne. (b) ^{1}H NMR of zanamivir-alkyne in CD_3OD at 500 MHz.

First, the protected Zanamivir-alkyne derivative **1** was synthesized by the procedure reported in the literature by Wen et al. (1). The zanamivir derivative **1** (100 mg) was treated with 1 N aq. NaOH (3 mL) at room temperature for 1 h. After the disappearance of starting material as monitored by TLC, the reaction mixture was neutralized with H^+ resin (Dowex 50WX8) and filtered off. The filtrate was concentrated to dryness and then taken with 5 mL TFA/DCM (1:1) and further stirred for 2 h at room temperature. The solvent was evaporated on rota-vapor. The obtained crude product was washed with diethyl ether to get the desired deprotected zanamivir-alkyne **2** as a white solid in 90% yield.

^{1}H NMR (500 MHz, CD_3OD): δ = 1.93 (s, 3H), 2.54 (t, 1H, J = 2.4 Hz), 3.46-3.49 (m, 1H), 3.62 (dd, 1H, *J* = 11.7, 2.6 Hz), 3.73-3.76 (m, 1H), 3.86-3.92 (m, 1H), 3.96-3.99 (m, 1H), 4.15 (t, 1H, *J* = 9.0 Hz), 4.37 (dd, 1H, *J* = 8.4, 2.1 Hz), 4.54 (dd, 1H, *J* = 9.5, 2.2 Hz), 4.98 (dd, 1H, *J* = 9.0, 1.7 Hz), 5.87 (d, 1H, *J* = 2.3 Hz); HRMS (ESI): m/z calculated for $C_{18}H_{24}N_4O_{10}$: 436.1439 [M+Na^+], found 436.1218.

6

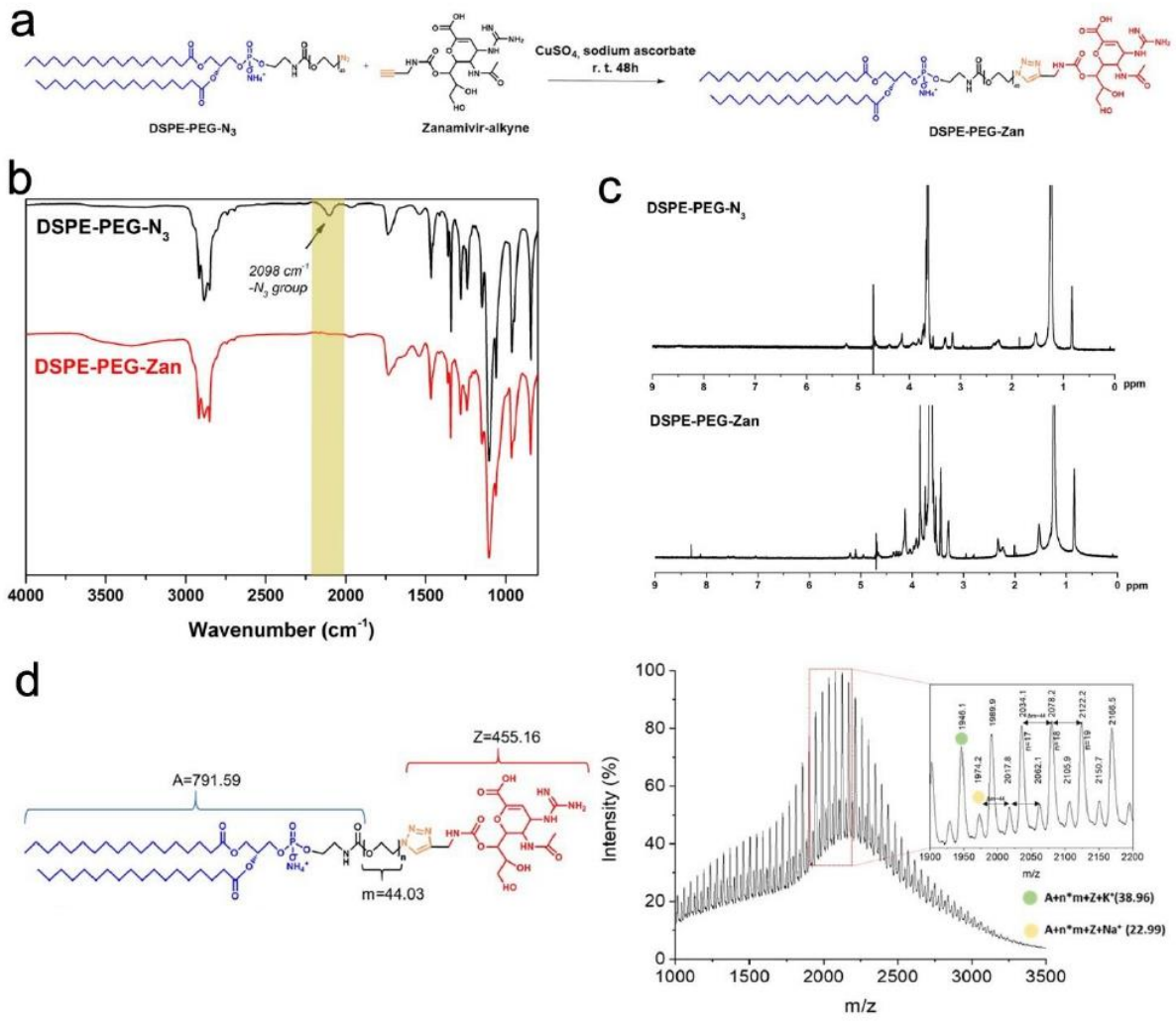

Fig. S3. Synthesis of DSPE-PEG conjugated zanamivir.

(a) Synthesis scheme for DSPE-PEG-Zan. (b) FTIR spectra DSPE-PEG-N_3 and DSPE-PEG-Zan, respectively. (c) ^{1}H NMR spectra for the DSPE-PEG-N_3 and DSPE-PEG-Zan in D_2O at 500 MHz, respectively. (d) MALDI-ToF MS spectra for the DSPE-PEG-Zan.

100 mg DSPE-PEG-N_3 (0.36 mmol) and 16.5mg Zanamivir-alkyne (0.4 mmol, 1.1 eq to N_3 groups) are firstly dissolved in 10mL DMF/DI water (50/50). Then, 34.0 mg $CuSO_4 \cdot 5H_2O$ (0.72 mmol, 2.0 eq to N_3 groups) is dissolved in 0.5mL DI water and then added sodium ascorbate (1432.2 mg, 7.2 mmol, 20 eq with respect to N_3 groups) in 1.0 ml H2O. The resulted solution is added to the solution of DSPE-PEG-N_3 and Zanamivir-alkyne, and the mixture was degassed for 5 min and stirred at room temperature. The reaction is monitored by Fourier transform infrared (FTIR) Spectroscopy (Nicolet iS50, Thermofisher) and ceased when the characteristic peak of -N_3 at 2100 cm^{-1} disappeared, which reveals the full conversion of DSPE-PEG-N_3 to DSPE-PEG-Zan. It takes 2 days to complete the reaction due to the large side group (DSPE-PEG) coupled to

-N_3. The reaction mixture is dialyzed against 5 mg/mL EDTA solution for 2 days to remove copper and then against DI water for 4 days. The final product is collected by lyophilization and again checked by IR, and no peak at 2100 cm^{-1} is detected, indicating the final compound is free of DSPE-PEG-N_3. The end group analysis from MALDI-ToF MS furthere verifies the synthesis of DSPE-PEG-Zan.

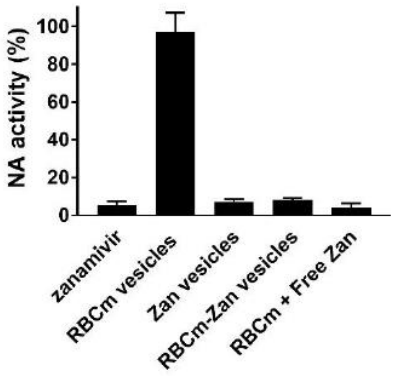

Fig. S4. NA inhibition by the lipid vesicles containing zanamivir.
NA activity of influenza A/X31 (H3N2) being incubated with the vesicles. Values are expressed as mean ±SD, n=6.

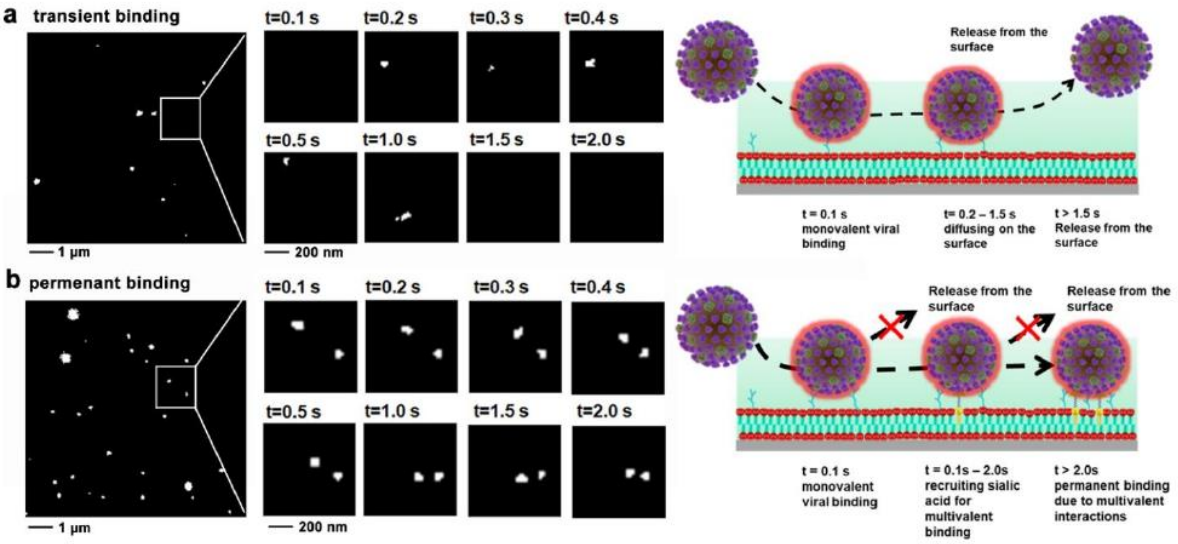

Fig. S5. Snapshots for the virus binding to the homomultivalent and heteromultivalent surfaces.

Single particle analysis for the transient viral binding (a) and permanent binding (b), respectively. Typically, when a virus is approaching the surface, it interacts with single sialic acid in a monovalent binding manner at the beginning. In the next few seconds, the virus circulates on the surface in order to recruit sialic acid to achieve multivalent and stable binding on the surface, and if enough sialic acid in recruited, the binding is stable, and the virus can stay at the surface permanently. Full videos are shown in Movie S1-S2.

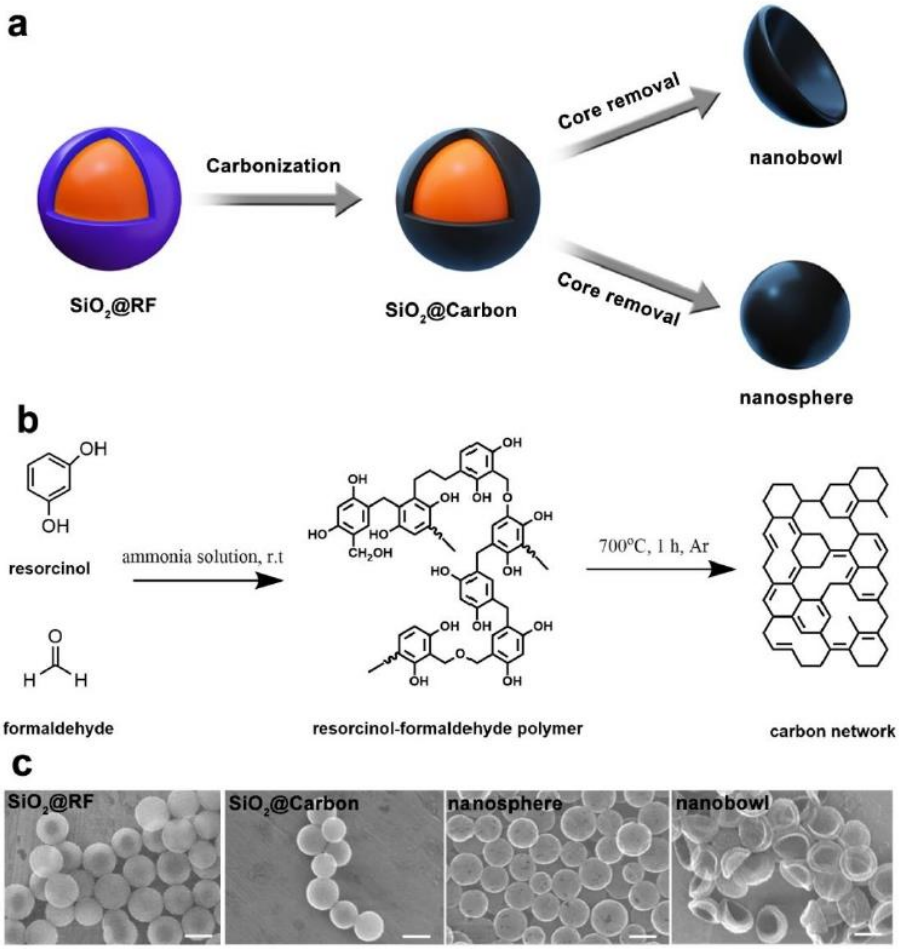

Fig. S6. Synthesis of nanoparticles with matched shape to IAV virions.
(a) Synthesis of the nanobowl and nanosphere via a carbonization-core removal process. RF: resorcinol-formaldehyde polymer. (b) Schemes for the synthesis procedure. (c) Corresponding SEM images for the nanoparticle at each step. Scale bar: 200 nm.

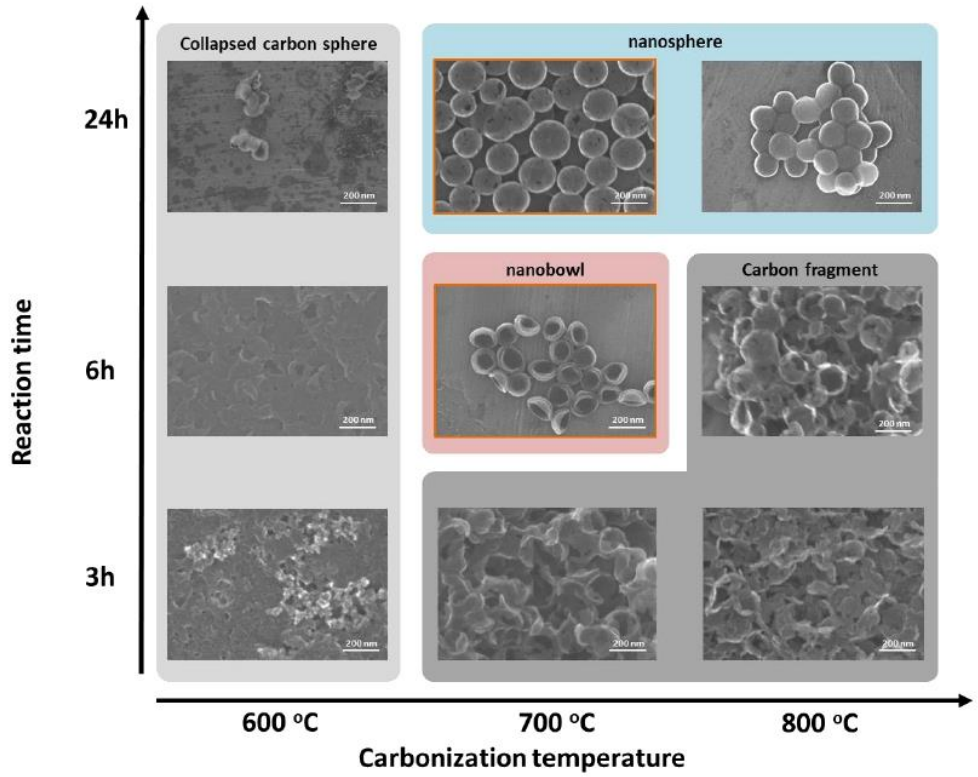

Fig. S7. Structures of the nanoparticles synthesized under different conditions.
Effects reaction time and carbonization temperatures on the morphologies of the nanoparticles.

To obtain a bowl-like nanoparticle, fine-tuning of the thickness and rigidity of the carbon layer is necessary. In our synthesis, the thickness of the carbon layer is tuned by the reaction time of the initial RF layer, where prolonged polymerizing time increases layer thickness. The layer rigidity is regulated by the carbonization temperature since that higher temperatures gave more sp^2- carbons into the carbon network. As shown, if the carbon layer is too flexible, the morphology cannot be maintained after removing the core material, and the hollow particle collapses like a soft hollow capsule. Increasing the carbonization temperature helps shape up the morphology, but in the case of low reaction time and high carbonization temperature, the particles are cracked into the fragments during the etching process. Therefore, to obtain a curved surface, a suitable carbonization temperature is necessary. In the case of suitable carbonization temperature, increasing the reaction time gives a spherical carbon nanoparticle, which is used as a spherical counterpart to study the effects of surface morphology on the interaction with IAV.

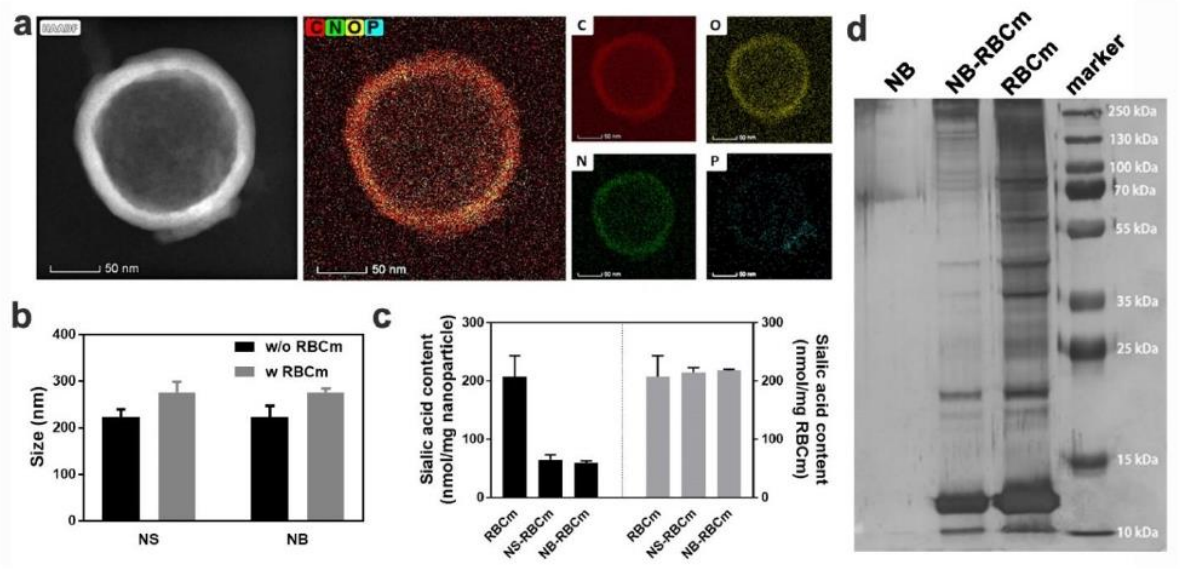

Fig. S8. Characterization of RBCm coated nanoparticles.

(a) HAADF–STEM images and corresponding elemental mapping for revealing the element distribution on the surface of NB-RBCm. Red: carbon; yellow: oxygen; green: nitrogen; violet: phosphorus. Nitrogen and phosphorus are the characteristic elements for the RBCm. (b) Dynamic light scattering (DLS) data for the nanocarbons with (w) and without (w/o) the coating of RBCm. Values are expressed as mean ± SD, n=4. (c) Sialic acid contents for the NS-RBCm and NB-RBCm. Values are expressed as mean ± SD, n=6. (d) SDS-PAGE for the RBCm and NB-RBCm.

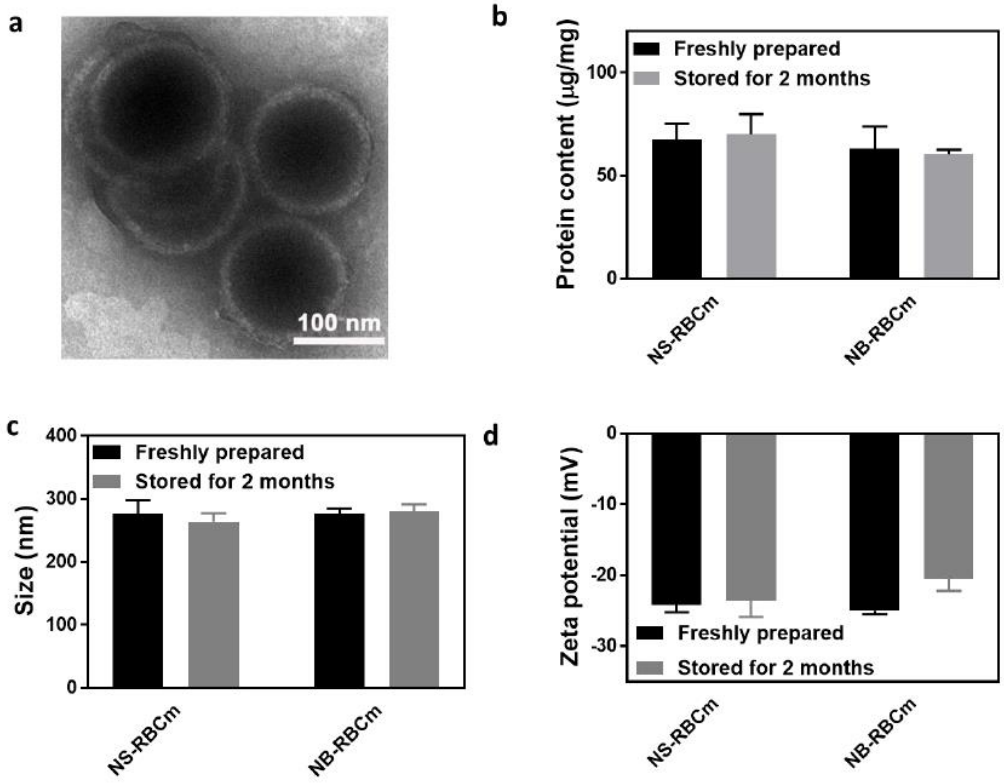

Fig. S9. Stability of RBCm coating on the nanoparticles.
(a) TEM image for the NB-RBCm that has been stored in PBS in 4 ºC for 2 months to demonstrate its good stability. (b) Protein amounts, (c) nanoparticle sizes, and (d) zeta potentials for the freshly prepared RBCm coated nanoparticles and the ones that have been stored in 4 ºC for 2 months. Values are expressed as mean ± SD, n=4.

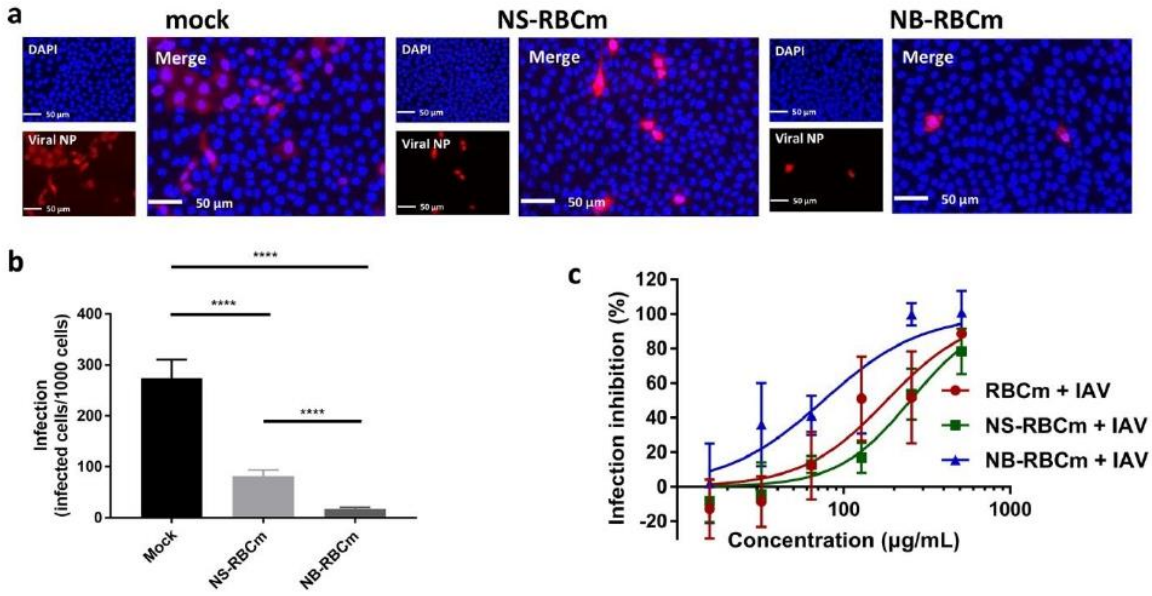

Fig. S10. Inhibition of IAV infection by RBCm coated homomultivalent nanostructures. (a) Typical immuno-fluorescent staining images of viral NP to show the infected cells with the treatment of the NS-RBCm and NB-RBCm. Scale bar: 50 μm. (b) the counting of infected cells from the fluorescent images. At least 4 images with more than 5, 000 cells are included in the counting. (c) Viability of the cells during the infection with the treatment of NS-RBCm. Values are expressed as mean ± SD, n=4.

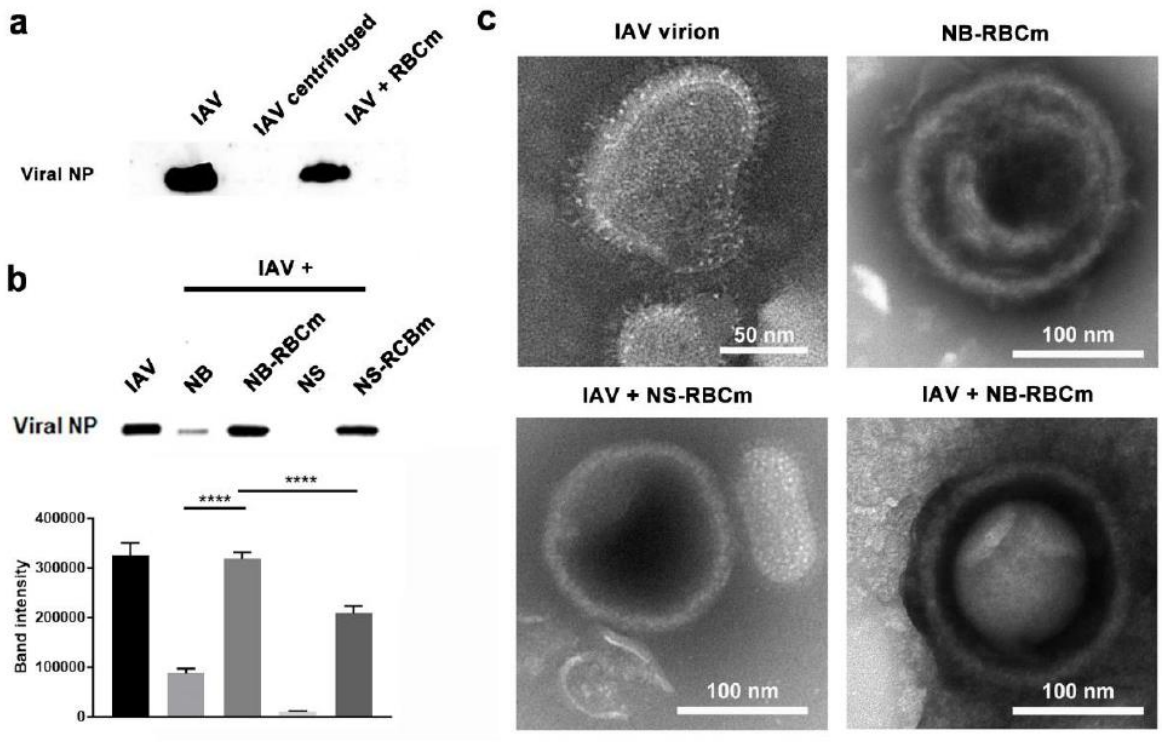

Fig. S11. . Binding of IAV virions by RBCm coated nanostructures.
(a) Western blot image for the IAV particles that have been centrifuged at 10, 000 rpm for 10 min in the absence and presence of RBCm. (b) Western blot images for the IAV centrifuged with the nano-inhibitors and the corresponding band intensity analysis. Values are expressed as mean ± SD, n=4. (c) Negatively stained TEM images for the virions of A/X31 (H3N2) and its binding to nanoparticles.

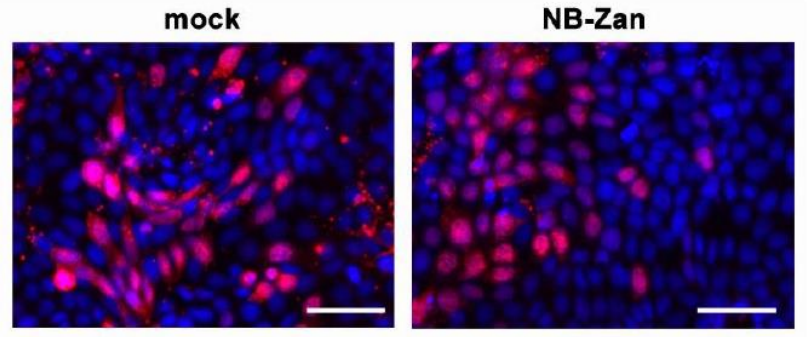

Fig. S12. Inhibition of IAV infection by zanamivir functionalized homomultivalent nanostructure.

Immunofluorescent staining images of cells infected with IAV in the presence or absence of NB-Zan for expression of viral NP. Scale bar: 50 μm. The infected cells are marked red by Alexa fluor 594, while the total cells are marked blue by DAPI.

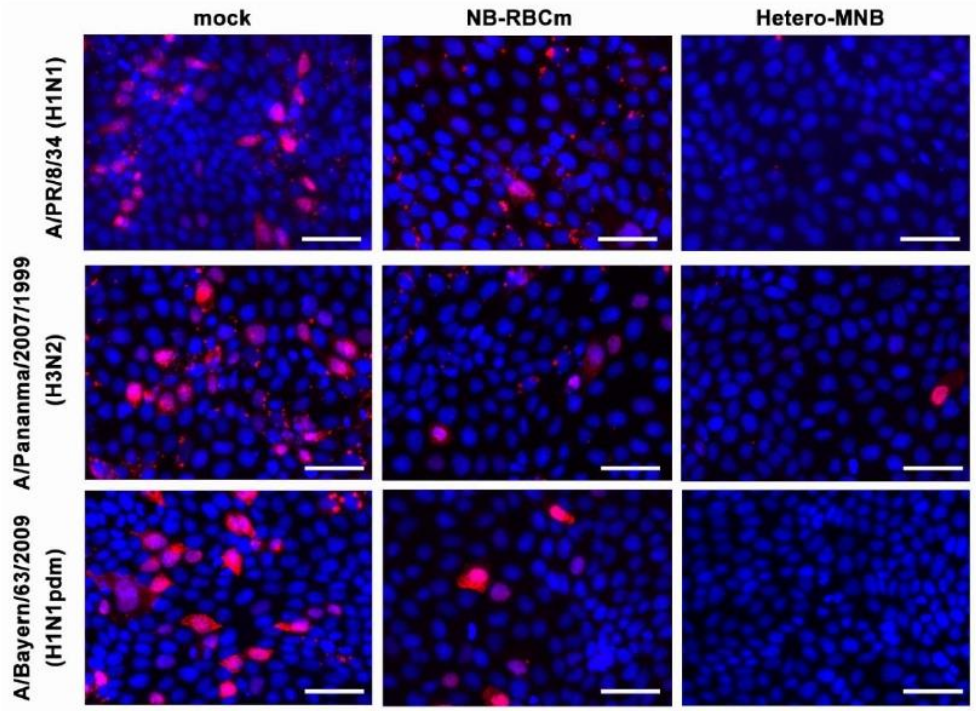

Fig. S13. Inhibition of IAV infection by homo- and hetero-multivalent topography-matching nanostructures.

Typical immunofluorescent staining images of viral NP to infection inhibition towards 3 typical human IAV strains, including A/PR/8/34 (H1N1), A/Panama/2007/1999 (H3N2) and A/Bayern/63/2009 (H1N1pdm). Scale bar: 50 μm. The infected cells are marked red by Alexa fluor 594 (red), while the total cells are marked blue by DAPI (blue).

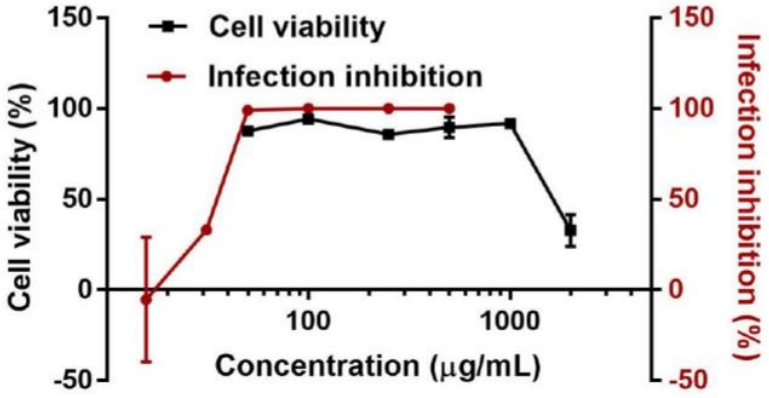

Fig. S14. Cellular toxicity of the hetero-multivalent topography-matching nanostructure. Cellular toxicity on MDCK-II cells and inhibition of infection for Hetero-MNB at different concentrations. Values are expressed at mean ±SD, n=4.

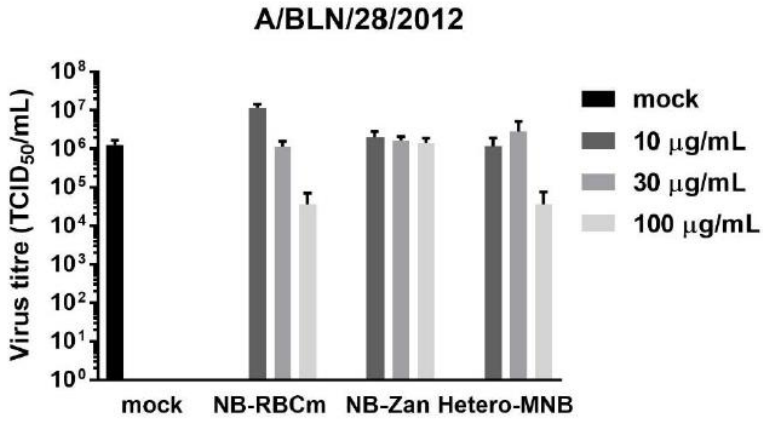

Fig. S15. Inhibition of zanamivir-resisting IAV infection by the hetero-multivalent topography-matching nanostructure.

Inhibition of viral propagation of the zanamivir resisting influenza strain (A/BLN/28/2012) for the inhibitors. The inhibitors were added to the culture medium after the initial infection of the cells. Values are expressed at mean ±SD, n=4.

Movie S1. Video for the transient viral binding to the surface.

Movie S2. Video for the permanent viral binding to the surface.

4 Summary and outlook

In this thesis, nanoparticle-based IAV inhibitors are developed via a combination of heteromultivalent structures and topography-matching nanoparticles. Firstly, the geometry-matching principle was studied by using nanoparticles with different spiky nanostructures on the surface. The topography of IAV virion was obtained from cryo-EM images, where a gap between HA and NA was noticed. With geometry modelling, it was revealed that compared with smooth surfaces, spiky surfaces were more favored for the virus interaction due to the increase of the interface area by spiky nanostructures. At a suitable spike length and spacing, the spikes could firmly insert into the gap of HA and NA, resulting in maximized area. Accordingly, the spiky nanoparticles were synthesized for the proof of concept and in a western-blot-based binding study. It was confirmed that nanoparticles with short spikes (approx. 10 nm in length and 10 nm spacing) were the best binders for IAV virions. The cryo-EM images further verified the insertion of spikes into the protein gap at this case.

Even the spiky nanoparticles bound IAV virions, they were not considered to effective IAV inhibitors, due to that the binding was not strong enough to compete IAV-cell interaction. To obtain a potent inhibitor, the surface of spiky nanoparticles was further functionalized by RBCm to enhance the virus-inhibitor interaction. The RBCm coat nanoparticle bound strongly to IAV virion, hence blocking the IAV interaction with its host cells, which was confirmed by confocal laser scanning microscopy (CLSM) and flow cytometry. The cellular infection study of IAV showed a clear decease of infected cells with RBCm coated nanoparticle dispersed in the medium. As expected, the RBCm coated the nanoparticle with short spikes was the best inhibitor, showing > 90% reduction of infected cells. The inhibitor was also able to reduce the viral replication, for which 99.9% reduction of viral titers after 24 hours of infection. Being co-used with a small dose of an NA inhibitor, zanamivir, the reduction of viral titers after 24 hours achieved 99.99%, possible due to the enhancement of IAV-inhibitor interaction by zanamivir.

In the second project, a potent IAV inhibitor was developed by combining spiky nanostructures with heteromultivalent surface functionalization. Two homo-multivalent polymeric structure, linear polyglycerol (LPG) functionalized 6'-silalylactose (LPG-SAL) and zanamivir (LPG-Zan) were synthesized and conjugated to the surface of nanoparticle with 10 nm spikes, the best viral binder from the first study, via click chemistry. After the functionalization, the inhibitor could engage HA and NA simultaneously for a robust binding,

while the matched geometry to IAV increased the interaction area and further enhanced the virus-inhibitor binding. In the CLSM-based virus binding assays, it was noticed that the inhibitor almost abolished the virions on the cell surface and the cellular infection assays showed few-to-none infected cells in the presence of the inhibitor at a MOI of 0.1. Being used after the first cycle of infection, the inhibitor showed virus-inhibition activity with a 6 order of magnitude reduction of viral propagation. Even being used 24 hours after the first cycle of infection, a 5 order of magnitude reduction of viral propagation was also noticed, demonstrating the potency of the inhibitor. The inhibitor was also found to be active against three IAV strained circulated in human, A/X31 (H3N2), A/PR/8/34 (H1N1), and A/Panama/2007/1999 (H3N2), revealing its potential to be a broad-spectrum IAV's inhibitor. It was noticed that the heteromultivalent inhibitor was much better than the homo-multivalent ones, which proves our hypothesis that heteromultivalency could further increase virus inhibition.

In the final project, a new geometry-matching nanostructure towards IAV virion was studied, a nanobowl with concave morphology that could cap the surface of virion. A carbon-based nanobowl was synthesized and functionalized by RBCm and zanamivir. For the generation of heteromultivalent surface, zanamivir was grafted to DSPE-PEG2000, which could be inserted into the lipid bilayer of RBCm via hydrophobic interactions. In this project, we also revealed the broad-spectrum virus binding ability of RBCm, which could bind the virions of A/X31 (H3N2), A/PR/8/34 (H1N1), and A/Panama/2007/1999 (H3N2) at a binding constant in nanomolar range. By TIRF microscopy, we noticed that zanamivir significantly increased the virion binding to RBCm, with increased 'on-rate.' The virions were also found to stay on the heteromultivalent surface of RBCm and zanamivir for a longer time with more tracks than RBCm, revealing the zanamivir could help stabilize the virions. The stabilization of virions increased the virion binding. The inhibitor, nanobowl functionalized with RBCm and zanamivir showed robust inhibition towards IAV, revealed by virion binding studies and cellular infection assays. Due to the broad-spectrum IAV-binding ability, the inhibitor was found to the active against A/X31 (H3N2), A/PR/8/34 (H1N1), A/Panama/2007/1999 (H3N2) and a newly emerged A/Bayern/2009 (H1N1pdm).

Conclusively, potent influenza inhibitors were obtained by combining heteromultivalency with geometry-matching topographies. The scientific goals were met by the three above-mentioned individual projects. As most of enveloped virions enter the host cells via similar pathways, it is envisioned such a strategy could be universal for the development of entry inhibitors for other virus strains. For example, the receptor of severe

acute respiratory syndrome coronavirus (SARS-CoV) and SARS-CoV-2 has been identified to angiotensin-converting enzyme 2 (ACE2) that is expressed in abundant cell lines.[2, 91-93] Taking the membrane of their host cells and combining with the geometry-matched nanoparticles is envisioned to result in a coronavirus inhibitor.[94]

The core materials used in these projects are indeed mesoporous nanoparticles that can be used as carrier systems. Loading pharmaceuticals into the nanostructures might promote the development of new heteromultivalent structures and multifunctional systems.[95-96] It should be noted that, for a proof-of-concept study, the nanoparticles in this PhD thesis are bioinert SiO_2 or carbon nanostructures and avoid the side effects of unspecific biological interactions. They are also not biodegradable in biological conditions, therefore may not be suitable as a clinical therapeutic for influenza infections. Nowadays, numerous new nanostructures with special topography are reported with higher potential for *in vivo* and clinical usages, which can be considered for the future development of virus inhibitors.[97-100]

4 Zusammenfassung und Ausblick

In der vorliegenden Arbeit wurden nanopartikelbasierte IAV-Inhibitoren über eine Kombination von heteromultivalenten Strukturen und topografischer Anpassung entwickelt. Zunächst wurde das Prinzip der Geometrieanpassung durch die Verwendung von Nanopartikeln mit unterschiedlich stacheligen Nanostrukturen auf der Partikelobberfläche untersucht. Die Topografie von Influenza A Viruspartikeln wurde aus Kryo-EM-Bildern gewonnen, wobei Freiräume zwischen den Spikeproteinen HA und NA festgestellt wurden. Bei der Oberflächenanpassung von Nanopartikeln stellte sich heraus, dass stachelige Oberflächen im Vergleich zu glatten Oberflächen für eine Interaktion mit Virengünstiger waren. Vermutlich lässt sich diese Beobachtung auf eine größere Interaktionsfläche zwischen viralen Spikeproteinen und den Nanostacheln der Nanopartikel zurückführen. Anhand von Bindungsstudien und Westernblotanalysen konnte gezeigt werden, dass Nanopartikel mit kurzen Stacheln (ca. 10 nm Länge) und einem durchschnittlichen Stachelabstand von 10 nm die besten Bindungseigenschaften gegenüber IAV-Partikel aufwiesen. Kryo-EM-Aufnahmen stützten weiter die Bindung und Verzahnung von stacheligen Nanopartikel mit viralen Spikeproteinen.

In zellbasierten Infektionsstudien konnten die stacheligen Nanopartikel jedoch keine effiziente IAV-Inhibition herbeiführen, weswegen weitere Optimierungsarbeiten notwendig waren. Erst über eine Oberflächenbeschichtung der Nanopartikel mit Erythrozytenmembranen (RBCm) konnte eine signifikante Virus-Nanopartikel-Interaktion in Zellbindungsstudienerzielt werden. Die Studie zur zellulären Infektion der IAV zeigte ein deutliches Absterben infizierter Zellen mit RBCm-beschichteten Nanopartikeln, die im Medium dispergiert waren. Wie erwartet, war das RBCm, das das Nanopartikel mit kurzen Spikes beschichtete, der beste Inhibitor und zeigte eine Reduktion der infizierten Zellen um > 90%. In Gegenwart von stacheligen und membranbeschichteten Nanopartikeln war eine virale Replikation 24 h nach Infektion drastisch reduziert (~99.9%). Bei gleichzeitiger Zugabe einer geringen Dosis des NA-Hemmers Zanamivir konnte der Titer sogar um 99,99% reduziert werden.

In einem zweiten Projekt wurde ein wirksamer IAV-Inhibitor entwickelt, bei dem stachelige Nanostrukturen einer heteromultivalenten Oberflächenfunktionalisierung unterzogen wurden. Die beiden homo-multivalenten Polymerstrukturen, lineares Polyglycerin (LPG) funktionalisiert mit 6'-Sialyllactose (LPG-SAL) oder Zanamivir (LPG-Zan) wurden synthetisiert und mittels Click-Chemie an die Oberfläche stacheliger

Nanopartikeln konjugiert. Durch diese Kombinationsstrategie soll die Virusbindung weiter verstärkt werden. In zellbasierten Infektionsstudien zeigte sich in Gegenwart dieser Inhibitoren eine stark reduzierte Infektion von Zellen. Bei Anwendung des Inhibitors nach dem ersten viralen Replikationszyklus zeigte der Inhibitor eine Reduktion der Virusvermehrung um 6 Größenordnungen. Selbst bei Anwendung 24 h nach dem ersten Replikationszyklus wurde eine Reduktion der Virusvermehrung um 5 Größenordnungen festgestellt, was die antivirale Wirksamkeit des Inhibitors untermauert. Es wurde auch festgestellt, dass der Inhibitor gegen drei beim Menschen zirkulierende IAV-Stämme (A/X31 (H3N2), A/PR/8/34 (H1N1) und A/Panama/2007/1999 (H3N2)) wirksam ist, was sein Potenzial als Breitband-IAV-Inhibitor offenbart. Es hat sich gezeigt, dass der heteromultivalente Inhibitor signifikant besser war als die homo-multivalenten Polyglycerole allein. Damit konnte unsere Hypothese, dass Heteromultivalenz die Virushemmung weiter erhöht bewiesen werden.

In einem weiteren Projekt wurden neue, der sphärischen Virusgeometrie angepasste Nanostruktur gegen IAV untersucht. Nanoschalen mit konkaver Morphologie, die der Oberfläche von Viruspartikeln angepasst sind eigneten sich hervorragend für eine Virusbindung. Hierfür wurde eine Nanoschale auf Kohlenstoffbasis synthetisiert und mit RBCm und Zanamivir funktionalisiert. Zur Erzeugung einer heteromultivalenten Oberfläche wurde Zanamivir auf DSPE-PEG2000 in die Lipiddoppelschicht eines RBCm Mantels von Nanopartikeln eingebracht. In diesem Projekt deckten wir auch eine breitwirksame Bindungsfähigkeit von Viren an die mit RBCm beschichteten Nanoschalen auf. Für die Virustypen A/X31 (H3N2), A/PR/8/34 (H1N1) und A/Panama/2007/1999 (H3N2) konnten bis zu nanomolare Bindungskonstanten ermittelt werden. Mit Hilfe der TIRF-Mikroskopie stellten wir fest, dass Zanamivir die Virionen Bindung an RBCm signifikant erhöht, was auf eine erhöhte Bindungsrate ('On-Rate') zurückgeführt werden konnte. Es zeigte sich auch, dass die Virionen länger auf der heteromultivalenten Oberfläche von RBCm und Zanamivir mit höheren Anteilen an RBCm verblieben, was zeigt, dass das Zanamivir zur Stabilisierung der Virionen beitragen könnte. Der Inhibitor, eine mit RBCm und Zanamivir funktionalisierte Nanoschale, zeigte darüber hinaus eine eindrucksvolle Hemmung gegenüber IAV, was durch Virionenbindungsstudien und zelluläre Infektionstests nachgewiesen wurde. Aufgrund des breiten Spektrums der IAV-Bindungsfähigkeit wurde der Inhibitor als aktiv gegen A/X31 (H3N2), A/PR/8/34 (H1N1), A/Panama/2007/1999 (H3N2) und A/Bayern/2009 (H1N1pdm) gefunden.

Fazit: Durch die Kombination von Heteromultivalenz mit geometrisch passenden

Topografien konnten wirksame Influenzahemmer generiert werden. Die wissenschaftlichen Ziele wurden durch die drei oben beschriebenen Einzelprojekte erreicht. Da die meisten umhüllten Virionen über ähnliche Mechanismen in die Wirtszellen gelangen, könnte eine solche Strategie universell für die Entwicklung von Eintritts Hemmern für andere Virusstämme eingesetzt werden. So wurde zum Beispiel der Rezeptor des Coronavirus des schweren akuten respiratorischen Syndroms (SARS-CoV) und des SARS-CoV2 für das Angiotensin-konvertierendes Enzym 2 (ACE2) identifiziert, das in einer Vielzahl von Zelllinien exprimiert wird.[2, 91-93] Man nimmt die Membran ihrer Wirtszellen und kombiniert sie mit den geometrisch angepassten Nanopartikeln, um einen Coronavirus-Inhibitor zu erhalten.[94]

Die Kernmaterialien, die in diesen Projekten verwendet werden, sind in der Tat mesoporöse Nanopartikel, die als Trägersysteme verwendet werden könnten. Das Einbringen von Pharmazeutika in die Nanostrukturen könnte die Entwicklung neuer heteromultivalenter Strukturen und multifunktionaler Systeme vorran bringen.[95-96] Es soll angemerkt werden, dass für eine „Proof-of-Concept“-Studie die Nanopartikel in dieser Doktorarbeit bioinerte SiO_2- oder Kohlenstoff-Nanostrukturen repräsentieren, um die Nebenwirkungen unspezifischer biologischer Wechselwirkungen zu vermeiden. Sie sind nicht biologisch abbaubar und eignen sich daher möglicherweise nicht als klinisches Therapeutikum zur Behandlung der Influenza. Heutzutage wird von zahlreichen neuen Nanostrukturen mit ausgeklügelten Topografien berichtet, für die ein höheres Potential in Tiermodellstudien gezeigt wurde. Diese Neuentwicklungen lassen auf einen vielversprechenden Trend hin zur Entwicklung von klinisch anwendbaren, antiviralen Virushemmern hoffen.[97-100]

References

[1] S. M. Kissler, C. Tedijanto, E. Goldstein, Y. H. Grad, M. Lipsitch, *Science* **2020**, *368*, 860-868.

[2] M. Hoffmann, H. Kleine-Weber, S. Schroeder, N. Krüger, T. Herrler, S. Erichsen, T. S. Schiergens, G. Herrler, N.-H. Wu, A. Nitsche, M. A. Müller, C. Drosten, S. Pöhlmann, *Cell* **2020**, *181*, 271-280.e278.

[3] Q. Li, X. Guan, P. Wu, X. Wang, L. Zhou, Y. Tong, R. Ren, K. S. M. Leung, E. H. Y. Lau, J. Y. Wong, X. Xing, N. Xiang, Y. Wu, C. Li, Q. Chen, D. Li, T. Liu, J. Zhao, M. Liu, W. Tu, C. Chen, L. Jin, R. Yang, Q. Wang, S. Zhou, R. Wang, H. Liu, Y. Luo, Y. Liu, G. Shao, H. Li, Z. Tao, Y. Yang, Z. Deng, B. Liu, Z. Ma, Y. Zhang, G. Shi, T. T. Y. Lam, J. T. Wu, G. F. Gao, B. J. Cowling, B. Yang, G. M. Leung, Z. Feng, *N. Engl. J. Med.* **2020**, *382*, 1199-1207.

[4] W. W. Thompson, D. K. Shay, E. Weintraub, L. Brammer, C. B. Bridges, N. J. Cox, K. Fukuda, *JAMA* **2004**, *292*, 1333-1340.

[5] J. D. Bloom, L. I. Gong, D. Baltimore, *Science* **2010**, *328*, 1272-1275.

[6] A. Trilla, G. Trilla, C. Daer, *Clin. Infect. Dis.* **2008**, *47*, 668-673.

[7] J. K. Taubenberger, J. C. Kash, D. M. Morens, *Sci. Transl. Med.* **2019**, *11*, eaau5485.

[8] J. K. Taubenberger, D. M. Morens, *Annu. Rev. Pathol.* **2008**, *3*, 499-522.

[9] R. Gao, B. Cao, Y. Hu, Z. Feng, D. Wang, W. Hu, J. Chen, Z. Jie, H. Qiu, K. Xu, X. Xu, H. Lu, W. Zhu, Z. Gao, N. Xiang, Y. Shen, Z. He, Y. Gu, Z. Zhang, Y. Yang, X. Zhao, L. Zhou, X. Li, S. Zou, Y. Zhang, X. Li, L. Yang, J. Guo, J. Dong, Q. Li, L. Dong, Y. Zhu, T. Bai, S. Wang, P. Hao, W. Yang, Y. Zhang, J. Han, H. Yu, D. Li, G. F. Gao, G. Wu, Y. Wang, Z. Yuan, Y. Shu, *N. Engl. J. Med.* **2013**, *368*, 1888-1897.

[10] H. Sun, Y. Xiao, J. Liu, D. Wang, F. Li, C. Wang, C. Li, J. Zhu, J. Song, H. Sun, Z. Jiang, L. Liu, X. Zhang, K. Wei, D. Hou, J. Pu, Y. Sun, Q. Tong, Y. Bi, K.-C. Chang, S. Liu, G. F. Gao, J. Liu, *Proc. Natl. Acad. Sci.* **2020**, 201921186.

[11] D. Liu, W. Shi, Y. Shi, D. Wang, H. Xiao, W. Li, Y. Bi, Y. Wu, X. Li, J. Yan, W. Liu, G. Zhao, W. Yang, Y. Wang, J. Ma, Y. Shu, F. Lei, G. F. Gao, *The Lancet* **2013**, *381*, 1926-1932.

[12] N. M. Bouvier, P. Palese, *Vaccine* **2008**, *26*, D49-D53.

[13] J. Wang, P. Li, Y. Yu, Y. Fu, H. Jiang, M. Lu, Z. Sun, S. Jiang, L. Lu, M. X. Wu, *Science* **2020**, *367*, eaau0810.

[14] M. Kanekiyo, M. G. Joyce, R. A. Gillespie, J. R. Gallagher, S. F. Andrews, H. M. Yassine, A. K. Wheatley, B. E. Fisher, D. R. Ambrozak, A. Creanga, K. Leung, E. S. Yang, S. Boyoglu-Barnum, I. S. Georgiev, Y. Tsybovsky, M. S. Prabhakaran, H. Andersen, W.-P. Kong, U. Baxa, K. L. Zephir, J. E. Ledgerwood, R. A. Koup, P. D. Kwong, A. K. Harris, A. B. McDermott, J. R. Mascola, B. S. Graham, *Nat. Immunol.* **2019**, *20*, 362-372.

[15] C. I. Paules, H. D. Marston, R. W. Eisinger, D. Baltimore, A. S. Fauci, *Immunity* **2017**, *47*, 599-603.

[16] C. Gerdil, *Vaccine* **2003**, *21*, 1776-1779.

[17] F. Carrat, A. Flahault, *Vaccine* **2007**, *25*, 6852-6862.

[18] L. V. Gubareva, L. Kaiser, F. G. Hayden, *The Lancet* **2000**, *355*, 827-835.

[19] R. Trebbien, S. S. Pedersen, K. Vorborg, K. T. Franck, T. K. Fischer, *Eurosurveillance* **2017**, *22*, 30445.

[20] A. C. Hurt, J. K. Holien, M. Parker, A. Kelso, I. G. Barr, *J. Virol.* **2009**, *83*, 10366-10373.

[21] N. Lee, A. C. Hurt, *Curr. Opin. Microbiol.* **2018**, *31*, 520-526.

[22] S. C. Harrison, *Virology* **2015**, *479-480*, 498-507.

[23] E. Vanderlinden, L. Naesens, *Med. Res. Rev.* **2014**, *34*, 301-339.

[24] G. Stiver, *Can. Med. Assoc. J.* **2003**, *168*, 49-57.
[25] C.-J. Wei, J. C. Boyington, P. M. McTamney, W.-P. Kong, M. B. Pearce, L. Xu, H. Andersen, S. Rao, T. M. Tumpey, Z.-Y. Yang, G. J. Nabel, *Science* **2010**, *329*, 1060-1064.
[26] R. B. Belshe, F. K. Newman, J. Cannon, C. Duane, J. Treanor, C. Van Hoecke, B. J. Howe, G. Dubin, *N. Engl. J. Med.* **2004**, *351*, 2286-2294.
[27] K. L. Nichol, J. D. Nordin, D. B. Nelson, J. P. Mullooly, E. Hak, *N. Engl. J. Med.* **2007**, *357*, 1373-1381.
[28] G. Neumann, T. Noda, Y. Kawaoka, *Nature* **2009**, *459*, 931-939.
[29] E. de Vries, W. Du, H. Guo, C. A. M. de Haan, *Trends Microbiol.* **2020**, *28*, 57-67.
[30] T. Sakai, S. I. Nishimura, T. Naito, M. Saito, *Sci. Rep.* **2017**, *7*, 45043.
[31] M. Müller, D. Lauster, H. H. K. Wildenauer, A. Herrmann, S. Block, *Nano Lett.* **2019**, *19*, 1875-1882.
[32] M. Zanin, P. Baviskar, R. Webster, R. Webby, *Cell Host Microbe* **2016**, *19*, 159-168.
[33] E. de Vries, W. Du, H. Guo, C. A. M. de Haan, *Trends Microbiol.* **2020**, *28*, 57-67.
[34] B. Button, L.-H. Cai, C. Ehre, M. Kesimer, D. B. Hill, J. K. Sheehan, R. C. Boucher, M. Rubinstein, *Science* **2012**, *337*, 937-941.
[35] M. D. Vahey, D. A. Fletcher, *eLife* **2019**, *8*, e43764.
[36] M. Ohuchi, N. Asaoka, T. Sakai, R. Ohuchi, *Microbes Infect.* **2006**, *8*, 1287-1293.
[37] D. Blumenkrantz, K. L. Roberts, H. Shelton, S. Lycett, W. S. Barclay, *J. Virol.* **2013**, *87*, 10539-10551.
[38] S. Bhatia, L. C. Camacho, R. Haag, *J. Am. Chem. Soc.* **2016**, *138*, 8654-8666.
[39] N. Parveen, G. E. Rydell, G. Larson, V. P. Hytönen, V. P. Zhdanov, F. Höök, S. Block, *J. Am. Chem. Soc.* **2019**, *141*, 16303-16311.
[40] V. Bandlow, S. Liese, D. Lauster, K. Ludwig, R. R. Netz, A. Herrmann, O. Seitz, *J. Am. Chem. Soc.* **2017**, *139*, 16389-16397.
[41] S. Bhatia, D. Lauster, M. Bardua, K. Ludwig, S. Angioletti-Uberti, N. Popp, U. Hoffmann, F. Paulus, M. Budt, M. Stadtmüller, T. Wolff, A. Hamann, C. Böttcher, A. Herrmann, R. Haag, *Biomaterials* **2017**, *138*, 22-34.
[42] D. Lauster, S. Klenk, K. Ludwig, S. Nojoumi, S. Behren, L. Adam, M. Stadtmüller, S. Saenger, S. Zimmler, K. Hönzke, L. Yao, U. Hoffmann, M. Bardua, A. Hamann, M. Witzenrath, L. E. Sander, T. Wolff, A. C. Hocke, S. Hippenstiel, S. De Carlo, J. Neudecker, K. Osterrieder, N. Budisa, R. R. Netz, C. Böttcher, S. Liese, A. Herrmann, C. P. R. Hackenberger, *Nat. Nanotech.* **2020**, *15*, 373-379.
[43] J. P. Amorij, A. Huckriede, J. Wilschut, H. W. Frijlink, W. L. J. Hinrichs, *Pharm. Res.* **2008**, *25*, 1256-1273.
[44] W. J. Lees, A. Spaltenstein, J. E. Kingery-Wood, G. M. Whitesides, *J. Med. Chem.* **1994**, *37*, 3419-3433.
[45] M. Nagao, Y. Fujiwara, T. Matsubara, Y. Hoshino, T. Sato, Y. Miura, *Biomacromolecules* **2017**, *18*, 4385-4392.
[46] S. Tang, W. B. Puryear, B. M. Seifried, X. Dong, J. A. Runstadler, K. Ribbeck, B. D. Olsen, *ACS Macro Lett.* **2016**, *5*, 413-418.
[47] Y. Yang, H.-P. Liu, Q. Yu, M.-B. Yang, D.-M. Wang, T.-W. Jia, H.-J. He, Y. He, H.-X. Xiao, S. S. Iyer, Z.-C. Fan, X. Meng, P. Yu, *Carbohydr. Res.* **2016**, *435*, 68-75.
[48] M. Nagao, T. Matsubara, Y. Hoshino, T. Sato, Y. Miura, *Biomacromolecules* **2019**, *20*, 2763-2769.
[49] M. Nagao, T. Matsubara, Y. Hoshino, T. Sato, Y. Miura, *Bioconjug. Chem.* **2019**, *30*, 1192-1198.
[50] M. Yamabe, K. Kaihatsu, Y. Ebara, *Bioconjug. Chem.* **2018**, *29*, 1490-1494.
[51] S. Liese, R. R. Netz, *Beilstein J. Org. Chem.* **2015**, *11*, 804-816.
[52] P. Kiran, S. Bhatia, D. Lauster, S. Aleksić, C. Fleck, N. Peric, W. Maison, S. Liese,

B. G. Keller, A. Herrmann, R. Haag, *Chem. Eur. J.* **2018**, *24*, 19373-19385.
[53] S. Liese, R. R. Netz, *ACS Nano* **2018**, *12*, 4140-4147.
[54] S.-J. Kwon, D. H. Na, J. H. Kwak, M. Douaisi, F. Zhang, E. J. Park, J.-H. Park, H. Youn, C.-S. Song, R. S. Kane, J. S. Dordick, K. B. Lee, R. J. Linhardt, *Nat. Nanotech.* **2016**, *12*, 48.
[55] V. Cagno, P. Andreozzi, M. D'Alicarnasso, P. Jacob Silva, M. Mueller, M. Galloux, R. Le Goffic, S. T. Jones, M. Vallino, J. Hodek, J. Weber, S. Sen, E.-R. Janeček, A. Bekdemir, B. Sanavio, C. Martinelli, M. Donalisio, M.-A. Rameix Welti, J.-F. Eleouet, Y. Han, L. Kaiser, L. Vukovic, C. Tapparel, P. Král, S. Krol, D. Lembo, F. Stellacci, *Nat. Mater.* **2018**, *17*, 195-203.
[56] S. T. Jones, V. Cagno, M. Janeček, D. Ortiz, N. Gasilova, J. Piret, M. Gasbarri, D. A. Constant, Y. Han, L. Vuković, P. Král, L. Kaiser, S. Huang, S. Constant, K. Kirkegaard, G. Boivin, F. Stellacci, C. Tapparel, *Sci. Adv.* **2020**, *6*, eaax9318.
[57] O. Kocabiyik, V. Cagno, L. Sedano, Y. Bhide, J. Mettier, C. Medaglia, B. Da Costa, Y. Zhu, S. Constant, S. Huang, L. Kaiser, W. L. J. Hinrichs, A. Huckeriede, R. Le Goffic, C. Tapparel, F. Stellacci, *bioRxiv* **2020**, 2020.2003.2018.996678.
[58] J. Vonnemann, S. Liese, C. Kuehne, K. Ludwig, J. Dernedde, C. Böttcher, R. R. Netz, R. Haag, *J. Am. Chem. Soc.* **2015**, *137*, 2572-2579.
[59] M. Wallert, C. Nie, P. Anilkumar, S. Abbina, S. Bhatia, J. N. Kizhakkedathu, R. Haag, S. Block, *Small* **2020**.
[60] I. Papp, C. Sieben, K. Ludwig, M. Roskamp, C. Böttcher, S. Schlecht, A. Herrmann, R. Haag, *Small* **2010**, *6*, 2900-2906.
[61] B. Ziem, H. Thien, K. Achazi, C. Yue, D. Stern, K. Silberreis, M. F. Gholami, F. Beckert, D. Gröger, R. Mülhaupt, J. P. Rabe, A. Nitsche, R. Haag, *Adv. Healthc. Mater.* **2016**, *5*, 2922-2930.
[62] P. Dey, T. Bergmann, J. L. Cuellar-Camacho, S. Ehrmann, M. S. Chowdhury, M. Zhang, I. Dahmani, R. Haag, W. Azab, *ACS Nano* **2018**, *12*, 6429-6442.
[63] S. Bhatia, M. Hilsch, J. L. Cuellar-Camacho, K. Ludwig, C. Nie, B. Parshad, M. Wallert, S. Block, D. Lauster, C. Böttcher, A. Herrmann, R. Haag, *Angew. Chem. Int. Ed.*, *n/a*.
[64] B. Ziem, H. Thien, K. Achazi, C. Yue, D. Stern, K. Silberreis, M. F. Gholami, F. Beckert, D. Gröger, R. Mülhaupt, J. P. Rabe, A. Nitsche, R. Haag, *Adv. Healthc. Mater.* **2016**, *5*, 2922-2930.
[65] G. Wu, S.-m. Yan, *Acta Pharmacol. Sin.* **2006**, *27*, 513-526.
[66] Q. Teng, D. Xu, W. Shen, Q. Liu, G. Rong, X. Li, L. Yan, J. Yang, H. Chen, H. Yu, W. Ma, Z. Li, *J. Virol.* **2016**, *90*, 9806-9825.
[67] K. L. Prachanronarong, A. S. Canale, P. Liu, M. Somasundaran, S. Hou, Y.-P. Poh, T. Han, Q. Zhu, N. Renzette, K. B. Zeldovich, T. F. Kowalik, N. Kurt-Yilmaz, J. D. Jensen, D. N. A. Bolon, W. A. Marasco, R. W. Finberg, C. A. Schiffer, J. P. Wang, *J. Virol.* **2019**, *93*, e01639-01618.
[68] M. B. Doud, J. M. Lee, J. D. Bloom, *Nat. Comm.* **2018**, *9*, 1386.
[69] J.-K. Park, Y. Xiao, M. D. Ramuta, L. A. Rosas, S. Fong, A. M. Matthews, A. D. Freeman, M. A. Gouzoulis, N. A. Batchenkova, X. Yang, K. Scherler, L. Qi, S. Reed, R. Athota, L. Czajkowski, A. Han, D. M. Morens, K.-A. Walters, M. J. Memoli, J. C. Kash, J. K. Taubenberger, *Nat. Med.* **2020**, *26*, 1240-1246.
[70] S. Jaiswal, C. H. M. Jamieson, W. W. Pang, C. Y. Park, M. P. Chao, R. Majeti, D. Traver, N. van Rooijen, I. L. Weissman, *Cell* **2009**, *138*, 271-285.
[71] P. L. Rodriguez, T. Harada, D. A. Christian, D. A. Pantano, R. K. Tsai, D. E. Discher, *Science* **2013**, *339*, 971-975.
[72] R. H. Fang, A. V. Kroll, W. Gao, L. Zhang, *Adv. Mater.* **2018**, *30*, 1706759.
[73] C.-M. J. Hu, R. H. Fang, K.-C. Wang, B. T. Luk, S. Thamphiwatana, D. Dehaini, P.

Nguyen, P. Angsantikul, C. H. Wen, A. V. Kroll, C. Carpenter, M. Ramesh, V. Qu, S. H. Patel, J. Zhu, W. Shi, F. M. Hofman, T. C. Chen, W. Gao, K. Zhang, S. Chien, L. Zhang, *Nature* **2015**, *526*, 118-121.
[74] C.-M. J. Hu, L. Zhang, S. Aryal, C. Cheung, R. H. Fang, L. Zhang, *Proc. Natl. Acad. Sci.* **2011**, *108*, 10980-10985.
[75] L. Rao, L.-L. Bu, J.-H. Xu, B. Cai, G.-T. Yu, X. Yu, Z. He, Q. Huang, A. Li, S.-S. Guo, W.-F. Zhang, W. Liu, Z.-J. Sun, H. Wang, T.-H. Wang, X.-Z. Zhao, *Small* **2015**, *11*, 6225-6236.
[76] Q. Hu, W. Sun, C. Qian, C. Wang, H. N. Bomba, Z. Gu, *Adv. Mater.* **2015**, *27*, 7043-7050.
[77] J.-Y. Zhu, D.-W. Zheng, M.-K. Zhang, W.-Y. Yu, W.-X. Qiu, J.-J. Hu, J. Feng, X.-Z. Zhang, *Nano Lett.* **2016**, *16*, 5895-5901.
[78] L. Rao, L.-L. Bu, B. Cai, J.-H. Xu, A. Li, W.-F. Zhang, Z.-J. Sun, S.-S. Guo, W. Liu, T.-H. Wang, X.-Z. Zhao, *Adv. Mater.* **2016**, *28*, 3460-3466.
[79] W. Chen, K. Zeng, H. Liu, J. Ouyang, L. Wang, Y. Liu, H. Wang, L. Deng, Y.-N. Liu, *Adv. Funct. Mater.* **2017**, *27*, 1605795.
[80] C.-M. J. Hu, R. H. Fang, J. Copp, B. T. Luk, L. Zhang, *Nat. Nanotech.* **2013**, *8*, 336-340.
[81] C.-M. J. Hu, R. H. Fang, B. T. Luk, L. Zhang, *Nat. Nanotech.* **2013**, *8*, 933-938.
[82] R. H. Fang, C.-M. J. Hu, B. T. Luk, W. Gao, J. A. Copp, Y. Tai, D. E. O'Connor, L. Zhang, *Nano Lett.* **2014**, *14*, 2181-2188.
[83] R. Yang, J. Xu, L. Xu, X. Sun, Q. Chen, Y. Zhao, R. Peng, Z. Liu, *ACS Nano* **2018**, *12*, 5121-5129.
[84] J. V. de Carvalho, R. O. de Castro, E. Z. M. da Silva, P. P. Silveira, M. E. da Silva-Januário, E. Arruda, M. C. Jamur, C. Oliver, R. S. Aguiar, L. L. P. daSilva, *PloS one* **2014**, *9*, e113691-e113691.
[85] X. Liu, L. Yuan, L. Zhang, Y. Mu, X. Li, C. Liu, P. Lv, Y. Zhang, T. Cheng, Q. Yuan, N. Xia, X. Chen, G. Liu, *Angew. Chem. Int. Ed.* **2018**, *57*, 12499-12503.
[86] H. Liao, J. H. Hafner, *Chem. Mater.* **2005**, *17*, 4636-4641.
[87] Y. Sun, Y. Xia, *Science* **2002**, *298*, 2176-2179.
[88] B. N. S. Thota, X. Lou, D. Bochicchio, T. F. E. Paffen, R. P. M. Lafleur, J. L. J. van Dongen, S. Ehrmann, R. Haag, G. M. Pavan, A. R. A. Palmans, E. W. Meijer, *Angew. Chem. Int. Ed.* **2018**, *57*, 6843-6847.
[89] Y. Chen, P. Xu, H. Chen, Y. Li, W. Bu, Z. Shu, Y. Li, J. Zhang, L. Zhang, L. Pan, X. Cui, Z. Hua, J. Wang, L. Zhang, J. Shi, *Adv. Mater.* **2013**, *25*, 3100-3105.
[90] W. Wang, P. Wang, X. Tang, A. A. Elzatahry, S. Wang, D. Al-Dahyan, M. Zhao, C. Yao, C.-T. Hung, X. Zhu, T. Zhao, X. Li, F. Zhang, D. Zhao, *ACS Cent. Sci.* **2017**, *3*, 839-846.
[91] M. M. Lamers, J. Beumer, J. van der Vaart, K. Knoops, J. Puschhof, T. I. Breugem, R. B. G. Ravelli, J. Paul van Schayck, A. Z. Mykytyn, H. Q. Duimel, E. van Donselaar, S. Riesebosch, H. J. H. Kuijpers, D. Schipper, W. J. van de Wetering, M. de Graaf, M. Koopmans, E. Cuppen, P. J. Peters, B. L. Haagmans, H. Clevers, *Science* **2020**, *369*, 50-54.
[92] B.-Z. Zhang, H. Chu, S. Han, H. Shuai, J. Deng, Y.-f. Hu, H.-r. Gong, A. C.-Y. Lee, Z. Zou, T. Yau, W. Wu, I. F.-N. Hung, J. F.-W. Chan, K.-Y. Yuen, J.-D. Huang, *Cell Res.* **2020**.
[93] R. Zang, M. F. G. Castro, B. T. McCune, Q. Zeng, P. W. Rothlauf, N. M. Sonnek, Z. Liu, K. F. Brulois, X. Wang, H. B. Greenberg, M. S. Diamond, M. A. Ciorba, S. P. J. Whelan, S. Ding, *Sci. Immunol.* **2020**, *5*, eabc3582.
[94] Q. Zhang, A. Honko, J. Zhou, H. Gong, S. N. Downs, J. H. Vasquez, R. H. Fang, W. Gao, A. Griffiths, L. Zhang, *Nano Lett.* **2020**, *20*, 5570-5574.

[95] Z. Li, J. C. Barnes, A. Bosoy, J. F. Stoddart, J. I. Zink, *Chem. Soc. Rev.* **2012**, *41*, 2590-2605.
[96] I. I. Slowing, B. G. Trewyn, S. Giri, V. S.-Y. Lin, *Adv. Funct. Mater.* **2007**, *17*, 1225-1236.
[97] J. Guo, B. L. Tardy, A. J. Christofferson, Y. Dai, J. J. Richardson, W. Zhu, M. Hu, Y. Ju, J. Cui, R. R. Dagastine, I. Yarovsky, F. Caruso, *Nat. Nanotech.* **2016**, *11*, 1105-1111.
[98] P. Zhang, X. Liu, P. Liu, F. Wang, H. Ariyama, T. Ando, J. Lin, L. Wang, J. Hu, B. Li, C. Fan, *Nat. Comm.* **2020**, *11*, 3114.
[99] G. Yao, J. Li, Q. Li, X. Chen, X. Liu, F. Wang, Z. Qu, Z. Ge, R. P. Narayanan, D. Williams, H. Pei, X. Zuo, L. Wang, H. Yan, B. L. Feringa, C. Fan, *Nat. Mater.* **2020**, *19*, 781-788.
[100] P. S. Kwon, S. Ren, S.-J. Kwon, M. E. Kizer, L. Kuo, M. Xie, D. Zhu, F. Zhou, F. Zhang, D. Kim, K. Fraser, L. D. Kramer, N. C. Seeman, J. S. Dordick, R. J. Linhardt, J. Chao, X. Wang, *Nat. Chem.* **2020**, *12*, 26-35.

5 Appendix

5.1 Publications and Conference Contributions

Publications

First author

1. **Chuanxiong Nie**, Marlena Stadtmüller, Hua Yang, Yi Xia, Thorsten Wolff, Chong Cheng, and Rainer Haag, Spiky Nanostructures with Geometry-matching Topography for Virus Inhibition, *Nano Lett.* 2020, 20, 7, 5367–5375. https://doi.org/10.1021/acs.nanolett.0c01723

2. **Chuanxiong Nie**, Badri Parshad, Sumati Bhatia, Chong Cheng, Marlena Stadtmüller, Alexander Oehrl, Yannic Kerkhoff, Thorsten Wolff, Rainer Haag, Topology-Matching Design of an Influenza-Neutralizing Spiky Nanoparticle-Based Inhibitor with a Dual Mode of Action, *Angew. Chem. Int. Ed.* 2020, 59, 15662-15666. https://doi.org/10.1002/anie.202004832

3. **Chuanxiong Nie**, Marlena Stadtmüller, Badri Parshad, Matthias Wallert, Yannic Kerkhoff, Sumati Bhatia, Stephan Block, Chong Cheng, Thorsten Wolff, Rainer Haag, Heteromultivalent topology-matched nanostructures as potent and broad-spectrum influenza A virus inhibitors, *Sci. Adv.*, 2020, Accepted.

4. **Chuanxiong Nie,** Lang Ma, Shuang Li, Xin Fan, Ye Yang, Chong Cheng, Weifeng Zhao，Changsheng Zhao, Recent progresses in graphene based bio-functional nanostructures for advanced biological and cellular interfaces, *Nano Today* 2019, 26, 57-97. https://doi.org/10.1016/j.nantod.2019.03.003

Co-authors

5. Rotsiniaina Randriantsilefisoa, **Chuanxiong Nie**, Badri Parshad, Yuanwei Pan, Sumati Bhatia and Rainer Haag, Double trouble for viruses: a hydrogel nanocomposite catches the influenza virus while shrinking and changing color, *Chem Comm.* 2020,56, 3547-3550. https://doi.org/10.1039/C9CC09069J

6. Michaël W. Kulka, **Chuanxiong Nie,** Philip Nickl, Yannic Kerkhoff, Arushi Garg, Dirk Salz, Jörg Radnik, Ingo Grunwald and Rainer Haag, Surface-Initiated Grafting of Dendritic Polyglycerol from Mussel-Inspired Adhesion-Layers for the Creation of Cell-Repelling

Coating. *Adv. Mater. Interf.*, 2020, 2000931. https://doi.org/10.1002/admi.202000931

7. Matthias Wallert, **Chuanxiong Nie**, Parambath Anilkumar, Srinivas Abbina, Sumati Bhatia, Kai Ludwig, Jayachandran N. Kizhakkedathu, Rainer Haag, Stephan Block, Mucin-Inspired, High Molecular Weight Virus Binding Inhibitors Show Biphasic Binding Behavior to Influenza A Viruses, *Small*, 2020, 16, 2004635. https://doi.org/10.1002/smll.202004635

8. Sumati Bhatia, Malte Hilsch, Jose Luis Cuellar-Camacho, Kai Ludwig, **Chuanxiong Nie**, Badri Parshad, Matthias Wallert, Stephan Block, Daniel Lauster, Christoph Böttcher, Andreas Herrmann, Rainer Haag, Adaptive Flexible Sialylated Nanogels as Highly Potent Influenza A Virus Inhibitors, *Angew. Chem. Int. Ed.* 2020, 59, 12417. https://doi.org/10.1002/anie.202006145

9. Yi Xia, Shuang Li, **Chuanxiong Nie,** Jianguang Zhang, Suqiong Zhou, Hua Yang, Mingjun Li, Wenzhong Li, Chong Cheng, Rainer Haag, A multivalent polyanion-dispersed carbon nanotube toward highly bioactive nanostructured fibrous stem cell scaffolds, *Appl. Mater. Today* 2019, 16, 518-528. https://doi.org/10.1016/j.apmt.2019.07.006

Conference Presentations

Oral and poster presentations:

Chuanxiong Nie, Chong Cheng, Rainer Haag

'Spiky nanostructures as the matching principle for the design of influenza virus inhibitor'

International Symposium of the SFB 765 "Multivalency in Chemistry and Biology"

Chuanxiong Nie, Sumati Bhatia, Klaus Osterrieder, Rainer Haag,

'Multivalent structures for the inhibition of SARS-CoV-2: progress report'

Kickoff-meeting for the BUA project for SARS-CoV-2.

5.2 Curriculum Vitae

For reasons of data protection, the curriculum vitae is not published in the electronic version.

Declaration of independence

Hereby, I certify that the work presented in this thesis has not previously been submitted for a degree nor has it been submitted as part of requirements for a degree except as fully acknowledged within the text.

I also certify that the thesis has been written by me. Any help that I have received in my research work and the preparation of the thesis itself has been acknowledged. In addition, I certify that all information sources and literature used are indicated in the thesis.

Chuanxiong Nie